

WIND ENGINEERING STUDY OF  
JOHNS-MANVILLE WORLD HEADQUARTERS

by

S.K. Nayak, J.A. Garrison\* and J.E. Cermak\*\*

for

Johns-Manville Corporation  
Greenwood Plaza  
Denver, Colorado 80217

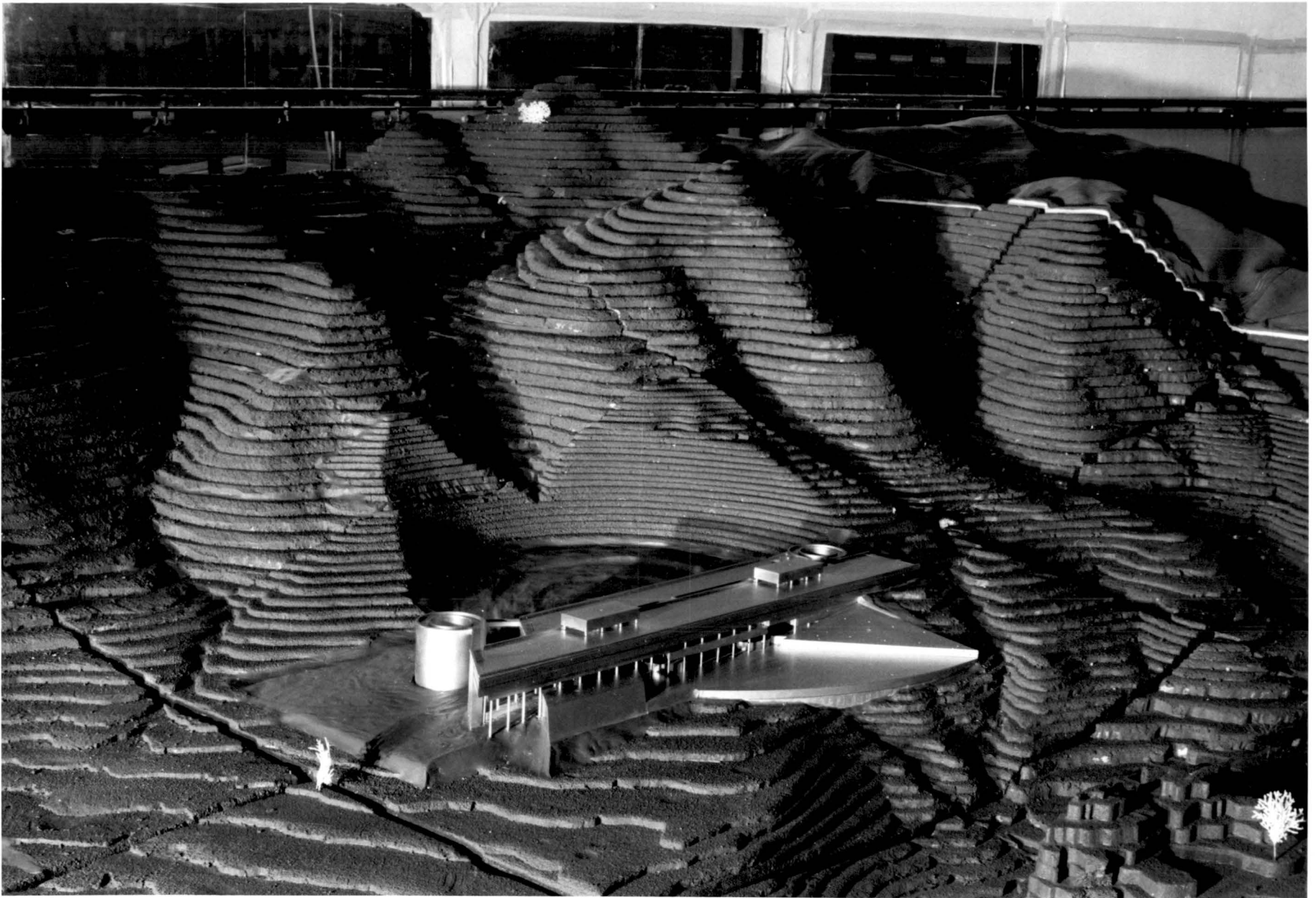
Fluid Mechanics Program  
Fluid Dynamics and Diffusion Laboratory  
Department of Civil Engineering  
Colorado State University  
Fort Collins, Colorado

October 1974

\*Research Associate

\*\*Professor-in-Charge, Fluid Mechanics Program

CER73-74SKN-JAG-JEC42



JOHNS-MANVILLE WORLD HEADQUARTERS  
(1:400 Scale Model)

## TABLE OF CONTENTS

<u>Section</u>	<u>Page</u>
ABSTRACT . . . . .	i
PURPOSE AND OBJECTIVES . . . . .	iii
CONCLUSIONS . . . . .	v
LIST OF TABLES . . . . .	vi
LIST OF FIGURES . . . . .	vii
LIST OF SYMBOLS . . . . .	x
I INTRODUCTION . . . . .	1
1.1 General . . . . .	1
1.2 Objectives . . . . .	2
II SIMULATION OF ATMOSPHERIC MOTION . . . . .	3
2.1 General . . . . .	3
2.2 Dynamic Similarity . . . . .	3
2.3 Thermal Similarity . . . . .	4
2.4 Kinematic Similarity . . . . .	4
III WIND TUNNEL AND MEASURING TECHNIQUES . . . . .	6
3.1 Wind Tunnel: General Description . . . . .	6
3.2 Model: Design and Construction . . . . .	6
3.3 Flow Visualization . . . . .	7
3.4 Snow-Drift Locations . . . . .	7
3.5 Tracer-Gas Concentrations . . . . .	8
3.6 Local Gusts and Mean Velocities . . . . .	8
3.7 Building Surface Pressures . . . . .	9
IV TEST PROGRAM AND RESULTS . . . . .	11
4.1 Test Program . . . . .	11
4.2 Approach Velocity Conditions . . . . .	12
4.3 Flow Visualization . . . . .	12
4.4 Snow-Drift Locations . . . . .	13
4.5 Local Automobile-Emission Concentrations . . . . .	14
4.6 Local Gusts . . . . .	15
4.7 Building Surface Pressures . . . . .	15
V CONCLUSIONS . . . . .	16
REFERENCES . . . . .	18
TABLES . . . . .	19

<u>Section</u>	<u>Page</u>
APPENDIX A . . . . .	28
APPENDIX B . . . . .	29
APPENDIX C . . . . .	32
APPENDIX D . . . . .	33
D.1 Local Automobile-Emission Concentrations . . .	33
D.2 Local Mean Velocities and Gust Intensities . .	35
D.3 Surface Pressures . . . . .	36

## ABSTRACT

Model tests of the Ken Caryl Ranch area were conducted in the Colorado State University environmental wind tunnel to determine: 1) general wind distribution, 2) snowdrift location, 3) distribution of gas concentration resulting from the automobile exhaust released in the ground level parking area, 4) local gust intensities, and 5) induced wind pressures on the Johns-Manville World Headquarters. The 1:400 scale model included the basic structure and all the significant local terrain features. Wind effects for eight significant wind directions at 45 degree intervals starting from north were examined in the study. General wind patterns were recorded by photographing the trajectories of smoke released at selected locations. Results of snow drifting simulation are documented by photographs. Local dispersion characteristics were obtained by measuring mean concentrations of tracer gas along vertical lines and at significant points while releasing a tracer gas in the parking area at a known uniform rate. Local gust-intensity measurements were made by using a hot-wire anemometer. Aerodynamic pressures on the building model were measured as the difference in local and freestream static pressures.

The present study has revealed that the heliport site is not associated with any serious problems of snowdrifts and surface winds. However, a significant snowdrift problem is seen to exist in the parking area at ground level, for cases of wind approaching from the S, SE, W and NW directions. The region on the northeast side of the building is found to be relatively free from problems due to snowdrifts and excessive concentrations of automobile exhausts. A high

concentration of automobile exhausts was induced at the terrace level by secondary flow behind the building. This occurred for the cases of wind approaching from the N, NE and E directions. Severe gust intensities were observed to persist in the valley regions of the adjacent mountainous terrain for the cases of wind approaching from S, SW, W and NW directions.

The maximum gust pressure on the building surface was found to be  $-48 \text{ lb/ft}^2$  behind the parapets at the southeast extreme of the Elevation-6335 level with a SE wind. Gust pressures on the glass surfaces did not exceed  $\pm 30 \text{ lb/ft}^2$  and were generally much smaller in magnitude.

## PURPOSE AND OBJECTIVES OF THE INVESTIGATION

The purpose of this investigation is to identify any potential adverse wind effects associated with the Johns-Manville World Headquarters (JMWH) at Ken Caryl Ranch. Quantitative data obtained from the model are selected to aid in the planning and design of the JMWH in an effort to minimize wind damage to the structure and discomfort to the occupants arising from environmental factors.

The objective of this study is to investigate the following wind characteristics and effects:

- 1) To define mean velocity distribution of approach winds and detailed flow patterns at selected locations around JMWH building
- 2) To identify snow-drift locations
- 3) To determine the concentration distribution in the region due to the automobile exhaust released at ground level parking area
- 4) To define the gust intensities to which a pedestrian will be subjected in the area
- 5) To determine the aerodynamic pressures induced on the building

The results obtained in the model study for each of the eight approach wind directions at 45-degree intervals beginning at north are presented in this report. The observations of flow visualization study are presented in a set of supplementary motion pictures. Snow-drift locations identified in this study are shown in black and white photographs. Concentration distributions in the region are shown as vertical profiles and radial plots of local concentration coefficients. Local gust intensities measured at 35 significant locations are presented in

tables and a radial plot. Surface gust pressures measured at 64 important locations on the building are expressed as pressure coefficients and summarized in tables.

Typical examples of how to use the data obtained in this investigation to predict prototype values are given in the appendices.

## CONCLUSIONS

The following conclusions are based on the data presented in this report, supplementary motion pictures and available climatological data available for the site.

1. The site for the heliport did not show any severe problems due to snow drifting and local surface winds for any of the eight approach wind directions studied.
2. A distinct snow-drift problem is found to exist in the ground-level parking area and also in between two parts of the building for cases of wind approaching from the S, SE, W, and NW directions.
3. The region on the northeast side of the building did not show any severe problems due to local snow-drifting, concentration of automobile exhaust and surface winds.
4. High concentrations of automobile exhaust released in the ground-level parking area were observed in the terrace region for cases of wind approaching from the N, NE and E directions.
5. Severe and persistent gust conditions were found to prevail in the valley regions of the mountainous terrain near the building for the cases of wind approaching from the S, SW, W and NW directions.
6. Pressure measurements on the building indicated that no unusually severe wind-gust pressures will prevail on the building.

## LIST OF TABLES

<u>Table</u>	<u>Description</u>	<u>Page</u>
1	LOCAL CONCENTRATION COEFFICIENTS . . . . .	20
2	LOCAL MEAN VELOCITIES AND GUST INTENSITIES AT 0.15 IN (5 FT PROTOTYPE) FROM SURFACE WIND APPROACHING FROM N AND NE . . . . .	21
3	LOCAL MEAN VELOCITIES AND GUST INTENSITIES AT 0.15 IN (5 FT PROTOTYPE) FROM SURFACE WIND APPROACHING FROM E AND SE . . . . .	22
4	LOCAL MEAN VELOCITIES AND GUST INTENSITIES AT 0.15 IN (5 FT PROTOTYPE) FROM SURFACE WIND APPROACHING FROM S AND SW . . . . .	23
5	LOCAL MEAN VELOCITIES AND GUST INTENSITIES AT 0.15 IN (5 FT PROTOTYPE) FROM SURFACE WIND APPROACHING FROM W AND NW . . . . .	24
6	SURFACE PRESSURE COEFFICIENTS WIND APPROACHING FROM N, NE, E AND SE . . . . .	25
7	SURFACE PRESSURE COEFFICIENTS WIND APPROACHING FROM S, SW, W AND NW . . . . .	26
8	LOCAL CONCENTRATIONS OF CARBON MONOXIDE: A typical case based on calculations presented in Appendix D1 (15 min average) . . . . .	27

## LIST OF FIGURES

<u>Figure</u>	<u>Description</u>	<u>Page</u>
1	Environmental Wind-Tunnel: Fluid Dynamics and Diffusion Laboratory, Colorado State University . . . .	40
2	Schematic of the Colorado State University Environmental Wind-Tunnel Showing the Model Location and Upwind Conditions . . . . .	41
3	Topography of the Site under Investigation . . . . .	42
4	Aerial View of Site under Investigation . . . . .	43
5	A Photograph of Styrofoam Particles used as a Drift Material . . . . .	44
6	Locations of Tracer-Gas Sources and their Details Wind Directions: N and NE . . . . .	45
7	Locations of Tracer-Gas Sources and their Details Wind Directions: E and SE . . . . .	46
8	Locations of Tracer-Gas Sources and their Details Wind Directions: S and SW . . . . .	47
9	Locations of Tracer-Gas Sources and their Details Wind Directions: W and NW . . . . .	48
10	Tracer-Gas Sampling and Analysis System . . . . .	49
11	Locations of Points where Local Concentrations and Gusts were Measured: Heliport, Parking Area and NE Side of the Building . . . . .	50
12	Plan View at Elevation 6322 Indicating Locations of Points where Local Concentrations and Pressures were Measured . . . . .	51
13	Plan View at Elevation 6335 Indicating Locations of Points where Local Concentrations, Gusts and Pressures were Measured . . . . .	52
14	Plan View at Elevation 6308 Indicating Pressure Points . . . . .	53
15	Plan View at Elevation 6294 Indicating Pressure Points . . . . .	54
16	Plan View at Elevation 6280 Indicating Pressure Points . . . . .	55

<u>Figure</u>	<u>Description</u>	<u>Page</u>
17	Plan View at Elevation 6266 Indicating Points where Local Concentrations, Gusts and Pressures were Measured . . . . .	56
18	Plan View at Elevation 6252 Indicating Locations of Points where Local Concentrations, Gusts and Pressures were Measured . . . . .	57
19	Locations of Pressure Taps on N and S Elevations . . .	58
20	Locations of Pressure Taps on E and W Elevations . . .	59
21	Typical Calibration of Hot Wire . . . . .	60
22	Mean Velocity Profiles at 300 ft Upwind of Building: Free Stream Wind Speed = 45 ft/sec . . . . .	61
23	Log-Log Plots of Mean Velocity Profiles at 300 ft Upwind of the Building . . . . .	62
24	Mean Velocity and Turbulence Intensity Profiles at the Heliport for the Case of Wind Approaching from W . . . . .	63
25	Mean Velocity and Turbulence Intensity Profiles in the Parking Area for the Case of Wind Approaching from W . . . . .	64
26	General Approach Flow Pattern: a) Wind Approaching from SW b) Wind Approaching from NW . . . . .	65
27	Wake Flow Due to the Building a) Wind Approaching from W b) Wind Approaching from N . . . . .	66
28	Snow-Drift Locations Due to Wind Approaching from the N . . . . .	67
29	Mean Drift Paths Due to N Wind . . . . .	68
30	Snow-Drift Locations Due to Wind Approaching from the NE . . . . .	69
31	Mean Drift Paths Due to NE Wind . . . . .	70
32	Snow-Drift Locations Due to Wind Approaching from E . . . . .	71

<u>Figure</u>	<u>Description</u>	<u>Page</u>
33	Mean Drift Paths Due to the E Wind . . . . .	72
34	Snow-Drift Locations Due to Wind Approaching from the SE . . . . .	73
35	Mean Drift Paths Due to the SE Wind . . . . .	74
36	Snow-Drift Locations Due to Wind Approaching from S . . . . .	75
37	Mean Drift Paths Due to the S Wind . . . . .	76
38	Snow-Drift Locations Due to Wind Approaching from the SW . . . . .	77
39	Mean Drift Paths Due to the SW Wind . . . . .	78
40	Snow-Drift Locations Due to Wind Approaching from the NW . . . . .	79
41	Mean Drift Paths Due to the W Wind . . . . .	80
42	Snow-Drift Locations Due to Wind Approaching from the NW . . . . .	81
43	Mean Drift Paths Due to NW Winds . . . . .	82
44	Vertical Profiles of Concentration Coefficients in the Parking Area for the Cases of Wind Approaching from the N, NE, E, SE, S, SW, W and NW . . . . .	83
45	Vertical Profiles of Concentration Coefficients on the Northeast Side of Building for the Cases of Wind Approaching from the N, NE, E, SE, S, W and NW . . . . .	84
46	Effect of Wind Directions on Concentration Coefficients at C3, C4, C5, C6, C7 and C8 . . . . .	85
47	Effect of Wind Direction on Concentration Coefficients at C1, C2, C9 and C10 . . . . .	86
48	Radial Plot of Local Mean Winds and Gusts in Heliport at W33, W34 and W35 . . . . .	87

## LIST OF SYMBOLS

A	= Calibration coefficient of hot wire
B	= Calibration coefficient of hot wire
C	= Local concentration
$c_p$	= Specific heat at constant pressure
$C_p$	= Pressure coefficient
E	= Hot-wire output voltage
$Ec$	= Eckert number $(U^2/c_p \Delta T)$
$Fg$	= Gust factor
$Fr$	= Froude number $\left(\frac{U}{gL} \frac{\Delta T}{T}\right)$
g	= Gravitational acceleration
H	= Building height
K	= Concentration coefficient $\left(\frac{CUL^2}{Q}\right)$
k	= Coefficient of thermal conductivity
L	= Characteristic length
n	= Exponent of velocity profile
P	= Local gust pressure
p	= Exponent of calibration relation of hot wire
$Pr$	= Prandtl number $(k/c_p \mu)^{-1}$
Q	= Source strength
$Re$	= Reynolds number $\left(\frac{\rho UL}{\mu}\right)$
$Ro$	= Rossby number $\left(\frac{U}{\Omega L}\right)$
T	= Temperature
U	= Wind speed
x,y,z	= Cartesian coordinates
$z_o$	= Effective roughness height

- $\rho$  = Mass density of fluid  
 $\mu$  = Dynamic viscosity  
 $\nu$  = Kinematic viscosity  $\mu/\rho$   
 $\Omega$  = Angular speed of Earth's rotation

### Suffixes

- 2H = At a height of 2H from ground level  
L = Local  
M = Mean  
m = Model  
O = Reference  
P = Prototype  
RMS = Root-mean-square of fluctuations  
S = Static  
 $S^\infty$  = Static at infinity  
 $\infty$  = At infinity  
 $\Delta$  = Difference

## I. INTRODUCTION

### 1.1 General

A wind-tunnel model study of Johns-Mansville World Headquarters building was motivated by the desire to identify any of the existing wind engineering problems due to the special features of surrounding topography, its orientation and wind conditions. Location of the building at the foot of the hills with special features makes the prediction of local wind field, local material-drift, pollution concentration distribution and induced surface pressures impossible through the use of present knowledge. Solutions to such complicated problems are attainable only through use of model testing in special environmental wind tunnels. Thus, the model of Johns-Manville World Headquarters was tested in the Environmental Wind-Tunnel of the Fluid Dynamics and Diffusion Laboratory at Colorado State University.

The headquarters is located at the Ken Caryl Ranch south of Denver, Colorado. Specific orientation and location of the building was chosen to blend with the natural topography; however, this may result in creation of some adverse wind effects. An objective of the wind-tunnel model study is to determine during the planning and design phase of the site development the location and nature of any potential wind problems.

Wind engineering aspects include the local snow-drift, dispersion, gusts and surface pressures induced by the local wind fields. Prediction of these quantities by employing present knowledge is possible in only very simple cases like those of simple structures standing in well defined velocity fields. The complicated hilly terrain on the southwest side, the excavation done to construct the parking area, orientation of

the building and also different directions of approach wind make the problem beyond the scope of conventional analytical approach.

## 1.2 Objectives

The object of the present study was to define the general wind distribution over the Ken Caryl Ranch, to determine the possible snow-drift problem locations, to assess the impact of automobile exhaust from the parking area on the surroundings and to evaluate the aerodynamic forces developed on the building by the local wind field. In order to accomplish these objectives, a 1:400 scale model of the building and the topography was subjected to rigorous wind-tunnel testing by simulating suitable approach wind conditions. The velocity field was established qualitatively by tracing trajectories of smoke released at selected locations. Hot-wire measurements were made to determine approach conditions of velocity and local gusts. An attempt was made to simulate precisely the snow-drift process and determine problem locations. Aerodynamic pressures at selected locations on the building were recorded as the difference between local surface pressure and free-stream static pressure. Impact of automobile exhaust on the surroundings was determined by noting the concentration of tracer gas at selected locations corresponding to a known amount of tracer gas released uniformly over the ground-level parking area. The results obtained in the systematic wind-tunnel model study are presented in this report.

## II. SIMULATION OF ATMOSPHERIC MOTION

### 2.1 General

For complete flow similarity in two systems of different length scales, geometric, dynamic and thermal similarity must be achieved. Geometric similarity is a requirement easily realized by using a scale model of prototype geometry. On the other hand, strict dynamic and thermal similarity as required by the identity of equations of motion and energy for the two systems can be achieved in rare cases. Therefore, it is necessary to relax the requirement of complete dynamic and thermal similarity and attempt to achieve the best approximations.

### 2.2 Dynamic Similarity

For complete dynamic similarity the dimensionless parameter Rossby number ( $Ro = \frac{U^2/L}{\Omega U}$ ), Reynolds number ( $Re = \frac{UL}{\nu}$ ) and Froude number ( $Fr = \frac{V}{gL} \cdot \frac{\Delta T}{T}$ ) would have to be the same for both model and prototype. Rossby number may be interpreted as the ratio of inertial forces for unit mass and a reference inertial force due to rotation of the earth system. Model Rossby number cannot be made equal to that of prototype. However, over short distances considered (up to 10,000 ft), the Coriolis acceleration has little influence on the flow (4). Accordingly, the standard practice is to relax the requirement of equal Rossby number (1,4). Reynolds number may be interpreted as the ratio of reference inertial force and viscous shear force due to unit mass. Reynolds number for the model exceeded  $10^4$  which is the lower critical value established by Golden (7) for the flow patterns to become independent of Reynolds number. The minimum Reynolds number encountered in the study was  $10^5$ , based on building model width 2.92 ft, and minimum wind velocity 6 ft/sec, strong atmospheric winds were found to have maximum influence on the flow field

in the region of the building. For such conditions, thermal stratification is of little significance. Therefore, the model was tested in isothermal boundary layer or for zero Richardson number. Correlation of tests of flow around the Rock of Gibraltar (6), flow over Pt. Arguello (3) and flow over San Nicolas Island, California (9) may be cited as examples of large Reynolds number flows which have been modeled successfully in wind tunnels.

### 2.3 Thermal Similarity

Thermal similarity requires equality of model and prototype Prandtl number and Eckert number. However, because only adiabatic flow was modeled these quantities did not apply.

### 2.4 Kinematic Similarity

Kinematic similarity requires similarity of mean velocity and turbulence intensity characteristics of the approach wind-tunnel flow with that of the atmospheric boundary layer (prototype). These requirements are automatically satisfied through the use of long wind-tunnel test sections and approach roughness (1). The simulated approach mean wind conditions are described by the velocity distribution power law

$$\frac{U(z)}{U(z_0)} = \left(\frac{z}{z_0}\right)^n .$$

The need for scaling of the atmospheric mean wind profile was demonstrated by Jensen (7). Substitution of a uniform velocity profile for a logarithmic profile resulted in a threefold variation in dimensionless pressure coefficients downstream of a model building. Such a variance in pressure field indicates a strong effect of the upstream wind profile on the kinematic behavior of the fluid near the building complex.

Complex topographical (mountain) features produce nonuniform fields of flow which perturb the regular upwind atmospheric flow profile. Around each hill a boundary layer exists where the velocity is zero at the surface but increases rapidly to a relatively constant value a short distance from the surface. Outside the boundary layer and downwind there exists a region of low velocity and pressure called the wake. In this region circulations are such that flow actually reverses direction with respect to upwind side. When the wakes of different hills interact, a complex velocity field is generated which strongly influences wind effects on structures in such regions. The Johns-Manville World Headquarters building presents such an example.

One of the difficulties of model testing in wind-tunnels is a possible effect of blockage. A ratio of projected model area to area of the wind-tunnel test section more than 0.10 produces an appreciable effect on the field. However, this problem is solved by using an adjustable test-section ceiling. This is achieved by adjusting the pressure gradient along the roof to zero.

The requirements of all the simulation criteria described above were satisfied in the model tests conducted in the Environmental Wind-Tunnel of Fluid Dynamics and Diffusion Laboratory at Colorado State University.

### III. WIND TUNNEL AND MEASUREMENT TECHNIQUES

#### 3.1 Wind Tunnel: General Description

The wind engineering study was conducted in the environmental wind tunnel (Fig. 1-2) located in the Fluid Dynamics and Diffusion Laboratory of Colorado State University. The wind tunnel is an open circuit facility driven by 180 HP, variable pitch, constant speed propeller. The test section is nominally 12 ft wide, 8 ft high and 52 ft long through a 4:1 contraction ratio. The roof is adjustable to maintain zero pressure gradient along the test section. Mean velocity in the test section can be varied continuously from 1 to 60 ft/sec.

#### 3.2 Model: Design and Construction

In order to obtain accurate assessment of local snow-drift locations, diffusion and advection of air pollutants, gust intensities and induced pressures the model was constructed to the largest scale that would not produce serious blockage in the wind tunnel. A 1:400 scale model was constructed. The building was made of Lucite plastic in order to permit drilling of pressure taps with desired precision. The topography within 2,000 ft radius surrounding the building was modeled using 0.3 in.-thick styrofoam sheets cut to fit the contour at 10 ft intervals. The building model and the surrounding topographical model (Fig. 3) were mounted on a 10 ft diameter turntable located at 24 ft from the entrance of the test section (Fig. 2). Topography within 8,000 ft radius from the center of the building was made from styrofoam blocks. The portion of the model that did not fit on the turntable was put at appropriate upwind and downwind locations. The turntable allowed orientation of the model with respect to the approaching wind. Figure 4 shows the building with respect to its natural setting.

### 3.3 Flow Visualization

Smoke produced by passing humid air over titanium tetrachloride located in a container outside the wind tunnel was used to define the general wind patterns around JMWH building. Smoke (titanium dioxide) was transported through Tygon tubes to selected locations on the model. Trajectories of smoke describing the wind pattern were recorded on 16 mm color motion pictures which form a supplementary part of this report. Descriptions of photographic equipment, films, exposures, etc., are detailed in Appendix A. Mean wind speed of 6 ft/sec was employed for flow-visualization studies. Effort was made to record not only the general wind distribution in the area but also the detailed flow patterns in and around locations of special interest such as parking area and the heliport. Special features of induced flow were documented by still photographs.

### 3.4 Snow-Drift Locations

Styrofoam particles of uniform size (approximately 1 mm, Fig. 5) tested as drift material, were employed to simulate this part of the study. Care was taken to see the surface properties of the particles did not interfere with the drifting process. Styrofoam particles were distributed in a ridge across the test section (6 ft) upwind of the building model and were allowed to drift under the influence of steady speed (15 ft/sec).

Particles were replenished in stages until a stable drift pattern was obtained. During this process the movement of particles was observed carefully and their general pattern of mean movement was recorded. The stable snow-drift pattern was tested at wind speeds up to 25 ft/sec

and was observed to be unaffected. The drift patterns were documented by photographing the model.

### 3.5 Tracer-Gas Concentrations

Krypton-85 was employed as a tracer gas for the diffusion measurements. After the flow in the wind tunnel was established, a mixture of Kr-85 and air of predetermined concentration (0.217  $\mu\text{ci/cc}$ ) was released at a constant rate from the parking area. Care was taken to see that the tracer gas was uniformly distributed over the entire parking area. Details of source locations are shown in Figs. 6-9. Samples were drawn from ten selected locations (Appendix B1) and also from seven points of each of the two vertical rakes so that the desired information on local dispersion characteristics could be predicted. Flow rate of Kr-85 gas mixture was controlled by a pressure regulator at the supply cylinder outlet and monitored by a Fischer and Porter precision flow meter (Appendix A). Source strength was 0.217  $\mu\text{ci/cc}$  of Kr-85, a beta emitter (half life time = 10.3 years), released at the rate of 300 cc/min. The samples collected were analyzed by using an Ultrascaler to determine their concentration. The local concentrations were expressed in the dimensionless form (concentration coefficients)

$$K = \frac{C U_{\infty} H^2}{Q} .$$

The sampling and detection systems are shown in Fig. 10 and described in Ref. 5. Appendix B1 and Figs. 11-20 show the details of locations where local concentration measurements were made.

### 3.6 Local Gusts and Mean Velocities

Mean velocity and turbulence (gust) intensity measurements were made at 0.15 in. (5 ft prototype) above the surface at 35 selected

locations on the model (Appendix B2, Figs. 7-16). These measurements were intended to indicate the environment to which pedestrians will be subjected.

The measurements were made using a single hot-wire mounted with its axis vertical. The instrument used was a CSU-made, constant-temperature type, hot-wire anemometer. The anemometer maintains the hot-wire at a predetermined constant temperature by employing the principles of feedback circuitry and bridge balance. Thus, the voltage impressed across the hot-wire becomes a function of the heat-transfer rate from the wire which in turn is dependent on the local convective velocity. King's Law,  $E^2 = A + BU^P$ , was used to relate the hot-wire output voltage and local wind speed. The constants A and B were determined by calibration. A typical calibration relation is presented in Fig. 21. Local root-mean-square values of gust velocities were obtained by measuring the root-mean-square values of the voltage fluctuations from the hot-wire output and using the following relationship:

$$U_{\text{RMS}} = \frac{2E_M E_{\text{RMS}} U_M^{1-P}}{B P} .$$

The mean wind speed was made dimensionless by dividing by the free-stream wind speed--( $U_M/U_\infty$ ). Turbulence (gust) intensities were represented in dimensionless form by dividing the root-mean-square (RMS) value of velocity fluctuations by the local mean velocity--( $U_{\text{RMS}}/U_M$ ). An alternate form of dimensionless turbulence intensity was obtained by dividing by the free-stream velocity--( $U_{\text{RMS}}/U_\infty$ ).

### 3.7 Building Surface Pressures

Surface pressures on the building at 64 selected locations (Appendix B3, Figs. 12-20) were measured as the difference between

local and free-stream static pressures. MKS Baratron pressure meter was used to make the measurements. The static pressure at 2,000 ft above the center of the building was taken as reference pressure. This was carefully selected in order to avoid disturbances of the wake due to the mountainous terrain. Surface pressures, thus obtained were expressed in two different dimensionless forms. In one case, the dynamic head of the free stream was taken as a reference and in the other case the dynamic head at two building heights was taken as a reference; i.e.,

$$C_{p^{\infty}} = \left( \frac{P_L - P_{S^{\infty}}}{\rho U_{\infty}^2 / 2} \right) \quad \text{and} \quad C_{p2H} = \left( \frac{P_L - P_{S^{\infty}}}{\rho U_{2H}^2 / 2} \right) .$$

Local surface pressures were also expressed in terms of prototype values by assuming a design wind speed of 230 ft/sec at 2,000 ft elevation and a design gust factor of 2.5 (Appendix D3).

## IV. TEST PROGRAM AND RESULTS

4.1 Test Program

The test program consisted of two stages. In the first stage a qualitative study of general wind distributions in the Ken Caryl Ranch area was made by visualizing the trajectories of smoke released from selected locations. Overall flow patterns were recorded by photographing the smoke released upwind of the model building. The details of local flow characteristics were identified by releasing smoke at locations of special interest, such as the parking area and the proposed heliport. A permanent record of flow fields was made by documenting the flow pattern on 16 mm color motion-picture film (Appendix C). Still pictures (black-and-white) were also taken to record mean flow patterns.

In the second stage of the study, detailed quantitative measurements were made. A thorough investigation of snow-drifts, dispersion of automobile exhausts, surface winds and induced wind pressures was conducted for each of the eight wind directions at 45-degree intervals starting from a north wind. Snow-drift patterns were obtained at free-stream wind speeds of 15 ft/sec and were tested for their stability at 25 ft/sec. Local tracer-gas concentration measurements were made at free-stream wind speeds of 6 ft/sec. Surface winds and induced wind pressures were measured for free stream wind speed of 45 ft/sec. Snow-drift locations were obtained by allowing the styrofoam particles supplied upwind of the model to drift under steady wind conditions until stable patterns were obtained. Snow-drift locations were documented by photographing the model. Local dispersion characteristics were obtained by measuring mean concentrations of tracer gas along

vertical lines and at significant points (Appendix B1) while releasing the tracer gas in the parking area at a known constant rate. Local mean winds and gust intensities were measured at 35 selected locations (Appendix B2) by using a hot-wire anemometer. Aerodynamic pressures on the building model were measured at 64 significant locations (Appendix B3) as the difference between local and free-stream static pressures.

#### 4.2 Approach Velocity Conditions

In order to determine the simulated velocity conditions in the model study, mean velocity profiles were measured at 300 ft upwind of the building. They were plotted for each of the wind directions tested (Figs. 22-23). Mean velocity and turbulence (gust) intensity profiles were also measured at the heliport and the ground level parking area. They are presented in their dimensionless form in Figs. 24-25.

#### 4.3 Flow Visualization

This part of the study was primarily aimed at defining the general wind distribution over the JMWH building area for the eight wind directions. Trajectories of smoke released at selected locations were photographed on 16 mm color film at 24 frames per sec and a permanent record of flow patterns was generated to supplement this report.

No severe gust conditions were observed in the heliport area for any of the approach wind directions tested. However, persistent and severe gusts were observed in the valley areas of mountainous terrain for winds approaching from the S, SW, W and NW directions. Similar phenomenon was observed during the snow-drift study. Secondary flow in the parking area, established by flow visualization study

(Figs. 26-27, Appendix C), for approach wind directions, N, NE and E indicates the nature and the extent to which the automobile exhausts will be trapped. Corresponding concentration measurements have also indicated higher values in the region. This study also points out the high degree of scavenging action on the northeast side of the building. This is also confirmed by the low concentration values observed during the local dispersion measurements. Thus, the northeast side of the building can be considered as a region with least impact due to the automobile exhaust released in the ground-level parking area. It must be noted that the terrace region has pronounced influence of automobile exhaust for conditions of wind approaching from the N, NE and E directions.

#### 4.4 Snow-Drift Locations

Principle aim of this part of study was to determine the possible problems due to snow-drift locations. An attempt was made to simulate the drift process by using specially selected styrofoam particles. The nature of simulation assumes that the snow is dry and snowfall occurs for indefinite periods of time. Only drift aspects are simulated. Thus, the results can be used only for qualitative interpretations.

The results of snow-drift simulation study that is the snow-drift locations and mean paths of particle movements are presented in Figs. 28-43. It is observed that the site for the heliport is free from any severe problems due to snow-drift in the cases of eight approach wind directions tested. However, marked snow-drift problems were observed in the ground-level parking area and also in the region between the two parts of the building for cases of wind approaching

from the southeast (Figs. 34-35), south (Figs. 36-37), west (Figs. 40-41) and northwest (Figs. 42-43) directions. The area on the northeast side of the building did not exhibit any serious snow-drift problem. For the purposes of general understanding of drift process, an attempt was made to record the general mean snow-drift paths for each of the eight wind directions.

#### 4.5 Local Automobile-Emission Concentrations

Local concentration measurements were primarily intended to determine the manner in which automobile exhaust released in the ground-level parking area dispersed near the building. Concentration measurements were made at selected locations corresponding to the release of tracer-gas at a known constant rate in the ground-level parking area. Source locations were oriented so that nearly a uniform distribution of tracer gas was achieved (Figs. 6-9). The results were expressed in dimensionless form (concentration coefficients) taking the source strength as a reference (Table 1, Figs. 44-47). Sample calculations to aid prototype predictions based on the model-study data are given in Appendix D1.

The following observations were made from a comparative study of the results presented. The vertical distributions of concentration coefficients (Figs. 44-45) confirm the existence of a region of secondary flow trapping the pollutant released in the ground-level parking area, as observed in the flow-visualization study. A high level of concentration was noted on the upper level (6,322) at sampling points C-1, C-2 and C-9 for winds approaching from the E, NE and N as a consequence of the secondary flow which traps the pollutants (Fig. 47). The measurements made on the northeast side of the building at C-10 conform with the flow-visualization results and reveal that

little of the automobile exhaust from the ground-level parking area reaches the terrace area.

#### 4.6 Local Gusts

Measurements of local gust intensities were made in order to predict the extent to which persons moving around the building will be affected by the local fluctuations in the wind. Root-mean-square value of local velocity fluctuations were measured at 0.15 in. (5 ft prototype) from the surface by using a single hot-wire anemometer at 35 locations (Appendix B2, Figs. 11-18). The results obtained are presented in Tables 2-5, in their normalized form. Distribution of surface winds in the heliport area is shown as radial plots in Fig. 48. Prediction of prototype conditions using these data is explained in Appendix D2.

#### 4.7 Building Surface Pressures

Surface pressure measurements were made to determine induced wind pressures on the building surface. Wind pressures at 64 selected locations (Appendix B3, Figs. 12-20) were measured with respect to free-stream static pressure (at 2,000 ft above the center of the building). These were expressed in dimensionless forms by dividing by the free-stream dynamic head. Auxillary dimensionless forms were obtained by using the dynamic head at two building heights as a reference. The results are summarized in Tables 6-7. A sample calculation indicating the prediction of prototype gust pressures is given in Appendix D3.

A detailed survey of pressure measurements indicated that the building was not subjected to any unusual conditions of severe wind pressures for any of the eight approach wind directions examined.

## CONCLUSIONS

The investigation was conducted on a 1:400 scale model of Johns-Manville World Headquarters and its surrounding topography using a large size wind-tunnel in order to predict the general wind distribution in the area of the Ken Caryl Ranch. Assessments were made of immediate environmental impact in terms of local snow-drift, dispersion of automobile exhaust released in the ground-level parking area, surface mean wind and gust intensities and aerodynamic pressures on the building. Following conclusions could be drawn from the data presented in this report and the supplementary motion pictures.

1. The site for the heliport did not show any severe problems due to snow-drifting and local surface winds for any of the eight approach wind directions studied.
2. A distinct snow-drift problem was found to exist in the ground-level parking area and also in between two parts of the building for cases of wind approaching from the S, SE, W, and NW directions.
3. The region on the northeast side of the building did not show any severe problems due to local snow-drifting, concentration of automobile exhaust and surface winds.
4. High concentrations of automobile exhaust released in the ground-level parking area were observed in the terrace region for cases of wind approaching from the N, NE and E directions.
5. Severe and persistent gust conditions were found to prevail in the valley regions of the mountainous terrain near the building for the cases of wind approaching from the S, SW, W and NW directions.

6. Pressure measurements on the building indicated that no unusually severe wind-gust pressures will prevail on the building.

## REFERENCES

1. Cermak, J.E., LABORATORY SIMULATION OF THE ATMOSPHERIC BOUNDARY LAYER, AIAA J1., Vol. 9, pp. 1746-1754, September 1971.
2. Cermak, J.E., F.H. Chaudhry, A.C. Hansen and J.A. Garrison, WIND AND AIR POLLUTION CONTROL STUDY OF YERBA BUENA CENTER, Colorado State University Report No. CER71-72JEC-FHC-ACH-JAG15, June 1972.
3. Cermak, J.E. and J.A. Peterka, SIMULATION OF WIND FIELDS OVER POINT ARGUELLO, CALIFORNIA BY WIND TUNNEL FLOW OVER TOPOGRAPHICAL MODEL, Field Report U.S. Navy Contract N126 (61756) 3U361A (PMR), Colorado State University Report No. CER65-JEC-JAP64, December 1965.
4. Cermak, J.E., V.A. Sandborn, E.J. Plate, G.J. Binder, H. Chuang, R.N. Merony and S. Ito, SIMULATION OF ATMOSPHERIC MOTION BY WIND TUNNEL FLOWS, Colorado State University Technical Report No. CER66-JEC-VAS-EJP-GJB-HE-RNM-SI17, May 1966.
5. Chaudhry, F.H. and R.N. Meroney, TURBULENT DIFFUSION IN A STABLY STRATIFIED SHEAR LAYER, U.S. Army Electronic Command Tech. Report C-042305, Colorado State University Report No. CER69-70FHC-JNM12, 1970.
6. Field, J.H. and R. Warden, SURVEY OF AIR CURRENTS IN THE BAY OF GIBRALTER, 192901930 Airministry Geophys., Mem. No. 59, London, 1933.
7. Halitsky, J., J. Golden, P. Halpern and P. Wu, WIND TUNNEL TEST ON GAS DIFFUSION FROM A LEAK IN SHELL OF A NUCLEAR POWER REACTOR AND NEARBY STACKS, Geophys. Sci. Lab. Report No. 63-2, New York University, April 1963.
8. Jensen, M. and N. Frank, MODEL SCALE TEST IN TURBULENT WIND, Part I, Danish Tech. Press, Copenhagen, 1963.
9. Meroney, R.N. and J.E. Cermak, WIND TUNNEL MODELING OF FLOW AND DIFFUSION OVER SAN NICOLAS ISLAND, CALIFORNIA, U.S. Navy Contract N123 (61756) 50192A (PMR), Colorado State University Report No. CER66-67-RNM-JEC44, September 1967.

TABLE I

LOCAL CONCENTRATION COEFFICIENTS

$$K = \frac{C_{max}}{C} \quad U_w = 185 \text{ cm/sec}, \quad Q = 1.085 \text{ m}^2/\text{sec}, \quad H = 8 \text{ cm}$$

Point Number	Approach Wind Directions							
	N	NE	E	SE	S	SW	W	NW
C-1	411.4	426.2	16.6	6.3	18.3	82	24.0	26.2
C-2	112.7	222.7	16.6	21.6	44.7	282	16.6	9.2
C-3	1.2	11.2	12.6	6.9	22.8	248	42.8	44.7
C-4	1.2	2.9	6.3	2.4	17.8	232	22.8	12.2
C-5	9.2	2.8	2.2	12.6	22.8	188	18.2	8.6
C-6	9.2	1.7	0	10.2	10.9	122	12.0	2.2
C-7	16.04	6.9	0	10.9	12.6	182	1.7	29.2
C-8	226.8	111.2	12.2	10.8	11.2	222	1092.2	197.1
C-9	92.4	266.0	246.0	10.9	8.6	170	22.2	12.8
C-10	14.2	22.6	10.9	8.0	7.2	102	2.8	6.9

Vertical profile in the ground-level parking area

C-11	82.7	229.7	8.6	2220	266.4	476	1100	124.9
C-12	142.1	222.2	8.6	1080	171.9	221	422.0	92.8
C-13	122.2	119.1	6.9	279	122.2	120	82.2	27.2
C-14	4.2	190.2	2.7	20.6	2.7	12.2	26.2	9.2
C-15	0.0	21.6	7.2	0	7.2	0	20.0	6.9
C-16	2.2	16.0	11.2	2.7	2.7	0	2.8	0
C-17	2.2	2.6	0.6	2.9	0	0	2.2	9.7

Vertical profile on the NE side of the building

C-18	0.8	2.2	4.0	24.7	162.2	26.7	7.2	12.2
C-19	2.1	9.2	9.8	22.7	120.9	60.8	8.6	6.9
C-20	10.2	0.6	1.2	10.2	71.0	22.6	6.9	9.2
C-21	12.0	2.2	6.2	0.0	110.7	22.4	1.7	9.8
C-22	10.9	0	0.0	2.2	22.9	22.2	9.2	9.8
C-23	8.6	2.2	6.2	4.6	14.9	2.2	2.2	8.6
C-24	6.2	1.7	1.7	2.2	20.6	6.9	0	10.9

TABLE 1

## LOCAL CONCENTRATION COEFFICIENTS

$$K = \frac{CU_{\infty}H^2}{Q}, \quad U_{\infty} = 185 \text{ cm/sec}, \quad Q = 1.085 \text{ } \mu\text{ci/sec}, \quad H = 8 \text{ cm}$$

Concentration Coefficients $K \times 10^3$	Approach Wind Directions							
	N	NE	E	SE	S	SW	W	NW
Point Number								
C-1	411.4	426.3	16.6	6.3	18.3	82	24.0	26.3
C-2	213.7	552.7	651.4	51.6	44.7	282	16.6	9.2
C-3	1.2	11.5	12.6	6.9	25.8	248	45.8	44.7
C-4	1.2	2.9	6.3	3.4	17.8	332	25.8	15.5
C-5	9.2	5.8	5.2	12.6	25.8	188	18.3	8.6
C-6	9.2	1.7	0	10.3	10.9	122	12.0	2.3
C-7	16.04	6.9	0	10.9	12.6	182	1.7	39.5
C-8	226.8	111.2	13.2	10.8	11.5	525	1092.5	197.1
C-9	93.4	566.0	346.0	10.9	8.6	170	33.3	13.8
C-10	14.3	55.6	10.9	8.0	7.5	105	5.8	6.9

## Vertical profile in the ground-level parking area

C-11	83.7	229.7	8.6	2350	266.4	476	1100	124.9
C-12	142.1	253.2	8.6	1080	171.9	231	452.0	92.8
C-13	152.5	119.1	6.9	279	125.5	120	82.5	37.8
C-14	4.5	190.2	5.7	20.6	5.7	15.5	56.2	9.2
C-15	0.0	51.6	7.5	0	7.5	0	20.0	6.9
C-16	3.5	16.0	11.5	5.7	5.7	0	5.8	0
C-17	2.3	8.6	0.6	2.9	0	0	2.3	9.7

## Vertical profile on the NE side of the building

C-18	0.6	5.2	4.0	24.7	163.2	56.7	7.5	13.2
C-19	5.1	9.2	9.8	32.7	120.9	60.8	8.6	6.9
C-20	10.3	0.6	1.2	10.3	71.0	75.6	6.9	9.2
C-21	12.0	3.5	6.3	0.0	110.7	53.4	1.7	9.8
C-22	10.9	0	0.0	5.2	22.9	33.3	9.2	9.8
C-23	8.6	5.2	6.3	4.6	14.9	3.5	5.2	8.6
C-24	6.3	1.7	1.7	2.3	20.6	6.9	0	10.9

TABLE 2

LOCAL MEAN VELOCITIES AND GUST INTENSITIES  
AT 0.15 IN. (5 FT PROTOTYPE) FROM SURFACE

Point No	North Wind $U_{\infty} = 42.6$ ft/sec			Northeast Wind $U_{\infty} = 43.0$ ft/sec		
	$\frac{U_M}{U_{\infty}}$	$\frac{U_{RMS}}{U_M}$	$\frac{U_{RMS}}{U_{\infty}}$	$\frac{U_M}{U_{\infty}}$	$\frac{U_{RMS}}{U_M}$	$\frac{U_{RMS}}{U_{\infty}}$
W1	0.464	0.189	0.088	0.248	0.382	0.095
W2	0.305	0.347	0.106	0.092	0.508	0.047
W3	0.222	0.450	0.100	0.140	0.523	0.073
W4	0.270	0.408	0.110	0.195	0.524	0.103
W5	0.304	0.398	0.121	0.222	0.460	0.102
W6	0.325	0.308	0.100	0.122	0.447	0.054
W7	0.352	0.312	0.110	0.119	0.444	0.053
W8	0.239	0.336	0.081	0.077	0.520	0.040
W9	0.138	0.532	0.074	0.221	0.456	0.101
W10	0.120	0.549	0.066	0.127	0.548	0.070
W11	0.416	0.283	0.118	0.150	0.541	0.081
W12	0.131	0.486	0.064	0.089	0.571	0.051
W13	0.301	0.406	0.122	0.150	0.541	0.081
W14	0.108	0.609	0.066	0.157	0.539	0.085
W15	0.272	0.421	0.115	0.225	0.407	0.092
W16	0.096	0.551	0.053	0.082	0.583	0.048
W17	0.249	0.443	0.110	0.098	0.583	0.058
W18	0.355	0.341	0.121	0.142	0.549	0.078
W19	0.412	0.316	0.130	0.165	0.558	0.092
W20	0.343	0.482	0.165	0.178	0.497	0.088
W21	0.462	0.363	0.168	0.228	0.477	0.109
W22	0.423	0.370	0.156	0.278	0.457	0.127
W23	0.392	0.358	0.140	0.248	0.501	0.125
W24	0.347	0.388	0.135	0.235	0.509	0.120
W25	0.378	0.381	0.144	0.164	0.520	0.085
W26	0.305	0.428	0.131	0.107	0.569	0.061
W27	0.305	0.442	0.135	0.125	0.562	0.070
W28	0.171	0.555	0.095	0.173	0.495	0.086
W29	0.241	0.439	0.106	0.156	0.566	0.089
W30	0.239	0.373	0.089	0.133	0.447	0.060
W31	0.367	0.271	0.100	0.179	0.518	0.093
W32	0.506	0.230	0.116	0.182	0.483	0.088
W33	0.648	0.178	0.115	0.344	0.266	0.092
W34	0.498	0.294	0.146	0.284	0.433	0.123
W35	0.498	0.186	0.093	0.313	0.515	0.099

TABLE 3

LOCAL MEAN VELOCITIES AND GUST INTENSITIES  
AT 0.15 IN. (5 FT PROTOTYPE) FROM SURFACE

Point No	East Wind $U_{\infty} = 43.4$ ft/sec			Southeast Wind $U_{\infty} = 43.3$ ft/sec		
	$\frac{U_M}{U_{\infty}}$	$\frac{U_{RMS}}{U_M}$	$\frac{U_{RMS}}{U_{\infty}}$	$\frac{U_M}{U_{\infty}}$	$\frac{U_{RMS}}{U_M}$	$\frac{U_{RMS}}{U_{\infty}}$
W1	0.182	0.396	0.072	0.342	0.331	0.113
W2	0.147	0.429	0.063	0.092	0.505	0.046
W3	0.229	0.387	0.089	0.379	0.308	0.117
W4	0.243	0.402	0.098	0.379	0.275	0.104
W5	0.152	0.468	0.072	0.220	0.326	0.072
W6	0.209	0.307	0.064	0.068	0.504	0.034
W7	0.192	0.366	0.070	0.065	0.570	0.037
W8	0.207	0.353	0.073	0.072	0.565	0.040
W9	0.207	0.450	0.093	0.343	0.293	0.101
W10	0.120	0.538	0.065	0.158	0.515	0.081
W11	0.224	0.505	0.113	0.384	0.375	0.144
W12	0.173	0.569	0.098	0.353	0.403	0.143
W13	0.221	0.447	0.099	0.282	0.354	0.100
W14	0.086	0.557	0.048	0.175	0.550	0.096
W15	0.120	0.560	0.067	0.379	0.282	0.107
W16	0.072	0.514	0.037	0.242	0.511	0.123
W17	0.121	0.553	0.067	0.328	0.308	0.101
W18	0.151	0.520	0.078	0.283	0.327	0.093
W19	0.327	0.355	0.116	0.323	0.332	0.107
W20	0.429	0.330	0.142	0.562	0.303	0.170
W21	0.312	0.367	0.114	0.684	0.156	0.107
W22	0.169	0.515	0.077	0.656	0.172	0.113
W23	0.184	0.502	0.093	0.691	0.246	0.121
W24	0.175	0.508	0.089	0.510	0.230	0.117
W25	0.180	0.471	0.085	0.691	0.220	0.108
W26	0.166	0.491	0.082	0.282	0.372	0.104
W27	0.131	0.526	0.069	0.452	0.239	0.108
W28	0.142	0.494	0.070	0.247	0.374	0.093
W29	0.304	0.360	0.110	0.190	0.468	0.089
W30	0.194	0.463	0.090	0.091	0.562	0.051
W31	0.226	0.396	0.089	0.283	0.331	0.096
W32	0.152	0.622	0.096	0.320	0.406	0.130
W33	0.228	0.293	0.067	0.366	0.252	0.092
W34	0.357	0.256	0.091	0.221	0.366	0.081
W35	0.207	0.326	0.067	0.393	0.260	0.102

TABLE 4

LOCAL MEAN VELOCITIES AND GUST INTENSITIES  
AT 0.15 IN. (5 FT PROTOTYPE) FROM SURFACE

Point No	South Wind $U_{\infty} = 41.5$ ft/sec			Southwest Wind $U_{\infty} = 42.8$ ft/sec		
	$\frac{U_M}{U_{\infty}}$	$\frac{U_{RMS}}{U_M}$	$\frac{U_{RMS}}{U_{\infty}}$	$\frac{U_M}{U_{\infty}}$	$\frac{U_{RMS}}{U_M}$	$\frac{U_{RMS}}{U_{\infty}}$
W1	0.334	0.252	0.084	0.041	0.748	0.031
W2	0.136	0.598	0.081	0.172	0.598	0.103
W3	0.180	0.413	0.075	0.096	0.660	0.063
W4	0.121	0.495	0.060	0.130	0.577	0.075
W5	0.063	0.522	0.033	0.097	0.570	0.055
W6	0.189	0.516	0.097	0.161	0.538	0.087
W7	0.174	0.461	0.080	0.177	0.591	0.105
W8	0.225	0.426	0.096	0.141	0.620	0.087
W9	0.100	0.451	0.045	0.032	0.964	0.031
W10	0.056	0.544	0.031	0.062	0.596	0.037
W11	0.207	0.462	0.095	0.209	0.573	0.120
W12	0.116	0.610	0.070	0.145	0.630	0.091
W13	0.250	0.388	0.097	0.212	0.536	0.113
W14	0.078	0.667	0.051	0.185	0.514	0.095
W15	0.290	0.380	0.110	0.202	0.561	0.109
W16	0.086	0.574	0.069	0.118	0.661	0.078
W17	0.176	0.478	0.083	0.183	0.512	0.096
W18	0.228	0.412	0.092	0.216	0.532	0.115
W19	0.209	0.613	0.086	0.262	0.569	0.137
W20	0.175	0.506	0.089	0.218	0.530	0.115
W21	0.165	0.538	0.089	0.163	0.617	0.100
W22	0.175	0.466	0.082	0.230	0.582	0.134
W23	0.229	0.613	0.095	0.243	0.560	0.131
W24	0.158	0.515	0.081	0.226	0.532	0.120
W25	0.200	0.443	0.089	0.198	0.625	0.124
W26	0.163	0.517	0.086	0.207	0.511	0.106
W27	0.198	0.426	0.085	0.156	0.568	0.088
W28	0.216	0.463	0.100	0.152	0.567	0.086
W29	0.220	0.369	0.077	0.170	0.563	0.092
W30	0.291	0.293	0.085	0.165	0.749	0.091
W31	0.260	0.303	0.079	0.163	0.600	0.086
W32	0.271	0.277	0.075	0.118	0.643	0.076
W33	0.331	0.361	0.123	0.245	0.396	0.097
W34	0.306	0.301	0.092	0.167	0.503	0.084
W35	0.354	0.250	0.089	0.150	0.571	0.086

TABLE 5

LOCAL MEAN VELOCITIES AND GUST INTENSITIES  
AT 0.15 IN. (5 FT PROTOTYPE) FROM SURFACE

Point No	West Wind $U_{\infty} = 44$ ft/sec			Northwest Wind $U_{\infty} = 42.1$ ft/sec		
	$\frac{U_M}{U_{\infty}}$	$\frac{U_{RMS}}{U_M}$	$\frac{U_{RMS}}{U_{\infty}}$	$\frac{U_M}{U_{\infty}}$	$\frac{U_{RMS}}{U_M}$	$\frac{U_{RMS}}{U_{\infty}}$
W1	0.07	0.232	0.017	0.062	0.431	0.027
W2	0.287	0.084	0.024	0.183	0.400	0.073
W3	0.156	0.085	0.024	0.119	0.543	0.065
W4	0.373	0.057	0.022	0.138	0.523	0.072
W5	0.422	0.046	0.019	0.129	0.499	0.064
W6	0.270	0.114	0.031	0.157	0.623	0.067
W7	0.378	0.065	0.025	0.170	0.681	0.082
W8	0.357	0.070	0.025	0.070	0.617	0.044
W9	0.097	0.042	0.041	0.057	0.642	0.037
W10	0.078	0.051	0.060	0.134	0.418	0.056
W11	0.671	0.055	0.026	0.264	0.328	0.087
W12	0.345	0.112	0.039	0.110	0.582	0.064
W13	0.500	0.046	0.023	0.200	0.456	0.092
W14	0.333	0.108	0.036	0.081	0.633	0.051
W15	0.326	0.093	0.030	0.161	0.569	0.077
W16	0.263	0.113	0.027	0.088	0.653	0.058
W17	0.259	0.130	0.034	0.123	0.598	0.073
W18	0.438	0.057	0.025	0.157	0.696	0.078
W19	0.465	0.057	0.026	0.186	0.470	0.087
W20	0.461	0.034	0.016	0.210	0.369	0.101
W21	0.330	0.088	0.029	0.160	0.568	0.088
W22	0.562	0.033	0.018	0.173	0.443	0.077
W23	0.562	0.043	0.026	0.156	0.571	0.089
W24	0.513	0.044	0.022	0.156	0.553	0.086
W25	0.257	0.104	0.027	0.080	0.627	0.050
W26	0.075	0.121	0.009	0.167	0.490	0.082
W27	0.286	0.115	0.033	0.193	0.442	0.085
W28	0.295	0.078	0.023	0.175	0.461	0.081
W29	0.312	0.076	0.023	0.218	0.392	0.085
W30	0.212	0.118	0.025	0.126	0.585	0.072
W31	0.369	0.061	0.023	0.321	0.257	0.083
W32	0.329	0.067	0.022	0.334	0.247	0.083
W33	0.278	0.063	0.018	0.221	0.316	0.070
W34	0.330	0.067	0.016	0.357	0.261	0.093
W35	0.239	0.112	0.027	0.116	0.514	0.060

TABLE 6

## SURFACE PRESSURE COEFFICIENTS

$$C_{P_{\infty}} = (P_L - P_{S_{\infty}}) / (PU_{\infty}^2 / 2) \quad C_{P_{2h}} = (P_L - P_{S_{2h}}) / (PU_{2h}^2 / 2) \quad P = 117 \text{ C}_{P_{\infty}} \text{ lb/ft}^2$$

Pressure Tap No.	North Winds			Northeast Winds			East Winds			Southeast Winds		
	$U_{\infty} = 41.6 \text{ FPS}, U_{2h}/U_{\infty} = 0.856$			$U_{\infty} = 41.9 \text{ FPS}, U_{2h}/U_{\infty} = 0.67$			$U_{\infty} = 43.5 \text{ FPS}, U_{2h}/U_{\infty} = 0.83$			$U_{\infty} = 43.4 \text{ FPS}, U_{2h}/U_{\infty} = 0.811$		
	$C_{P_{\infty}}$	$C_{P_{2h}}$	$\frac{P}{\text{lb/ft}^2}$	$C_{P_{\infty}}$	$C_{P_{2h}}$	$\frac{P}{\text{lb/ft}^2}$	$C_{P_{\infty}}$	$C_{P_{2h}}$	$\frac{P}{\text{lb/ft}^2}$	$C_{P_{\infty}}$	$C_{P_{2h}}$	$\frac{P}{\text{lb/ft}^2}$
P1	-0.133	-0.18	-15.57	0.395	0.088	4.63	0.168	0.243	19.66	+0.125	+0.191	14.63
P2	+0.025	+0.034	+2.93	0.122	0.271	14.25	0.202	0.282	23.57	-0.199	-0.303	-23.26
P3	-0.183	-0.25	-21.41	0.020	0.044	2.31	0.162	0.234	18.83	+0.141	+0.215	16.47
P4	-0.267	-0.364	-31.23	0.089	0.198	10.4	0.168	0.243	19.66	-0.184	-0.280	-21.48
P5	-0.20	-0.273	-23.4	0.026	0.059	3.09	0.188	0.212	21.98	+0.080	+0.1212	9.31
P6	-0.20	-0.273	-23.4	-0.0082	-0.018	-0.97	0.192	0.278	22.46	+0.098	+0.149	11.46
P7	0.10	0.137	11.7	0.128	0.286	15.01	0.186	0.270	21.79	-0.089	-0.135	-10.38
P8	0.033	0.045	3.87	0.125	0.279	14.63	0.157	0.228	18.41	-0.067	-0.103	7.87
P9	0.082	0.125	6.47	0.099	0.22	11.54	0.153	0.221	17.87	-0.040	-0.061	-4.65
P10	0.032	0.034	2.93	0.109	0.242	12.71	0.168	0.263	19.66	-0.034	-0.051	-3.93
P11	0.042	0.057	4.92	0.122	0.271	14.25	0.128	0.186	15.01	-0.037	-0.0559	-4.3
P12	0.017	0.023	1.99	-0.016	-0.037	-1.93	0.00	0.00	0.00	-0.025	-0.0373	-2.86
P13	0.02	0.027	2.34	-0.013	-0.029	-1.54	0.034	0.049	3.93	-0.037	-0.0559	-4.3
P14	0.013	0.018	1.53	-0.008	-0.018	-0.97	0.070	0.102	8.22	+0.006	+0.0093	0.72
P15	-0.008	-0.0113	-0.97	-0.008	-0.018	-0.97	0.086	0.124	10.00	+0.034	+0.0513	3.93
P16	0.008	0.0113	0.97	0.0162	0.032	1.94	0.073	0.106	8.58	0.00	0.00	0.00
P17	0.025	0.034	2.93	0.0242	0.055	2.91	0.034	0.049	3.93	-0.018	-0.028	-2.15
P18	0.00	0.00	0.00	0.0362	0.058	4.23	0.128	0.186	15.01	+0.037	+0.056	4.3
P19	0.013	0.018	1.53	0.030	0.066	3.47	0.095	0.137	11.08	+0.0184	+0.028	2.15
P20	0.00	0.00	0.00	-0.008	-0.018	-0.97	0.131	0.190	15.36	+0.0734	+0.42	8.58
P21	0.008	0.0113	0.97	0.058	0.128	6.74	0.211	0.305	24.65	+0.049	+0.075	5.72
P22	0.067	0.091	7.83	0.132	0.293	15.39	0.174	0.252	20.37	0.00	0.00	0.00
P23	0.053	0.072	6.21	0.069	0.154	8.08	0.153	0.221	17.87	+0.0184	+0.028	2.15
P24	-0.042	-0.057	-4.92	-0.0164	-0.037	-1.92	0.079	0.115	9.29	+0.0153	+0.023	1.79
P25	-0.06	-0.082	-7.02	-0.060	-0.088	-4.61	0.046	0.066	5.36	+0.092	+0.0140	1.07
P26	0.063	0.086	7.37	0.030	0.066	3.47	0.140	0.203	16.43	+0.0214	+0.033	2.51
P27	0.033	0.045	3.87	0.023	0.051	2.69	0.131	0.190	15.36	+0.0275	+0.042	3.22
P28	0.03	0.041	3.52	0.016	0.037	1.92	0.168	0.243	19.66	+0.034	+0.0513	3.93
P29	0.03	0.041	3.52	0.026	0.059	3.09	0.128	0.186	15.01	+0.031	+0.0467	3.57
P30	-0.113	-0.154	-13.23	-0.046	-0.103	-5.39	0.079	0.115	9.29	+0.037	+0.056	4.28
P31	-0.10	-0.136	-11.70	-0.043	-0.095	-5.01	0.043	0.062	5.01	-0.0153	-0.023	1.79
P32	-0.093	-0.127	-10.89	-0.049	-0.110	-5.77	0.052	0.075	6.07	-0.0077	-0.012	-0.88
P33	-0.20	-0.273	-23.40	-0.145	-0.323	-16.93	-0.095	-0.137	-11.08	+0.251	+0.382	29.29
P34	-0.167	-0.228	-19.53	-0.158	-0.353	-18.48	-0.083	-0.119	-9.64	+0.242	+0.368	28.25
P35	-0.00	-0.00	-0.00	0.151	0.337	17.70	0.269	0.389	31.44	-0.1835	-0.280	-21.49
P36	-0.103	-0.141	-12.08	-0.053	-0.117	-6.15	0.00	0.00	0.00	-0.0077	-0.012	-0.88
P37	-0.097	-0.132	-11.35	-0.04	-0.088	-4.61	0.058	0.084	0.75	+0.023	+0.035	+2.69
P38	0.058	0.079	6.79	+0.089	0.198	10.4	0.186	0.270	21.79	-0.018	-0.028	-2.15
P39	0.063	0.086	7.37	-0.013	-0.029	-1.54	0.119	0.172	13.96	+0.0077	+0.012	0.88
P40	0.047	0.064	5.49	0.016	0.037	0.92	0.079	0.115	9.29	+0.0122	+0.0186	1.44
P41	0.025	0.034	2.93	-0.032	-0.073	-3.84	0.034	0.049	3.93	-0.018	-0.028	-2.15
P42	0.233	0.318	-37.23	0.063	0.095	5.01	-0.040	-0.058	-4.64	-0.0214	-0.033	-2.51
P43	0.063	0.086	7.37	0.217	0.484	25.39	0.049	0.071	5.72	-0.076	-0.117	-8.94
P44	-0.123	-0.168	-14.39	-0.059	-0.132	-6.93	-0.153	-0.222	-1.79	-0.086	-0.131	-10.02
P45	-0.167	-0.228	-19.53	-0.086	-0.192	-10.00	-0.040	-0.040	-3.22	-0.064	-0.098	-7.51
P46	-0.103	-0.140	-12.05	-0.043	-0.095	-5.01	0.034	0.486	3.93	-0.0214	-0.033	-2.51
P47	-0.123	-0.168	-14.39	-0.049	-0.110	-5.77	0.024	0.035	2.86	+0.0077	+0.012	0.88
P48	-0.103	-0.140	-12.05	-0.049	-0.110	-5.77	0.021	0.031	2.50	+0.012	+0.0186	1.44
P49	-0.160	-0.218	-18.72	-0.026	-0.059	-3.09	0.086	0.124	10.00	+0.028	+0.042	3.22
P50	-0.08	-0.109	-9.36	-0.053	-0.117	-6.15	0.049	0.071	5.72	+0.0214	+0.033	2.51
P51	-0.11	-0.150	-12.88	-0.0263	-0.059	-3.09	0.076	0.110	8.93	+0.058	+0.089	6.79
P52	-0.143	-0.195	-16.73	-0.109	-0.242	-12.71	-0.153	-0.221	-17.87	+0.254	+0.387	28.69
P53	-0.217	-0.296	-25.39	-0.164	-0.366	-19.24	-0.144	-0.21	-16.80	-0.101	-0.154	-11.81
P54	0.08	0.109	9.36	+0.197	+0.440	+23.10	0.171	0.248	20.00	-0.095	-0.145	-11.19
P55	-0.183	-0.250	-21.41	-0.079	-0.176	-9.23	0.043	0.062	5.01	-0.089	-0.135	-10.38
P56	-0.043	-0.059	-5.03	-0.008	-0.018	-0.97	0.113	0.164	13.23	-0.00	-0.00	-0.00
P57	-0.167	-0.228	-19.53	-0.089	-0.198	-10.38	-0.049	-0.071	-5.72	-0.0153	+0.0233	1.79
P58	0.063	0.086	7.37	-0.076	-0.169	-8.84	0.043	0.062	4.99	-0.0306	-0.0467	-3.58
P59	-0.058	-0.079	-6.79	0.086	-0.191	-10.00	0.031	0.044	3.57	+0.0245	+0.0373	2.86
P60	-0.008	-0.0113	-0.97	-0.036	-0.081	-4.23	0.040	0.0574	4.65	-0.0183	-0.028	-2.15
P61	-0.150	-0.205	-17.56	-0.020	-0.044	-2.31	0.061	0.088	7.14	-0.0077	-0.012	-0.88
P62	-0.183	-0.250	-21.41	-0.072	-0.161	-8.46	-0.034	-0.0486	-3.93	-0.089	-0.135	-10.38
P63	-0.160	-0.218	-18.72	-0.0395	-0.088	-4.63	-0.098	-0.141	-11.44	-0.098	-0.149	-11.46
P64	-0.147	-0.200	-17.10	-0.151	-0.337	-17.70	-0.147	-0.212	-17.14	-0.413	-0.629	-48.31

TABLE 7

SURFACE PRESSURE COEFFICIENTS

$$C_{P_{\infty}} = (P_L - P_{S_{\infty}}) / (U_{\infty}^2 / 2) \quad C_{P_{2h}} = (P_L - P_{S_{2h}}) / (U_{2h}^2 / 2) \quad P = 117 \text{ C}_{psw} \text{ lb/ft}^2$$

Pressure Tap No.	South Winds			Southwest Winds			West Winds			Northwest Winds		
	$U_{\infty} = 41.5 \text{ FPS}, U_{2h}/U_{\infty} = 0.525$			$U_{\infty} = 44.2 \text{ FPS}, U_{2h}/U_{\infty} = 0.661$			$U_{\infty} = 43.3 \text{ FPS}, U_{2h}/U_{\infty} = 0.644$			$U_{\infty} = 42.0 \text{ FPS}, U_{2h}/U_{\infty} = 0.707$		
	$C_{P_{\infty}}$	$C_{P_{2h}}$	$P$ lb/ft <sup>2</sup>									
P1	-0.118	-0.428	-13.75	0.062	0.14	7.23	+0.0123	+0.030	1.44	-0.0246	-0.0492	-2.88
P2	-0.193	-0.704	-23.05	0.018	0.041	2.08	-0.0246	-0.059	-2.88	-0.0164	-0.0338	-1.91
P3	-0.092	-0.337	-10.80	0.041	0.095	4.82	-0.0154	-0.037	-1.80	-0.0246	-0.0492	-2.88
P4	-0.210	-0.765	-24.54	0.012	0.027	1.37	-0.0200	-0.048	-2.34	-0.030	-0.0600	-3.45
P5	-0.186	-0.673	-21.60	0.027	0.061	3.10	-0.0277	-0.067	-3.26	-0.0082	-0.0164	-0.95
P6	-0.138	-0.502	-16.10	0.035	0.081	4.13	-0.0154	-0.037	-1.80	-0.0164	-0.0328	-1.92
P7	-0.186	-0.673	-21.60	0.015	0.034	1.17	-0.0310	-0.074	-3.60	-0.0197	-0.0396	-2.31
P8	-0.186	-0.673	-21.60	0.007	0.017	0.87	-0.0230	-0.056	-2.69	-0.0082	-0.0164	-0.95
P9	-0.168	-0.612	-19.64	0.027	0.061	3.10	-0.0400	-0.096	-4.68	-0.0295	-0.0590	-3.45
P10	-0.148	-0.538	-17.28	0.015	0.034	1.72	-0.0154	-0.037	-1.80	-0.033	-0.066	-3.84
P11	-0.168	-0.612	-19.64	0.007	0.017	0.87	-0.0520	-0.126	-6.12	-0.0165	-0.033	-1.92
P12	-0.134	-0.489	-15.71	-0.012	-0.027	-1.37	-0.040	-0.096	-4.68	-0.0246	-0.0692	-2.88
P13	-0.128	-0.465	-14.92	0.015	0.034	1.72	-0.029	-0.067	-3.40	-0.0426	-0.052	-4.99
P14	-0.141	-0.514	-16.48	0.000	0.000	0.00	+0.0154	+0.037	1.80	-0.0360	-0.072	-4.21
P15	-0.106	-0.380	-12.17	0.022	0.051	2.58	+0.031	+0.074	3.60	-0.0295	-0.0590	-3.45
P16	-0.134	-0.489	-15.71	-0.015	-0.034	-1.72	-0.0123	-0.030	-1.44	-0.0197	-0.0394	-2.31
P17	-0.144	-0.526	-16.83	-0.007	-0.017	-0.87	-0.034	-0.082	-3.96	-0.0164	-0.0328	-1.92
P18	-0.134	-0.489	-15.71	-0.007	-0.017	-0.87	-0.0246	-0.059	-2.88	-0.0393	-0.0786	-4.61
P19	-0.134	-0.489	-15.71	0.007	0.017	0.87	-0.0185	-0.044	-2.17	-0.0164	-0.0328	-1.92
P20	-0.114	-0.416	-13.35	0.015	0.034	1.72	-0.042	-0.096	-4.91	-0.0082	-0.0164	-0.95
P21	-0.131	-0.477	-15.31	0.007	0.017	0.87	-0.059	-0.140	-6.85	-0.0130	-0.0260	-1.53
P22	-0.155	-0.563	-18.06	0.022	0.051	2.59	-0.0154	-0.037	-1.80	+0.0246	+0.0492	2.88
P23	-0.151	-0.551	-17.66	0.022	0.051	2.58	-0.0185	-0.044	-2.17	+0.0295	+0.0590	3.45
P24	-0.104	-0.379	-12.17	0.079	0.183	9.29	+0.071	+0.170	8.29	-0.0164	-0.0328	-1.92
P25	-0.092	-0.337	-10.80	0.091	0.210	10.68	+0.092	+0.222	10.80	-0.0246	-0.0492	-2.88
P26	-0.141	-0.514	-16.48	-0.007	-0.017	-0.87	-0.034	-0.082	-3.97	-0.0246	-0.0492	-2.88
P27	-0.128	-0.465	-14.91	0.007	0.017	0.87	-0.025	-0.059	-2.88	-0.0330	-0.066	-3.84
P28	-0.131	-0.477	-15.31	0.015	0.034	1.72	-0.043	-0.104	-5.04	+0.0164	+0.0228	1.92
P29	-0.128	-0.465	-14.91	0.015	0.034	1.72	-0.039	-0.093	-4.51	+0.0295	+0.0590	3.45
P30	-0.057	-0.208	-6.67	0.091	0.021	10.68	+0.080	+0.193	9.36	+0.0360	+0.0720	4.21
P31	-0.101	-0.367	-11.79	0.062	0.142	7.23	+0.051	+0.122	5.95	-0.0230	-0.0460	-2.69
P32	-0.092	-0.337	-10.80	0.079	0.183	9.29	+0.046	+0.111	5.41	-0.0164	-0.0328	-1.92
P33	+0.044	+0.159	-5.11	0.068	0.156	7.92	-0.039	-0.093	-4.51	-0.0164	-0.0328	-1.92
P34	+0.054	+0.195	+6.29	0.062	0.142	7.23	-0.022	-0.052	-2.51	+0.0197	+0.0394	+2.31
P35	-0.024	-0.856	-27.49	-0.015	-0.034	-1.72	-0.085	-0.045	-2.17	+0.0082	+0.0164	+0.95
P36	-0.111	-0.404	-12.97	0.077	0.176	8.94	+0.074	+0.178	8.65	-0.0246	-0.0492	-2.88
P37	-0.091	-0.330	-10.61	0.088	0.203	10.33	+0.092	+0.222	10.97	-0.0295	-0.059	-3.45
P38	-0.154	-0.563	-18.06	0.007	0.017	0.87	-0.042	-0.100	-4.87	-0.033	-0.066	-4.21
P39	-0.148	-0.538	-17.28	0.00	0.00	0.00	-0.077	-0.259	-9.00	-0.069	-0.138	-8.06
P40	-0.134	-0.489	-15.70	0.007	0.017	0.87	-0.034	-0.082	-3.97	-0.062	-0.124	-7.28
P41	-0.121	-0.441	-14.13	-0.015	-0.034	-1.72	-0.040	-0.096	-4.68	-0.0197	-0.0394	-2.31
P42	-0.138	-0.502	-16.10	-0.00	-0.000	-0.00	-0.0123	-0.030	-1.44	+0.0164	+0.0328	+1.92
P43	-0.151	-0.551	-17.66	0.077	0.176	8.94	+0.034	+0.082	6.68	-0.0082	-0.0164	-0.95
P44	-0.128	-0.465	-14.92	0.065	0.149	7.57	+0.022	+0.052	2.51	-0.0246	-0.0492	-2.88
P45	-0.154	-0.563	-18.06	0.044	0.102	5.16	+0.037	+0.089	4.32	-0.0164	-0.0328	-1.92
P46	-0.101	-0.367	-11.8	0.071	0.163	8.27	+0.034	+0.082	3.97	-0.0082	0.0164	-0.95
P47	-0.097	-0.355	-11.39	0.082	0.190	9.64	+0.059	+0.141	6.85	+0.0197	+0.0394	+2.31
P48	-0.121	-0.441	-16.13	0.05	0.115	5.86	+0.092	+0.222	10.80	-0.0131	0.0262	-1.54
P49	-0.074	-0.269	-8.63	0.08	0.186	9.46	+0.110	+0.267	12.97	+0.0082	+0.0164	0.95
P50	-0.124	-0.453	-14.53	0.044	0.102	5.17	+0.092	+0.222	10.8	-0.0246	-0.0492	-2.88
P51	-0.087	-0.318	-10.21	0.071	0.162	-8.27	+0.089	+0.204	10.38	-0.0164	-0.0328	-1.92
P52	+0.023	+0.086	+2.74	0.053	0.122	6.19	-0.0015	-0.004	-0.17	-0.0295	-0.0590	-3.45
P53	-0.226	-0.826	-26.50	0.027	0.061	3.10	+0.0075	+0.019	0.87	-0.0295	-0.0590	-3.45
P54	-0.185	-0.673	-21.60	0.012	0.027	1.37	-0.035	-0.085	-4.14	-0.0328	-0.0656	-3.84
P55	-0.118	-0.428	-13.75	0.059	0.136	6.88	+0.046	-0.111	5.41	-0.0246	-0.0492	-2.88
P56	-0.144	-0.526	-16.88	0.007	0.017	0.87	-0.068	-0.163	7.92	-0.0410	-0.0820	-3.07
P57	-0.134	-0.489	-15.7	0.053	0.122	6.19	+0.068	+0.163	7.92	-0.0082	-0.0164	-0.95
P58	-0.154	-0.563	-18.06	-0.018	-0.041	-2.06	-0.0123	-0.030	-1.39	-0.0246	-0.0492	-2.88
P59	-0.128	-0.465	-14.92	0.012	0.027	1.37	+0.039	+0.093	4.64	-0.0164	-0.0328	-1.92
P60	-0.141	-0.5114	-16.48	-0.022	-0.051	-2.58	+0.037	+0.082	1.80	-0.0131	-0.0262	-1.54
P61	-0.158	-0.575	-18.46	-0.015	-0.034	-1.72	+0.055	+0.133	6.48	-0.0426	-0.0852	-4.99
P62	-0.121	-0.441	-14.16	0.068	0.156	7.92	+0.059	+0.141	6.85	-0.000	-0.000	-0.00
P63	-0.201	-0.734	-23.56	0.015	0.034	1.72	-0.059	-0.141	6.85	-0.0164	-0.0328	-1.92
P64	-0.302	-0.918	-35.34	0.012	0.027	1.37				-0.0197	-0.0396	-2.31

TABLE 8

LOCAL CONCENTRATIONS OF CARBON MONOXIDE: A typical case  
based on calculations presented in Appendix D1 (15 min average)

$$U_{\infty} = 4.5 \text{ mph} \quad H = 105 \text{ feet} \quad Q = 2.475 \times 10^4 \text{ ft}^3/\text{hr}$$

Concentration	Approach Wind Directions							
	N	NE	E	SE	S	SW	W	NW
Point Number	ppm	ppm	ppm	ppm	ppm	ppm	ppm	ppm
C-1	38.9	40.3	1.7	0.6	1.70	7.8	2.3	2.5
C-2	20.2	52.2	61.6	4.9	4.2	26.7	1.6	0.9
C-3	0.1	1.1	1.2	0.6	2.5	23.4	4.3	4.2
C-4	0.1	6.3	0.6	0.3	1.7	31.4	2.4	1.5
C-5	0.9	0.6	0.5	1.2	2.5	17.8	1.7	0.8
C-6	0.9	0.2	0.0	1.0	1.0	11.5	1.1	0.2
C-7	1.5	0.6	0.0	1.0	1.2	1.7	0.2	3.7
C-8	21.4	10.5	1.2	102.1	1.1	5.0	10.3	18.6
C-9	8.8	53.5	32.7	1.0	0.8	16.1	3.2	1.3
C-10	1.4	5.3	1.0	0.8	0.7	9.9	0.6	0.6
Vertical profile in the ground level parking area								
C-11	7.9	21.7	0.8	222.1	25.2	45.0	104.0	11.8
C-12	13.4	23.9	0.8	102.1	16.2	21.8	42.7	8.8
C-13	14.4	11.3	0.6	26.4	11.9	11.3	7.8	3.6
C-14	0.4	18.0	0.5	20.0	0.5	1.5	5.3	0.9
C-15	0.0	4.9	0.7	0.0	0.7	0.0	1.9	0.7
C-16	0.3	1.5	1.1	0.5	0.5	0.0	0.6	0.0
C-17	0.2	0.8	0.1	0.37	0.0	0.0	0.2	0.9
Vertical profile on the northeast side of the building								
C-18	0.1	0.5	0.4	2.3	15.4	5.4	0.7	1.2
C-19	0.5	0.9	0.9	3.1	11.4	5.7	0.8	0.7
C-20	1.0	0.1	0.1	1.0	6.7	7.1	0.6	0.9
C-21	1.1	0.3	0.6	0.0	3.9	5.1	0.2	0.9
C-22	1.0	0.0	0.0	0.5	2.2	3.2	0.9	0.9
C-23	0.8	0.5	0.6	0.5	1.4	0.3	0.5	0.8
C-24	0.6	0.1	0.2	0.2	1.9	0.7	0.0	1.0

## APPENDIX A: INSTRUMENTATION AND MATERIALS

Model: Main building model, made of Lucite plastic, surrounding topography made of styrofoam sheets (0.3 in. thick) and blocks

Camera: Movie: Bolex H16-16 mm camera  
 Still: Supergraphic Camera 4 in. x 5 in., Kodak Retina III, 35 mm; Hasselblad EL/M, 2 1/4 x 2 1/4

Film: Movie: Ektachrome 7242 ASA 125, forced developed to ASA 500  
 Still: Royal-Pan-4164, Kodak film, Ektachrome EHB

Exposure: Movie:  $f = \text{variable}$ , 24 frames per sec  
 Still:  $f = 8-16$ ,  $t = 1/50$  sec

Smoke: Titanium dioxide generated by passing humid air over titanium tetrachloride

Lighting System: Flood lights, 650 watts each, type Berkey Colortran

Simulated Snow-Drift Particles: Styrofoam particles, uniform, average size approximately 1 mm

Tracer Gas: Krypton-85, concentration 0.217  $\mu\text{ci/cc}$

Flow Meters: Fischer & Porter Co. Precision flow rator No. F.P. 1/8-14-G-6 3/4/61

Sampling Panel: 25 point sampling system made at CSU (Fig. 10)

Tracer Gas Analyzer: Ultrascaler-Model 192A of Nuclear Chicago

Hot-Wire Anemometer: Constant temperature type, made at CSU

Hot Wire: Pt(80%) Ir(20%) wire dia. = 0.01 mm, length - 2 mm

Traversing mechanism: Made at CSU, range = 0.8 m, precision = 0.5 mm

R.M.S. Meter: DISA RMS meter type 55D35

Oscilloscope: Tektronix Oscilloscope type 561A

Counter: H.P. Counter with external control, model 522B, precision  $\pm 0.01$  sec

D.V.M.: 1) HP Integrating digital volt meter model 2401C  
 2) HP digital volt meter model 3440A

Thermometers: Precision thermometer, range 0-200°F

Barometer: Ideal-Arrowsmith, precision  $\pm 0.001$  in. Hg

Pressure Meter: MKS Baratron pressure meter type 77; range 0-30 mm Hg; precision  $\pm 0.0002$  mm Hg

## APPENDIX B

Details of the locations for each of 64 pressure taps, 35 local gust measurements and 24 local concentration measurements are described in the following tables. Locations are specified by grid coordinates and elevations taken from drawings supplied by TAC. Additional remarks are added wherever necessary to fully describe the locations.

B.1 Points for Local Concentration Measurements

Point No.	Fig. No.	Grid Coordinates		Elevations	Remarks
		x	y		
C1	12	8.5	H.2	6322	facing up
C2	12	20.5	H.2	6322	facing up
C3	17	12.5	G.4	6252	facing up
C4	18	13.5	G.3	6252	facing up
C5	18	15.7	G.3	6252	facing up
C6	18	17.3	F.0	6252	facing up
C7	17	20.0	F.5	6266	facing up
C8	11	9.0	0.0	Ground	facing NW
C9	11	18.5	G.5	6336	facing NW
C10	11	16.0	D.0	Ground	facing NW
*C11 to C17	11	12.0	0.5	Ground	facing NW, Fig. 44
*C18 to C24	11	11.0	D.5	6266	facing NW, Fig. 45

\*represents vertical rakes of sample points

B.2 Points for Local Gust (Turbulence) Measurements

Point No.	Fig. No.	Grid Coordinate		Level	Remarks
		x	y		
W1	18	2.0	F.5	Ground	NE Corner
W2	18	8.5	H-5	Ground	SW Side
W3	18	20.5	B.5	Ground	NE Side
W4	18	14.9	C.5	Ground	NE Side
W5	18	10.8	E.5	Ground	NE Side
W6	17	14.5	J.5	Ground	SW Side
W7	17	14.5	G.8	Ground	SW Side
W8	17	21.5	K.2	Ground	SW Side
W9	17	19.3	E.5	6266	NE Side
W10	17	22.7	E.5	6266	NE Side
W11	13	8.5	J.0	6322	Roof
W12	13	8.5	H.0	6322	Roof
W13	13	14.5	J.2	6322	Roof
W14	13	14.5	H.1	6322	Roof
W15	13	20.5	J.0	6322	Roof
W16	13	20.5	H.0	6322	Roof
W17	13	22.5	J.8	6322	Roof
W18	13	17.7	J.8	6322	Roof
W19	13	11.2	J.8	6322	Roof
W20	13	1.7	F.4	6336	Roof
W21	13	6.9	F.4	6336	Roof
W22	13	10.2	F.4	6336	Roof
W23	13	13.6	F.4	6336	Roof
W24	13	15.5	F.4	6336	Roof
W25	13	18.7	F.4	6336	Roof
W26	13	22.2	F.4	6336	Roof
W27	13	26.3	F.4	6336	Roof
W28	11			Ground	Parking
W29	11			Ground	Parking
W30	11			Ground	Parking
W31	11			Ground	Parking
W32	11			Ground	Parking
W33	11			Ground	Heliport
W34	11			Ground	Heliport
W35	11			Ground	Heliport

B.3 Points for Mean Surface Pressure Measurement

Pressure Tap No.	UP	Opening Directed				SE	S	Elevation	Fig. No.	Grid No. x-y	Remarks
		Incline UP	NE	NW	SW						
P1							X	6256	20		
P2		X						6266	16		inclined face-Greenhouse
P3							X	6271	20		
P4	X							6280	16		Greenhouse
P5							X	6277	20		
P6							X	6263	20		
P7		X						6266	16		Inclined face-Greenhouse
P8	X							6280	16		Greenhouse roof
P9		X						6266	16		Inclined face-Greenhouse
P10					X			6252	18		Doorway
P11	X							6280	16		Greenhouse roof
P12		X						6260	16	19.E	Cafeteria roof
P13		X						6264	16	19.C	Cafeteria roof
P14		X						6285	16	21.D	Cafeteria roof
P15		X						6260	16	22.C	Cafeteria roof
P16		X						6264	16	22.E	Cafeteria roof
P17					X			6285	16	19.E	Cafeteria SW face
P18					X			6260	16	23.E	Cafeteria SW face
P19					X			6285	16	21.E	Cafeteria SW face
P20						X		6277	16		Cafeteria SE face
P21						X		6259	16		Cafeteria SE face
P22			X					6252	18		Doorway
P23	X							6266	17		
P26					X			6266	17		Doorway
P25					X			6252	18		Doorway
P26						X		6252	18		Doorway
P27	X							6266	17		
P28						East		6252	18		Doorway
P29		X						6266	17		Doorway
P30				X				6280	16		Doorway
P31				X				6294	15		
P32				X				6294	15		
P33						X		6308	14		
P34						X		6315	14		
P35			X					6308	14		
P36					X			6308	14	1.F	
P37					X			6308	14	11.H	
P38			X					6308	14	18.H	
P39			X					6308	14	7.F	
P40			X					6308	14	14.F	
P41			X					6308	14	23.F	
P42			X					6315	14	27.F	
P43			X					6322	14	27.F	
P44					X			6308	14	25.F	
P45	X							6322	14	8.K	Roof
P46					X			6308	14	8.K	
P47					X			6308	14	11.K	
P48	X							6322	14	15.K	Roof
P49					X			6308	14	14.K	
P50	X							6322	14	19.K	Roof
P51					X			6308	14	20.K	
P52							X	6222	14	23.K	
P53	X							6336	13	1.F	Roof
P54			X					6322	14	3.G	
P55					X			6322	14	4.F	Doorway
P56			X					6322	14		
P57	X							6336	13	14.F	
P58					X			6322	14	12.G	
P59	X							6336	13	27.F	Roof
P60					X			6322	14	25.G	
P61						X		6322	14	27.G	
P62					X			6336	13	27.H	Doorway
P63			X					6336	13	8.G	Doorway
P64	X							6332	13	1.F	

## APPENDIX C: CONTENTS OF MOTION PICTURES

Details of the content and order of scenes visualized by smoke and recorded on motion pictures are given in the following table:

Wind Direction	Source Location	Remarks
General Introduction		
	General view of the model outside the wind tunnel	
	General view of the model oriented in the wind tunnel	
North	Upwind	General wind distribution
North	Parking area	
North	Heliport	
Northeast	Upwind	General approach wind
Northeast	Parking area	
Northeast	Heliport	
East	Upwind	Approach wind
East	Parking area	
East	Heliport	
Southeast	Upwind	Approach wind
Southeast	Parking area	
Southeast	Heliport	
South	Upwind	Approach wind
South	Parking area	
South	Heliport	
Southwest	Upwind	Approach wind
Southwest	Parking area	
Southwest	Heliport	
West	Upwind	Approach wind
West	Parking area	
West	Heliport	
Northwest	Upwind	Approach wind
Northwest	Parking area	
Northwest	Heliport	

## APPENDIX D: TYPICAL EXAMPLES ON USE OF THE MODEL DATA

Results obtained in the present investigation are presented in dimensionless form with respect to appropriate reference quantities. These dimensionless results represent both the model and the prototype behavior.

D.1 Local Automobile-Emission Concentrations

In the model study, a known amount of tracer gas was released over the ground-level parking area and concentration measurements were made at 24 selected locations (Appendix B.1). The results were expressed in dimensionless form as follows,

$$K = \frac{CU_{\infty} H^2}{Q}$$

where  $K$  is the local concentration coefficient,  $C$  is the local concentration,  $U_{\infty}$  is the free stream wind speed,  $H$  is a characteristic dispersion length equal to the building height and  $Q$  is the source strength or rate of tracer gas release. From the principles of model prototype similitude

$$(K)_m = (K)_p = \left( \frac{CU_{\infty} H^2}{Q} \right)_m = \left( \frac{CU_{\infty} H^2}{Q} \right)_p$$

Thus,  $C_p = K_m \left( \frac{Q}{U_{\infty} H^2} \right)_p$  where subscripts  $m$  and  $p$  refer to model and

prototype, respectively. When the prototype conditions of prevailing wind speed, building height and source strength of any pollutant in the parking area are known, local concentrations can be calculated when the coefficient has been determined by measurement in the model. As

an illustration to demonstrate the versatility of the data, the following typical calculations are presented:

Prediction of concentrations of automobile exhaust:

Source Strength

parking capacity at ground level = 630 cars

parking capacity at terrace level = 470 cars

Total parking capacity = 1100 cars

Assume a cold starting condition of 50 percent of cars at full capacity of the parking areas as a probable maximum source condition.

Also assume typical concentration data for exhaust gases as follows (2):

Total exhaust = 1500 ft<sup>3</sup>/hr/car

CO<sub>2</sub> Content = 11.4 percent by volume

CO Content = 3.0 percent by volume

Hydrocarbons = 460 ppm/car

Hexane = 69.1 gm/hr/car

Total exhaust from 550 automobiles = 825,000 ft<sup>3</sup>/hr.

Thus, the source strength will be

$$\left\{ \begin{array}{l} \text{CO}_2 \quad : \quad 0.114 \times 825000 = 9.405 \times 10^4 \text{ ft}^3/\text{hr} \\ \text{CO} \quad : \quad 0.03 \times 825000 = 2.475 \times 10^4 \text{ ft}^3/\text{hr} \\ \text{Hydrocarbons} \quad : \quad 460 \times 825000 = 3.795 \times 10^{10} \text{ ppm ft}^3/\text{hr} \\ \text{Hexane} \quad : \quad 69.1 \times 550 = 38005 \text{ gm/hr} \end{array} \right.$$

Approach Velocity:

The dispersal rate will be minimal during light variable conditions of wind. Survey of limited wind data available for the area indicates that such winds occur at mean speed of 4.5 mph. Therefore,

$$U_{\infty} = 23,760 \text{ ft/hr.}$$

Local Concentrations:

Local concentrations can be evaluated using the formula:

$$C_p = K_m \frac{Q}{U_\infty H^2} \quad .$$

Thus, with a building height  $H$  of 105 ft,

$$\left\{ \begin{array}{l} \text{CO}_2 \\ \text{CO} \\ \text{Hydrocarbons} \\ \text{Hexane} \end{array} \right. = K_m \left\{ \begin{array}{l} \frac{9.405 \times 10^4 \text{ (ft}^3\text{/hr)}}{23760 \text{ (ft/hr)} \times (105)^2 \text{ ft}^2} \\ \frac{2.475 \times 10^4 \text{ (ft}^3\text{/hr)}}{23760 \text{ (ft/hr)} \times (105)^2 \text{ ft}^2} \\ \frac{3.795 \times 10^{10} \text{ ppm ft}^3\text{/hr}}{23760 \text{ (ft/hr)} \times (105)^2 \text{ ft}^2} \\ \frac{38005 \text{ gm/hr}}{23760 \text{ ft/hr} \times (105)^2 \text{ ft}^2} \end{array} \right\} = \left\{ \begin{array}{l} 359.03 K_m \text{ ppm} \\ 94.5 K_m \text{ ppm} \\ 1.45 K_m \text{ ppm} \\ 1.4508 \times 10^{-4} K_m \text{ gm/ft}^3 \\ = 5.12 K_m \text{ mlg/m}^3 \end{array} \right. .$$

From the above relations concentration distributions of  $\text{CO}_2$ ,  $\text{CO}$ , Hydrocarbons and Hexane can be computed. Similar calculations can be extended to any other constituent of the source released in the parking area. Local concentrations of carbon monoxide at the 24 locations are given in Table 8.

## D.2 Local Mean Velocities and Gust Intensities

Model data on local mean velocity and gust intensities in this report are in dimensionless form taking local mean and free-stream wind speed as a reference. Prototype local mean wind speed and root-mean-square of velocity fluctuations at corresponding locations can be predicted by using the principle of similitude. Root-mean-square values of the local velocity fluctuations are a measure of local gust

intensity. Dimensionless local mean and RMS velocities are the same for both the model and prototype. Thus,

$$\left(\frac{U_{RMS}}{U_{\infty}}\right)_m = \left(\frac{U_{RMS}}{U_{\infty}}\right)_p, \text{ and } \left(\frac{U_M}{U_{\infty}}\right)_m = \left(\frac{U_M}{U_{\infty}}\right)_p.$$

Therefore,  $(U_{RMS})_p = \left(\frac{U_{RMS}}{U_{\infty}}\right)_m (U_{\infty})_p$  and

$$(U_M)_p = \left(\frac{U_M}{U_{\infty}}\right)_m (U_{\infty})_p.$$

Model values of  $\left(\frac{U_{RMS}}{U_{\infty}}\right)$  and  $\left(\frac{U_M}{U_{\infty}}\right)$  at 35 selected locations are presented in Table 2-5, corresponding prototype mean and RMS values of local velocity can be calculated from the above relations.

### D.3 Surface Pressures

Model surface pressures are measured as difference in surface pressure and free-stream static pressure and expressed in dimensionless form taking dynamic head of the free stream and flow at two building heights at the center of building--

$$C_{p\infty} = \left\{ \frac{P_L - P_{s\infty}}{\rho U_{\infty}^2 / 2} \right\} \text{ and } D_{P2H} = \left\{ \frac{P_L - P_{s\infty}}{\rho U_{2H}^2 / 2} \right\}.$$

Pressure on the prototype at corresponding locations can be predicted from either of the two model pressure coefficients depending on the type available information of prototype velocity. From the principles of model similitude

$$(C_p)_m = (C_p)_p = \left(\frac{\Delta P}{\rho U^2 / 2}\right)_m = \left(\frac{\Delta P}{\rho U^2 / 2}\right)_p.$$

Thus,

$$(\Delta P)_p = \frac{\Delta P}{\rho U^2/2} \left( \rho U^2/2 \right)_m = C_{pm} \frac{\rho U^2}{2} p .$$

Prototype pressures at corresponding locations can be worked out from the model pressure coefficients using the above formula. For ready reference surface gust pressures are calculated for design wind speed of 230 ft/sec at 2,000 ft and a gust factor  $F_g$  of 2.5 and presented in Tables 6-7. Surface gust pressures  $P$  are related to the local pressure coefficients and reference pressure as

$$P = C_p \text{ (reference pressure)}$$

where

$$\text{reference pressure} = F_g \frac{\rho U_\infty^2}{2} .$$

Reference Gust Pressure for the Prototype

The reference gust pressure is defined as  $Fg \frac{\rho U_{\infty}^2}{2}$ . In the present study a mean velocity at 2,000 ft was chosen as reference velocity  $U_{\infty}$ . The gust factor  $Fg$  is taken to be 2.5 as specified in the Canadian Building Code. The exponent of power-law velocity distribution is taken as 0.16. The 50-year recurrence design wind speed for Denver was taken to be 80 mph at 30 ft in accordance with the ANSI A58.1, Building Code.

Thus,

$$\frac{U_{2000}}{U_{30}} = \left(\frac{2000}{30}\right)^{0.16} = 1.9582$$

$$U_{2000} = 1.9582 U_{30} = 1.9582 \times 80 = 156.66 \text{ mph} = 229.76 \text{ ft/sec}$$

A correction for air density to account for the one-mile elevation of Denver was taken as:

$$\rho = 0.84 \rho_{\text{sea level}}$$

$$= 0.84 (0.00211)$$

$$= 0.001773 \text{ slugs/ft}^3$$

$$\text{The reference gust pressure} = 2.5 \times \frac{0.001773}{2} \times (229.76)^2$$

$$= 117 \text{ lb/ft}^2$$

Thus, the building surface pressure is given by

$$P = 117 C_p$$

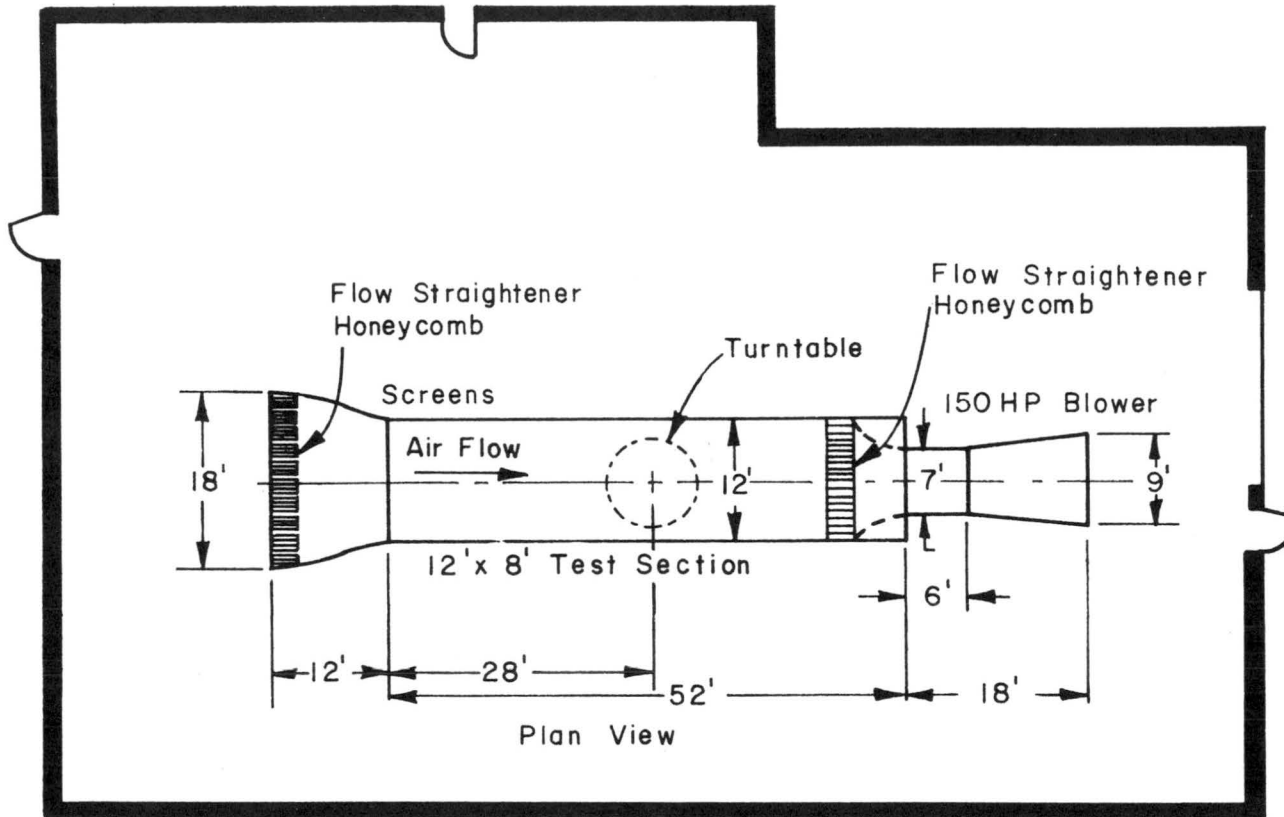


Fig. 1 Environmental Wind-Tunnel: Fluid Dynamics and Diffusion Laboratory, Colorado State University.

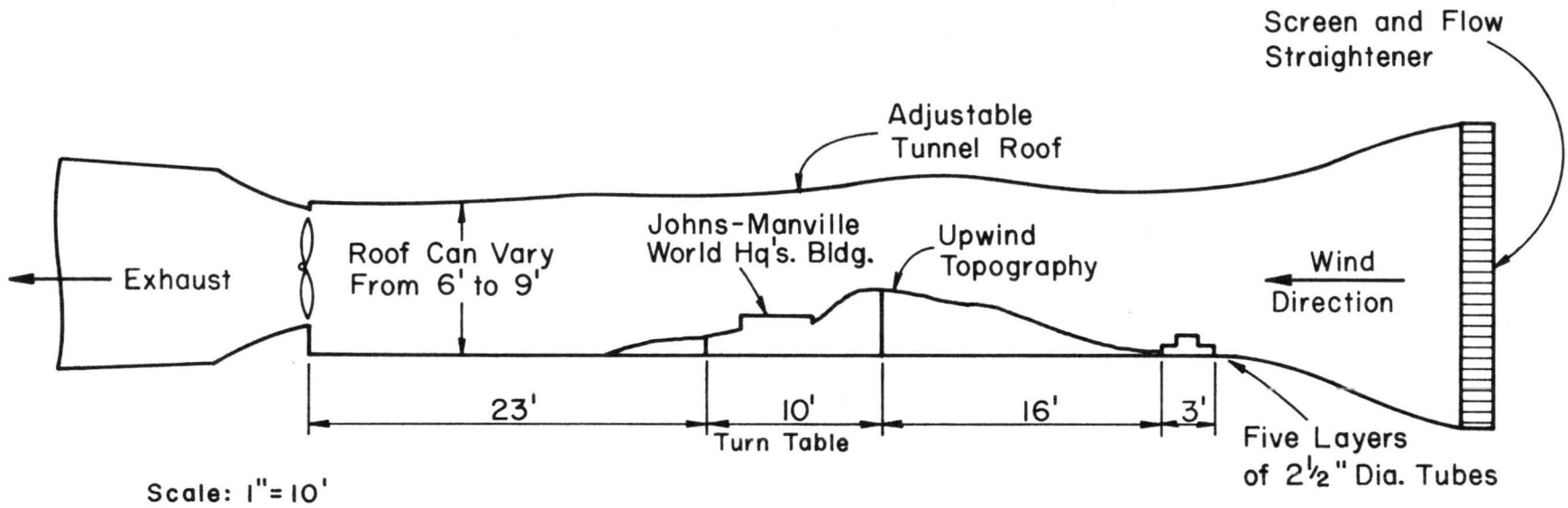


Fig. 2 Schematic of the Colorado State University Environmental Wind-Tunnel Showing the Model Location and Upwind Conditions.

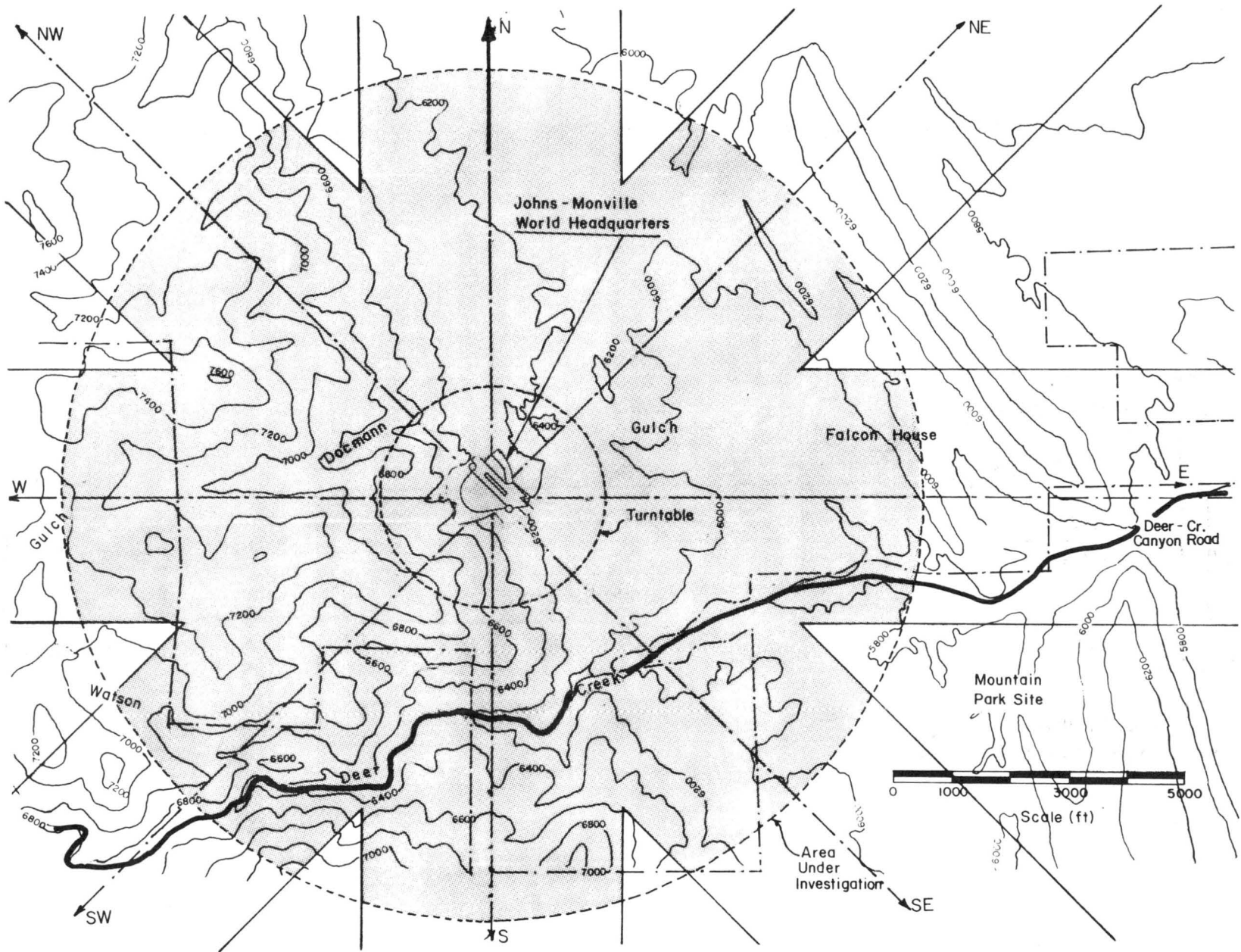


Fig. 3 Topography of the Site under Investigation.



Figure 4 Aerial View of Site Under Investigation.

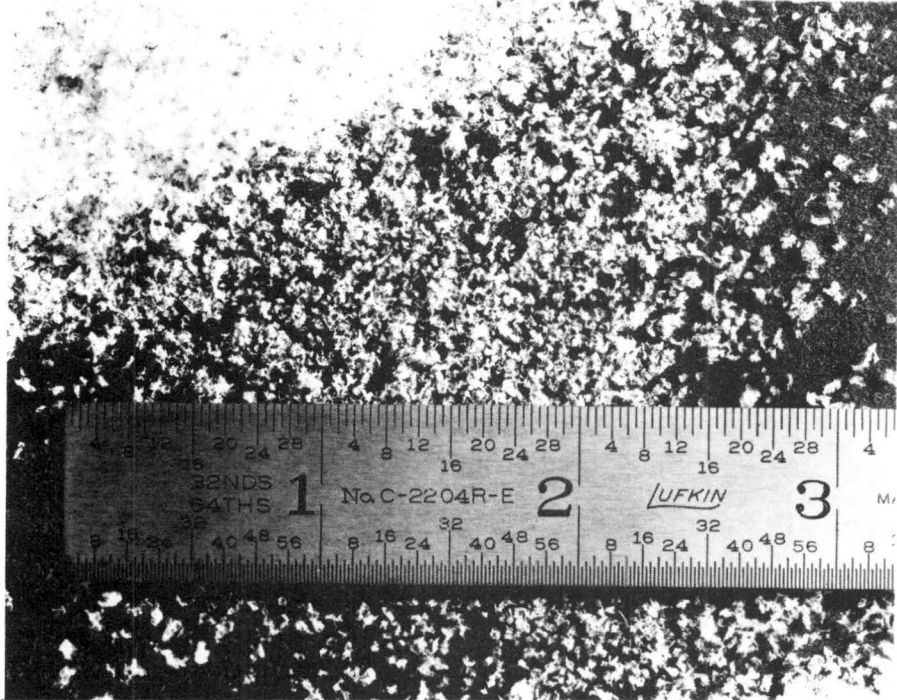


Figure 5 Photograph of Styrofoam Particles Used as a Drift Material.

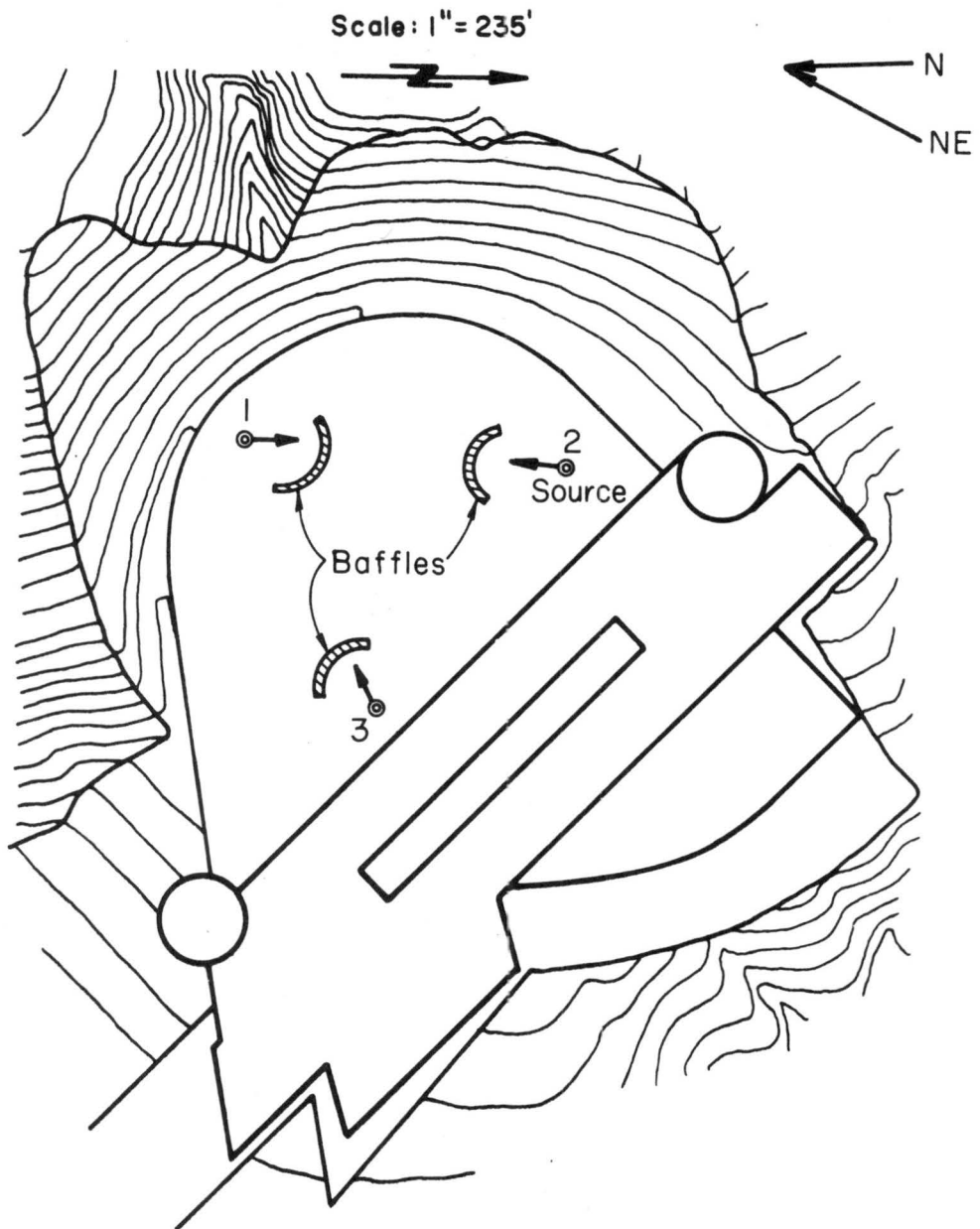


Fig. 6 Locations of Tracer-Gas Sources and their Details  
Wind Directions: N and NE.

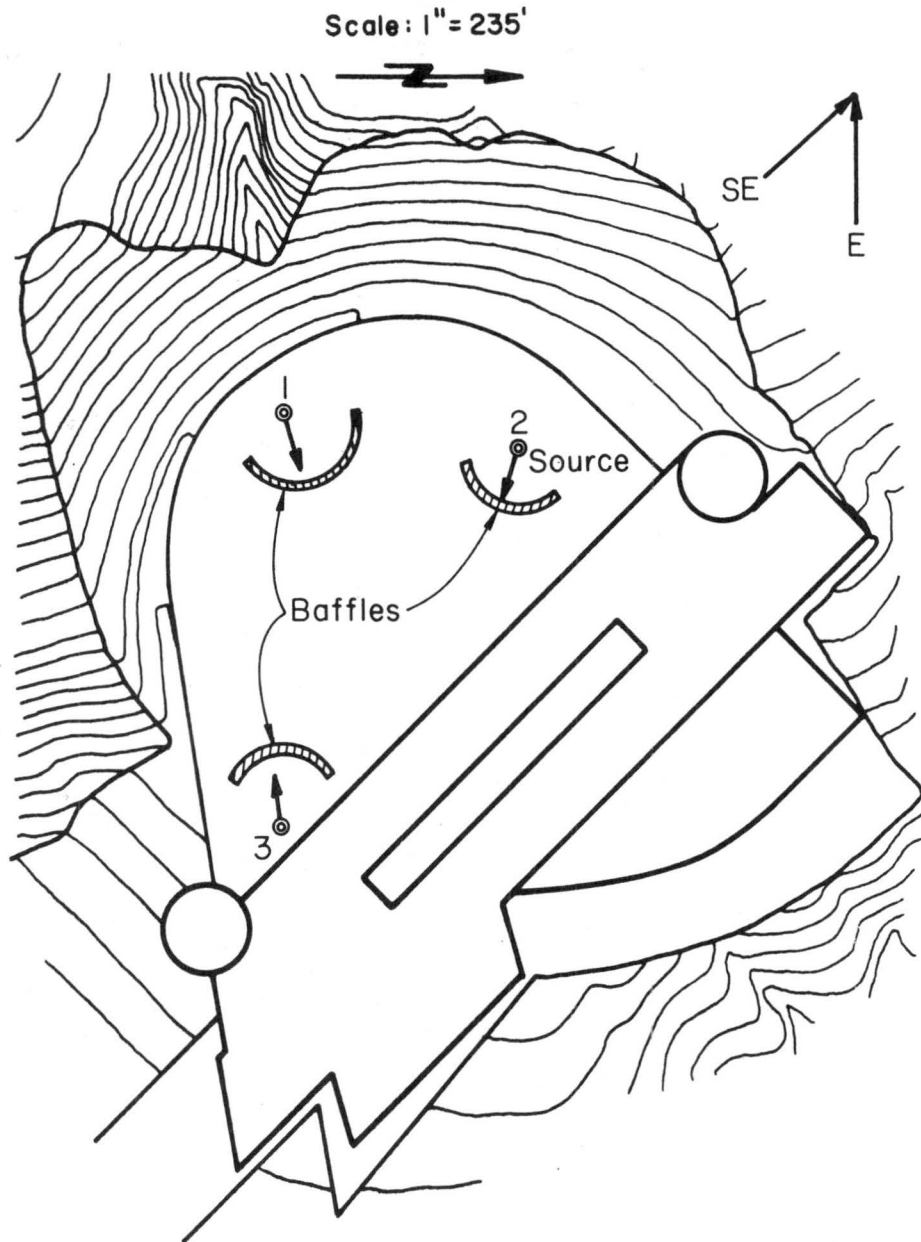


Fig. 7 Locations of Tracer-Gas Sources and their Details  
Wind Directions: E and SE.

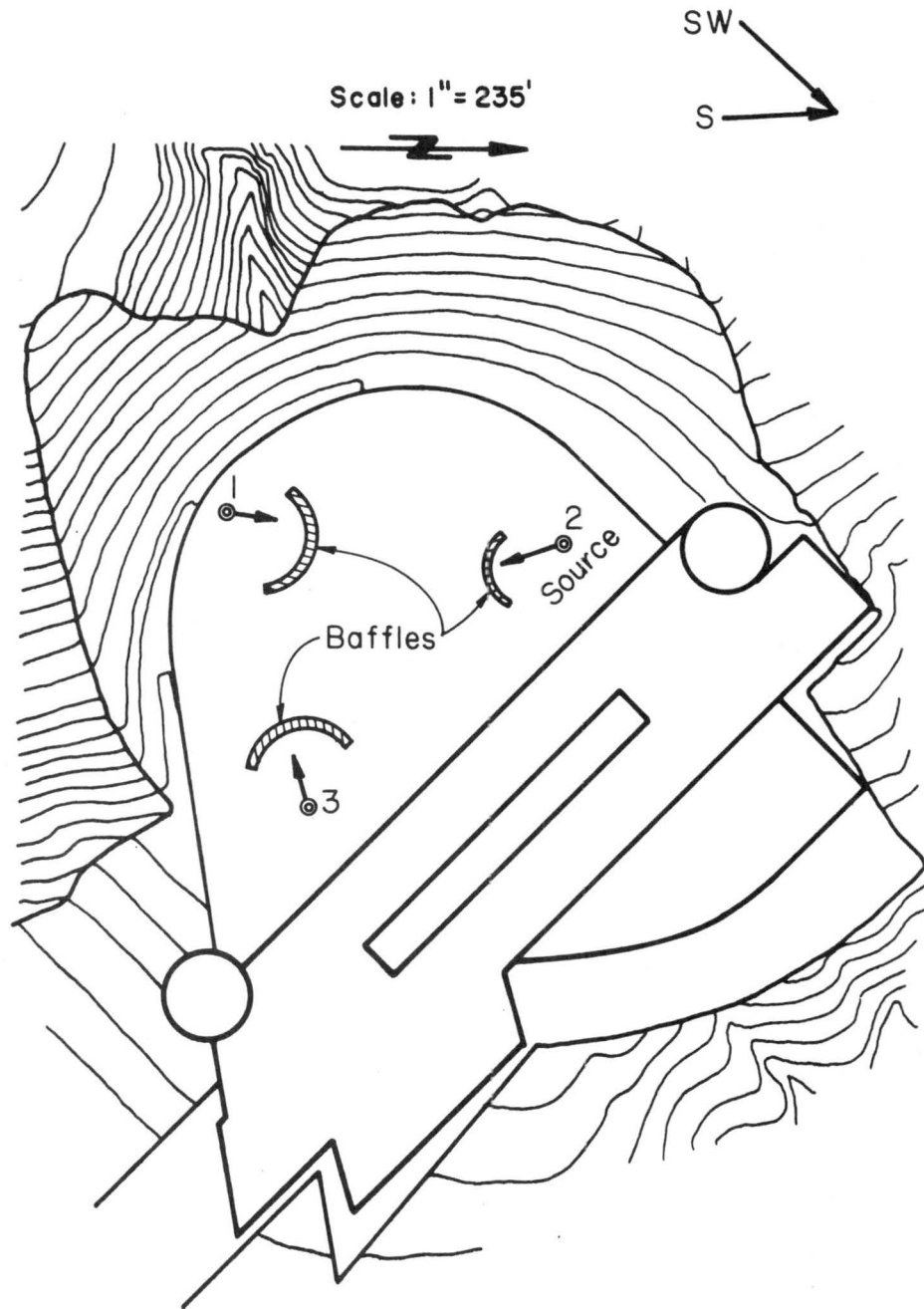


Fig. 8 Locations of Tracer-Gas Sources and their Details  
Wind Directions: S and SW.

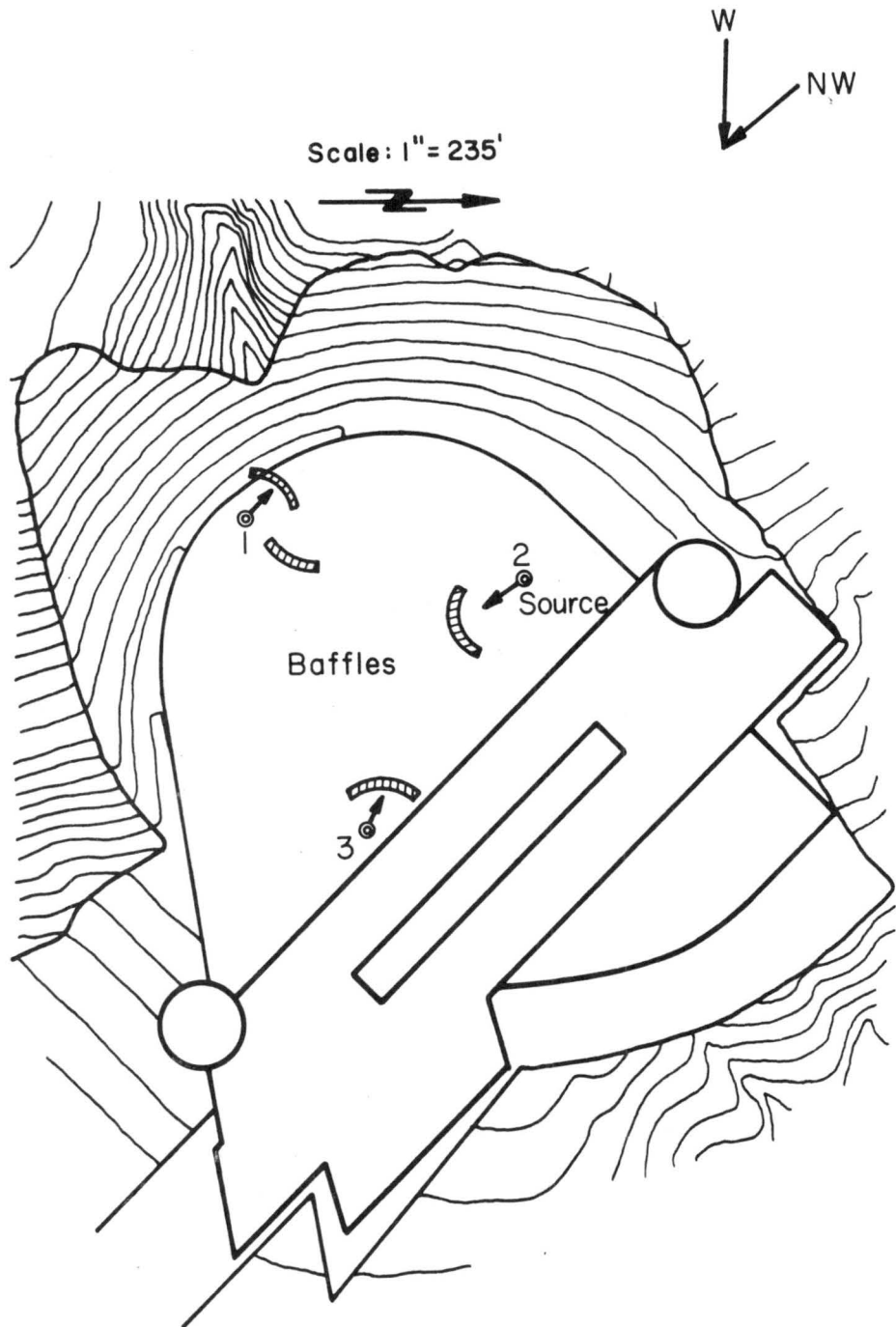


Fig. 9 Locations of Tracer-Gas Sources and their Details  
Wind Directions: W and NW.

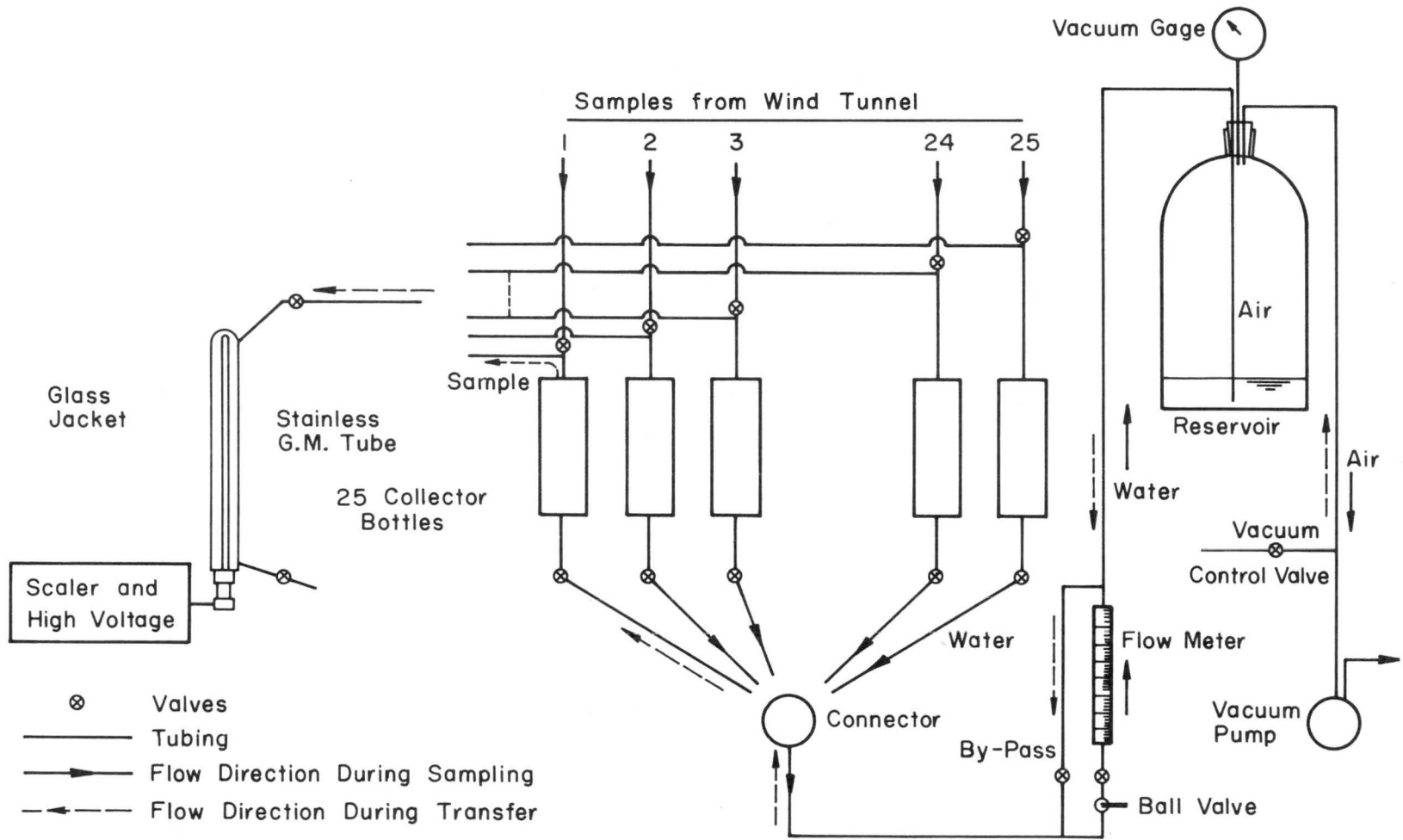


Fig. 10 Tracer-Gas Sampling and Analysis System.

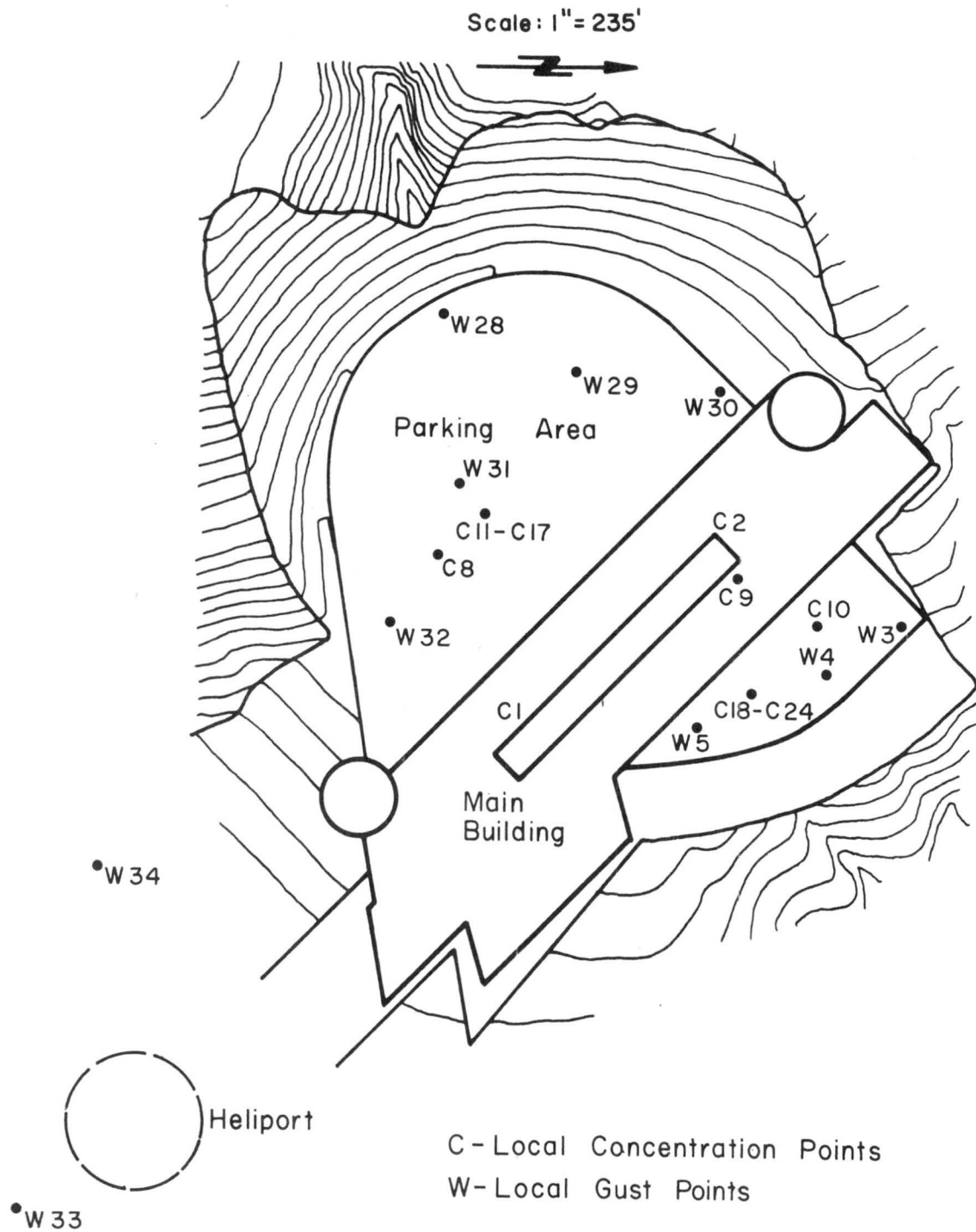


Fig.11 Locations of Points where Local Concentrations and Gusts were Measured: Heliport, Parking Area and NE Side of the Building.

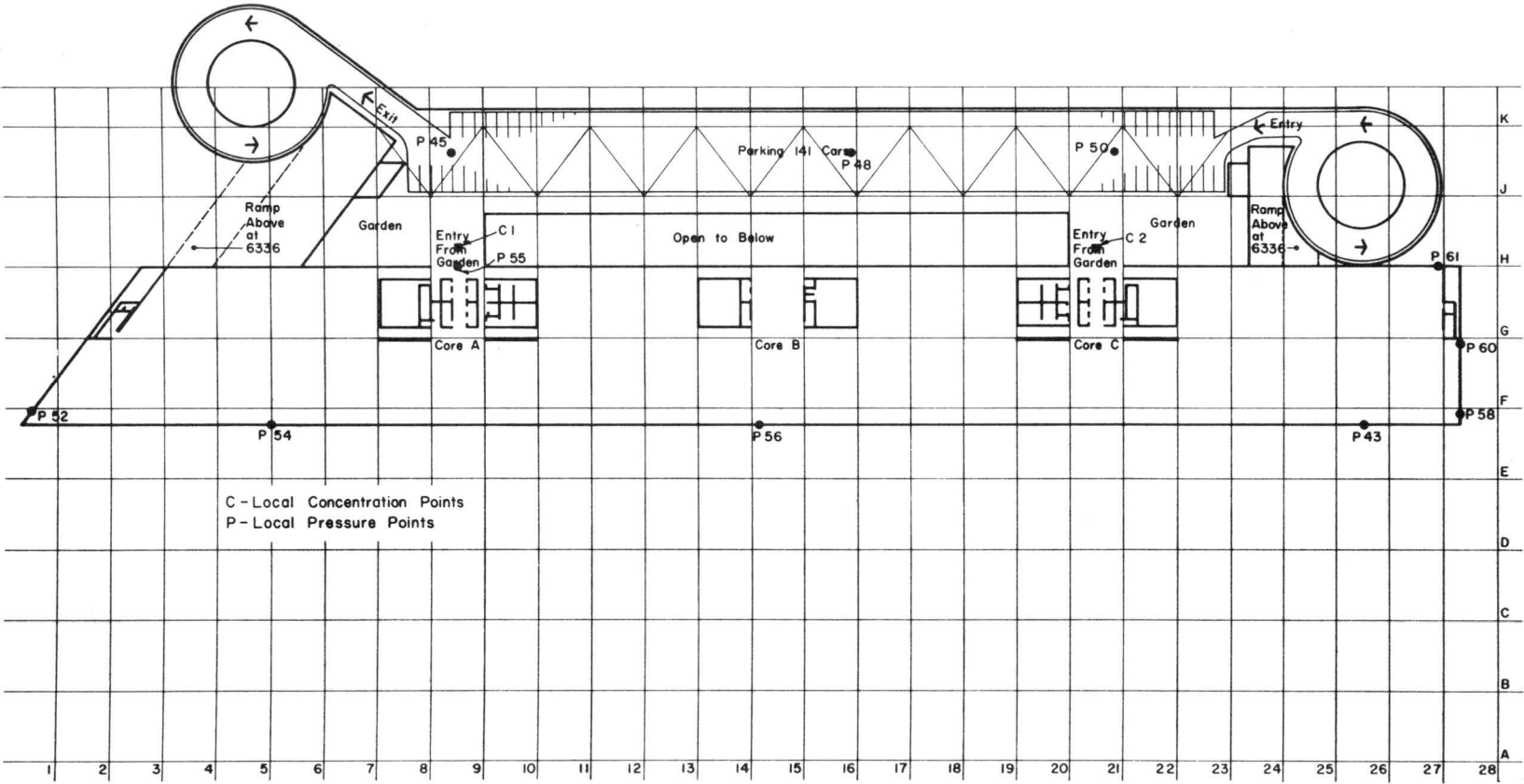


Fig. 12 Plan View at Elevation 6322 Indicating Locations of Points where Local Concentrations and Pressures were Measured.

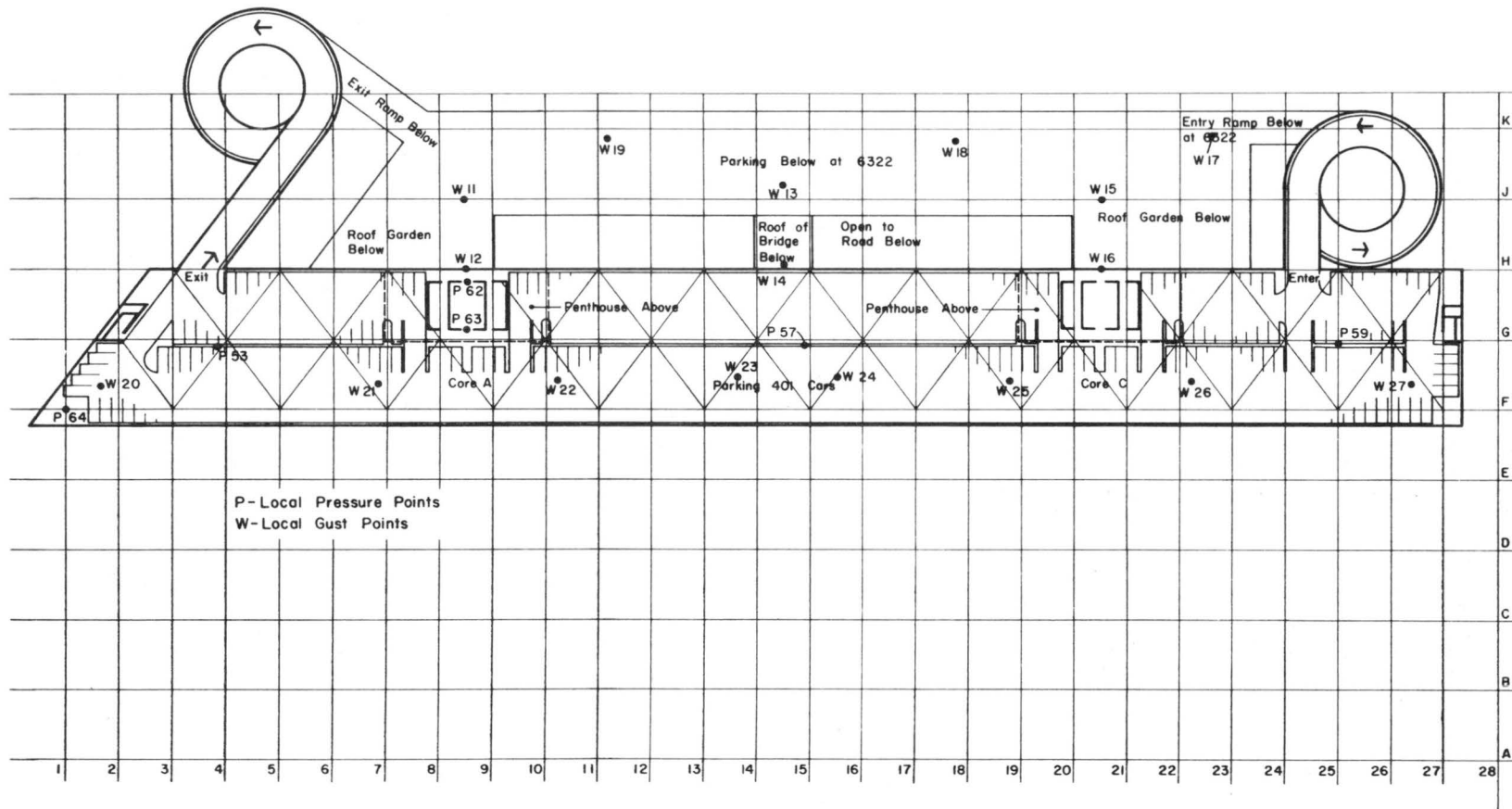


Fig. 13 Plan View of Elevation 6335 Indicating Locations of Points where Local Concentrations, Gusts and Pressures were Measured.

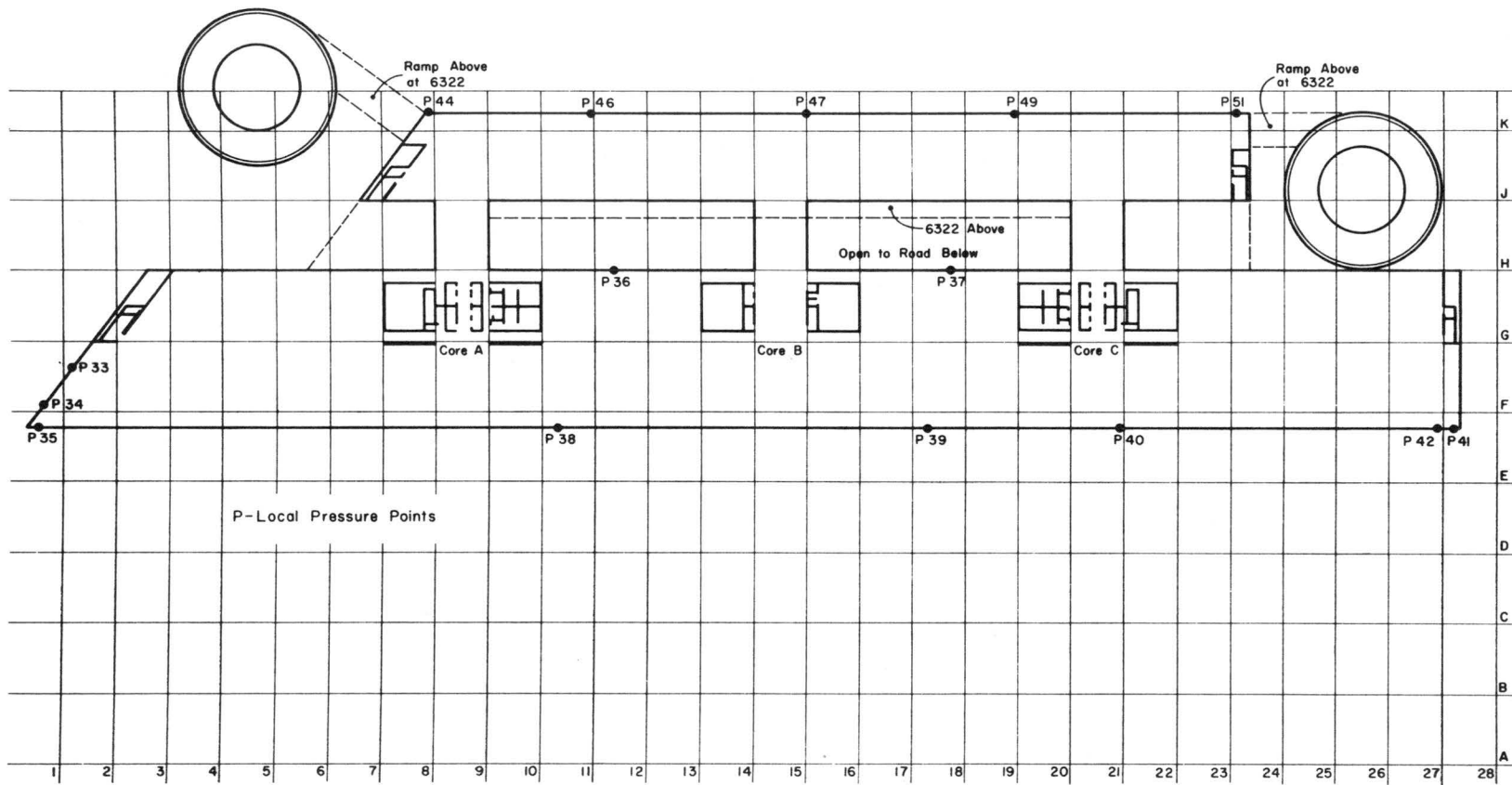


Fig. 14 Plan View at Elevation 6308 Indicating Pressure Points.

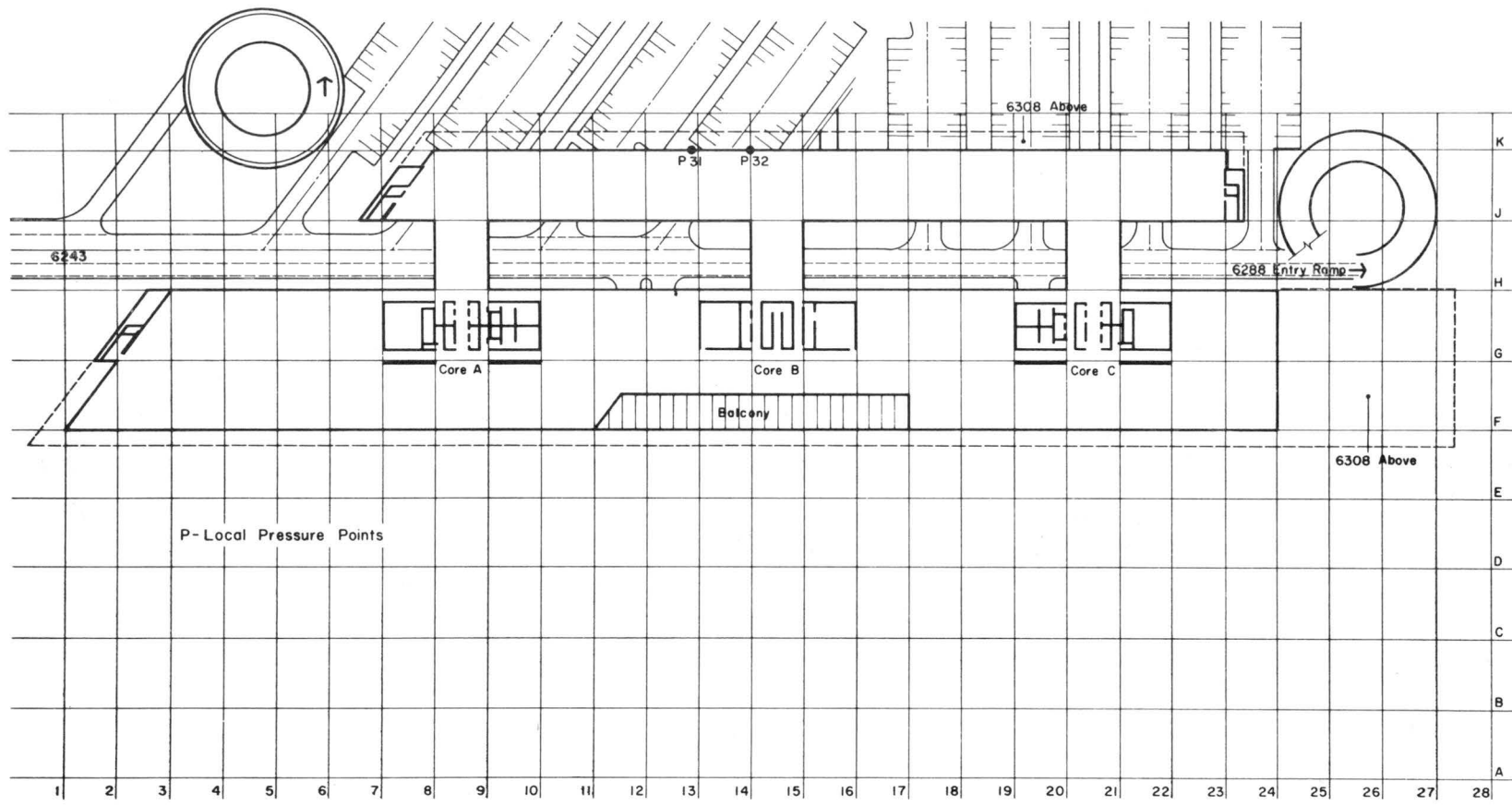


Fig. 15 Plan View at Elevation 6294 Indicating Pressure Points.

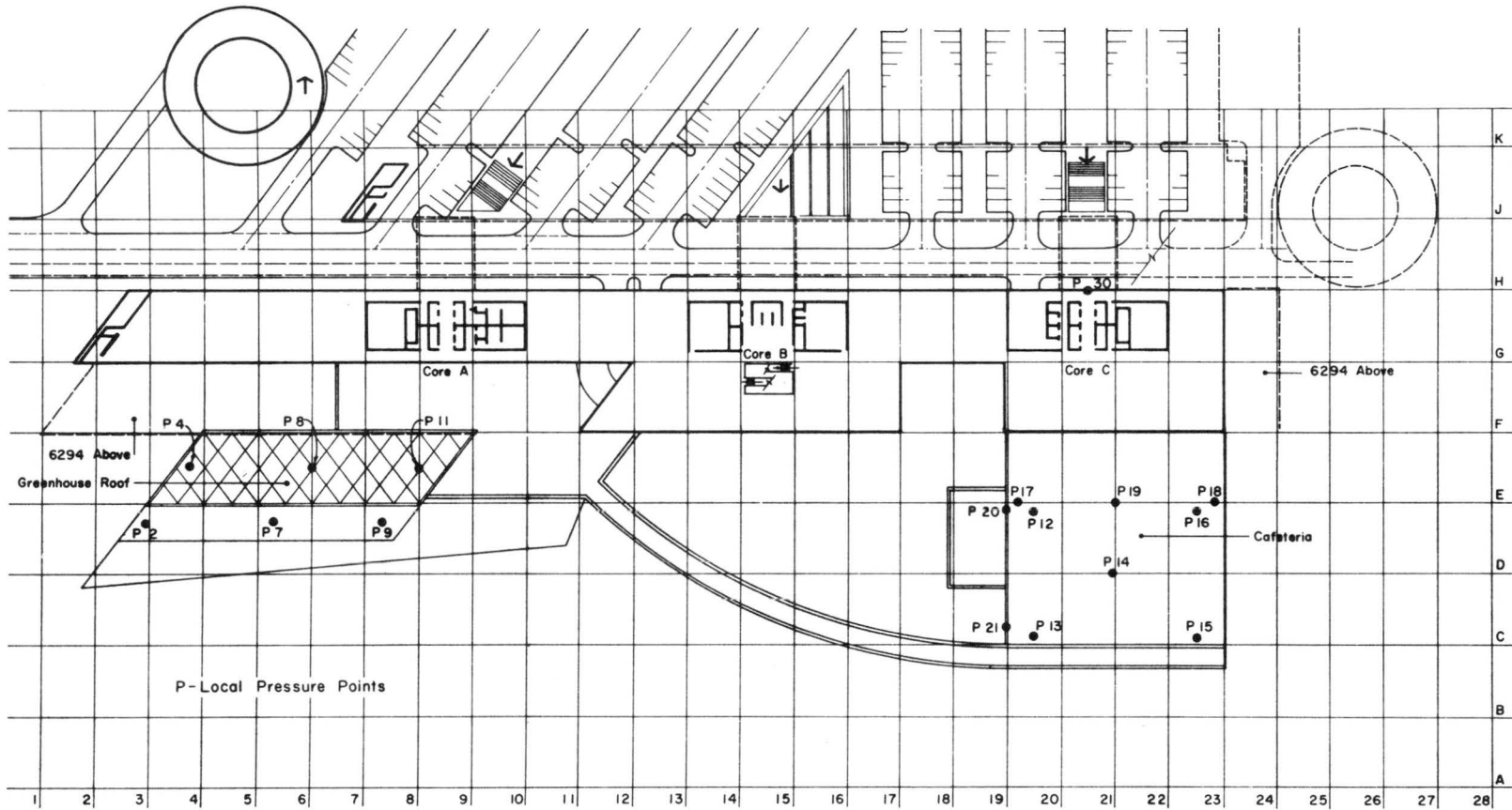


Fig. 16 Plan View at Elevation 6280 Indicating Pressure Points.

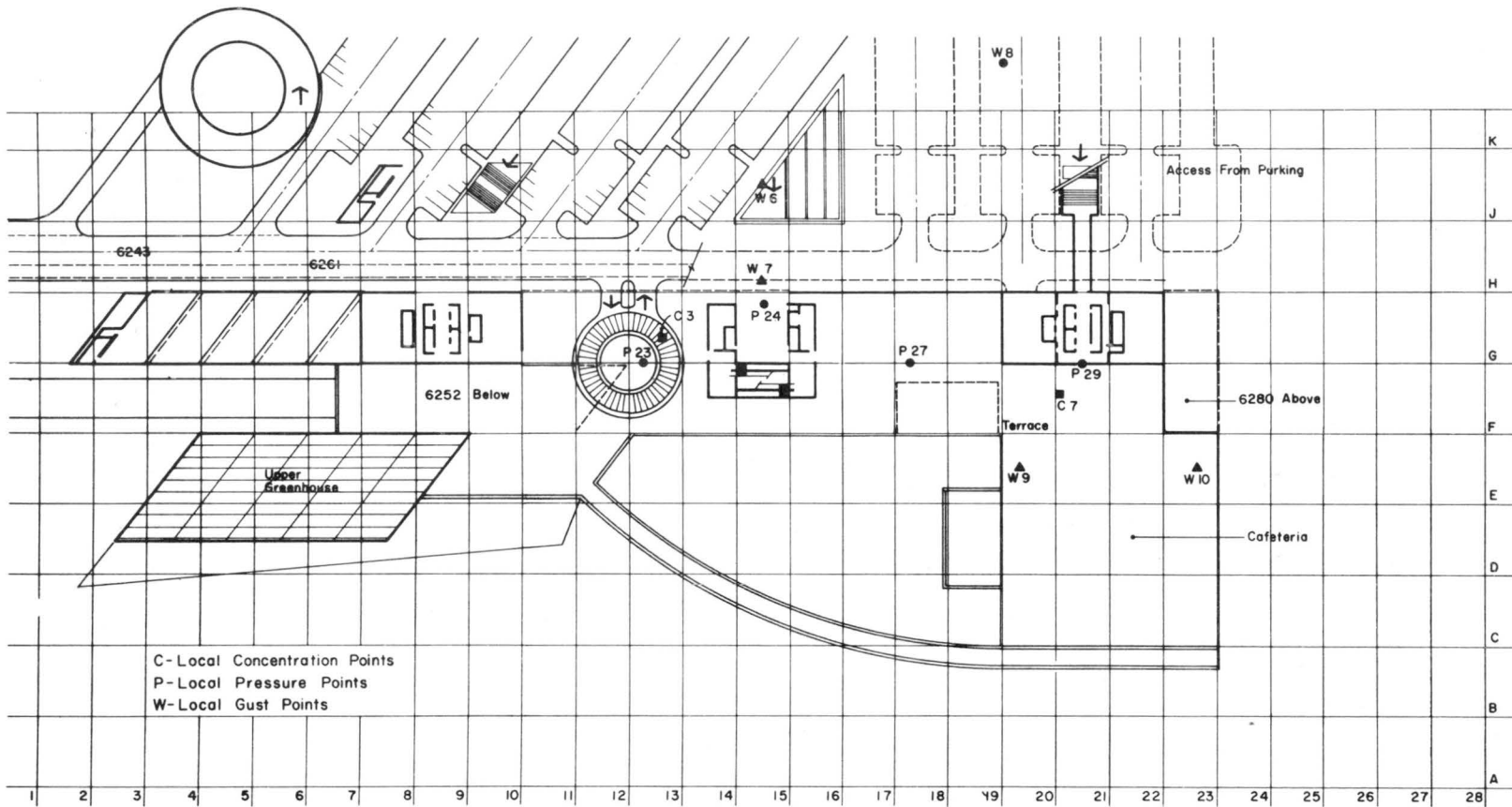


Fig. 17 Plan View at Elevation 6266 Indicating Points where Concentrations, Gusts and Pressures were Measured.

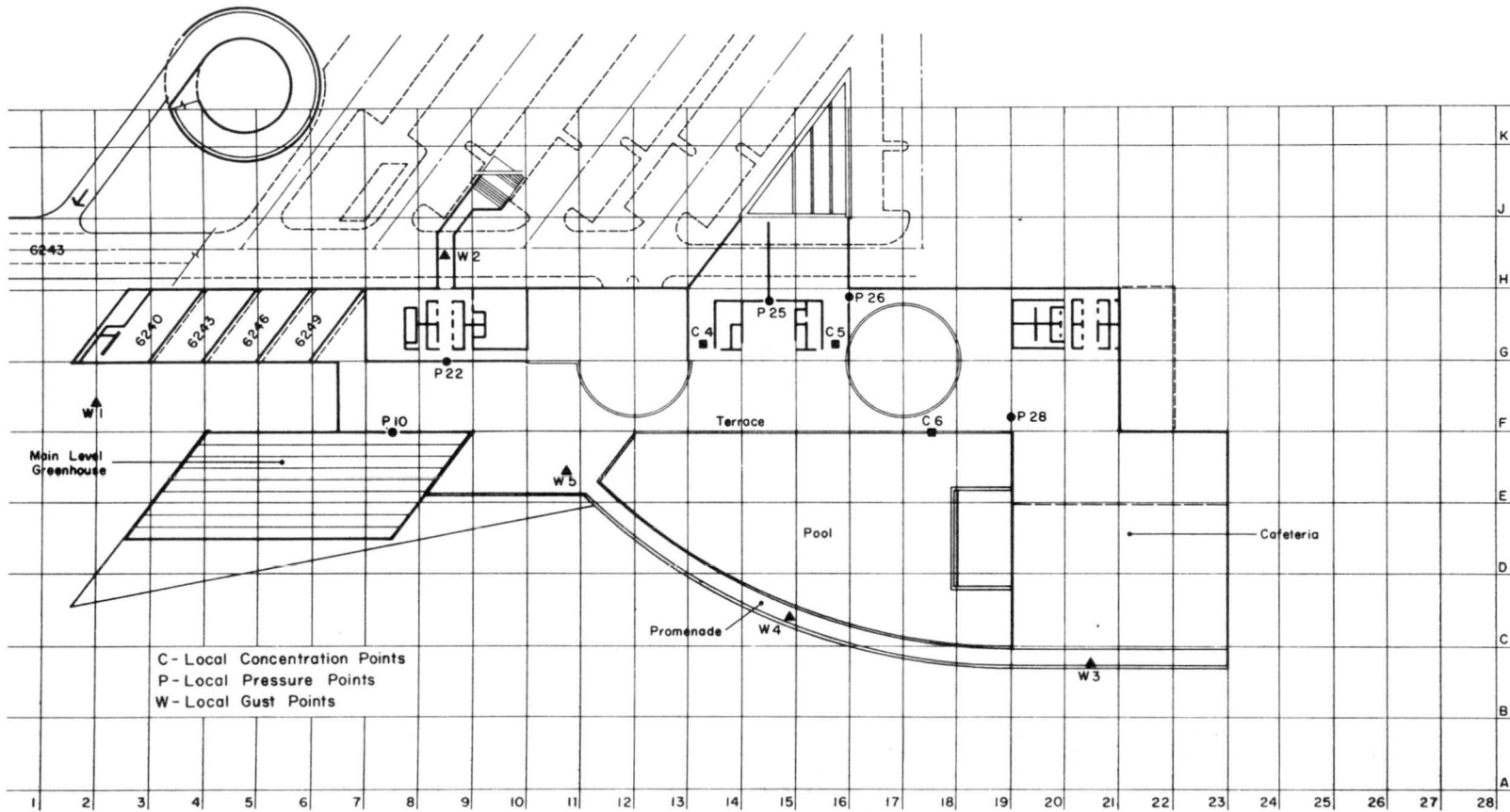
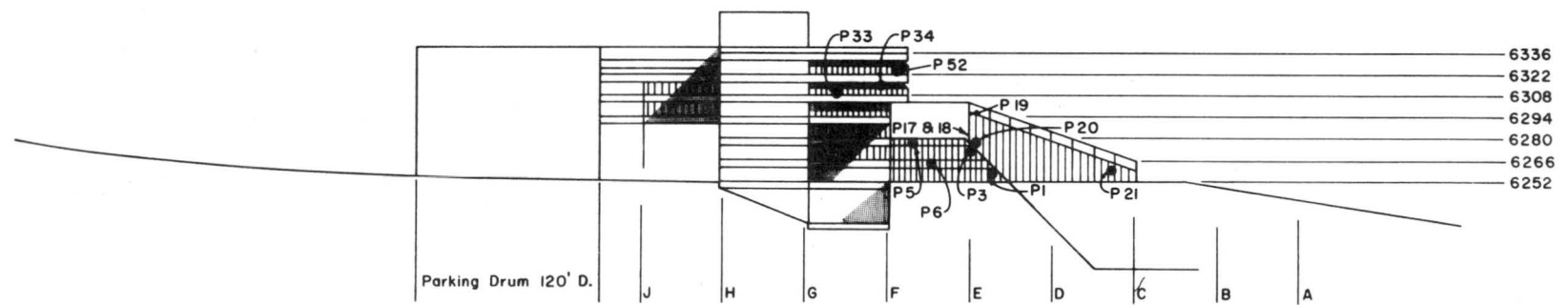
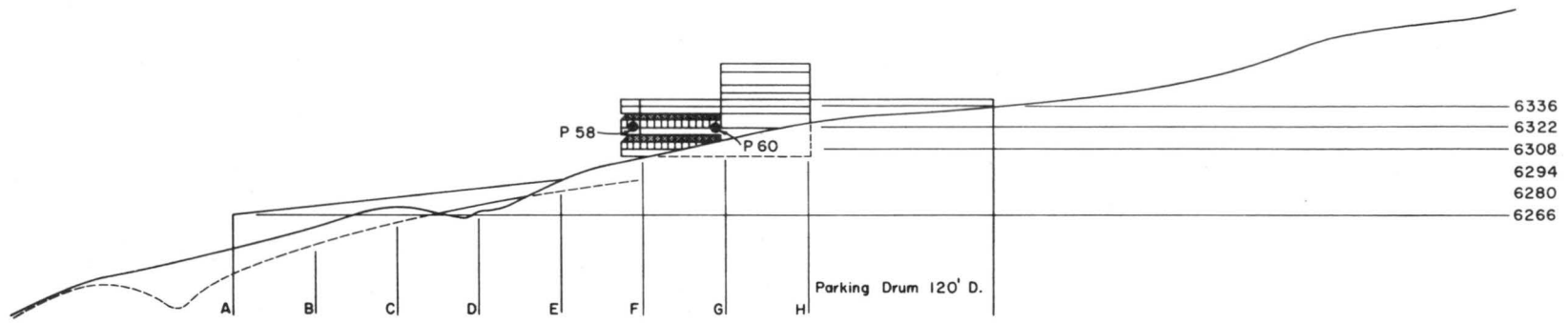
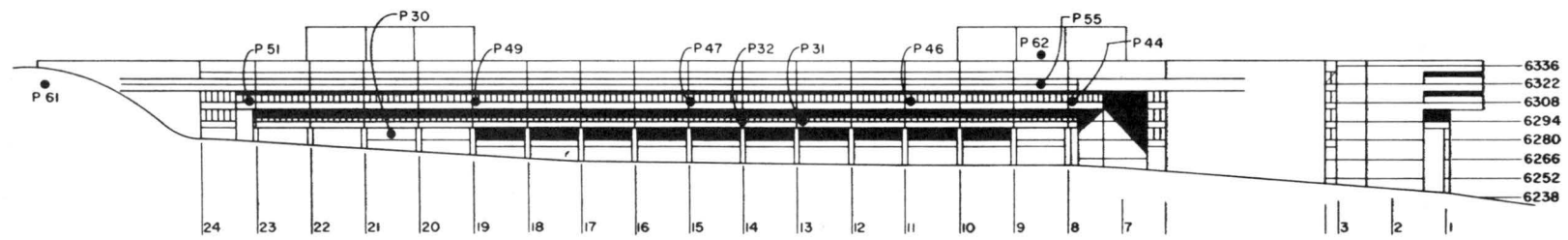


Fig. 18 Plan View at Elevation 6252 Indicating Locations of Points where Local Concentrations, Gusts and Pressures were Measured.

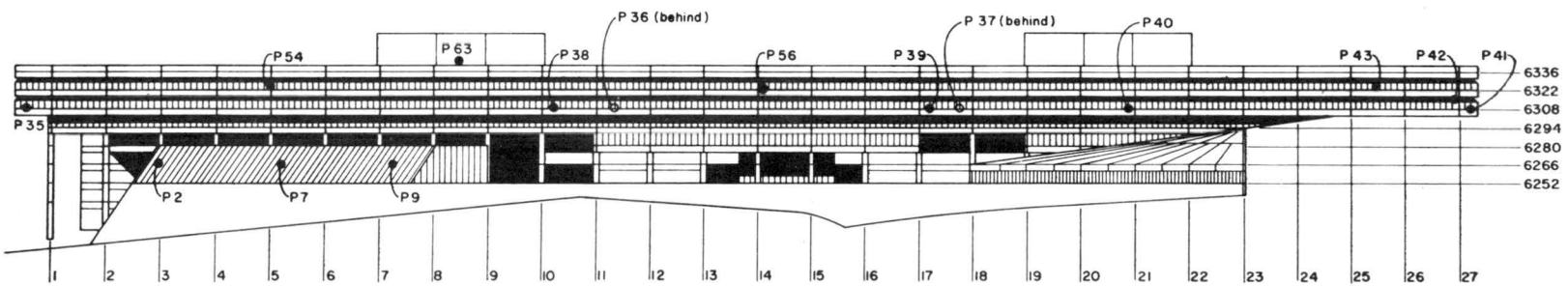


P-Local Pressure Points

Fig. 19 Locations of Pressure Taps on N and S Elevations.



West Elevation



East Elevation

P-Local Pressure Points

Fig. 20 Locations of Pressure Taps on E and W Elevations.

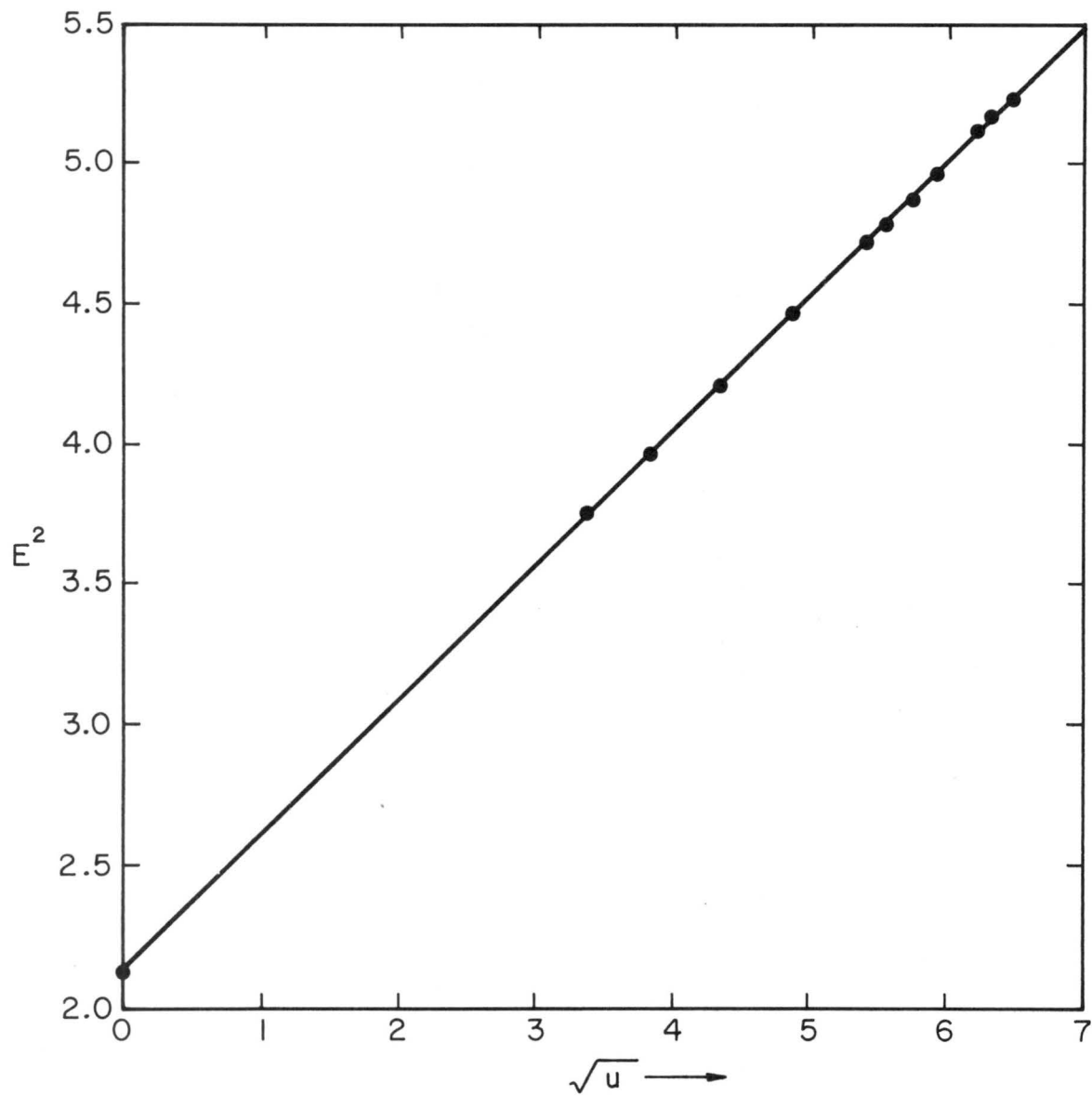


Fig. 21 Typical Calibration of Hot Wire.

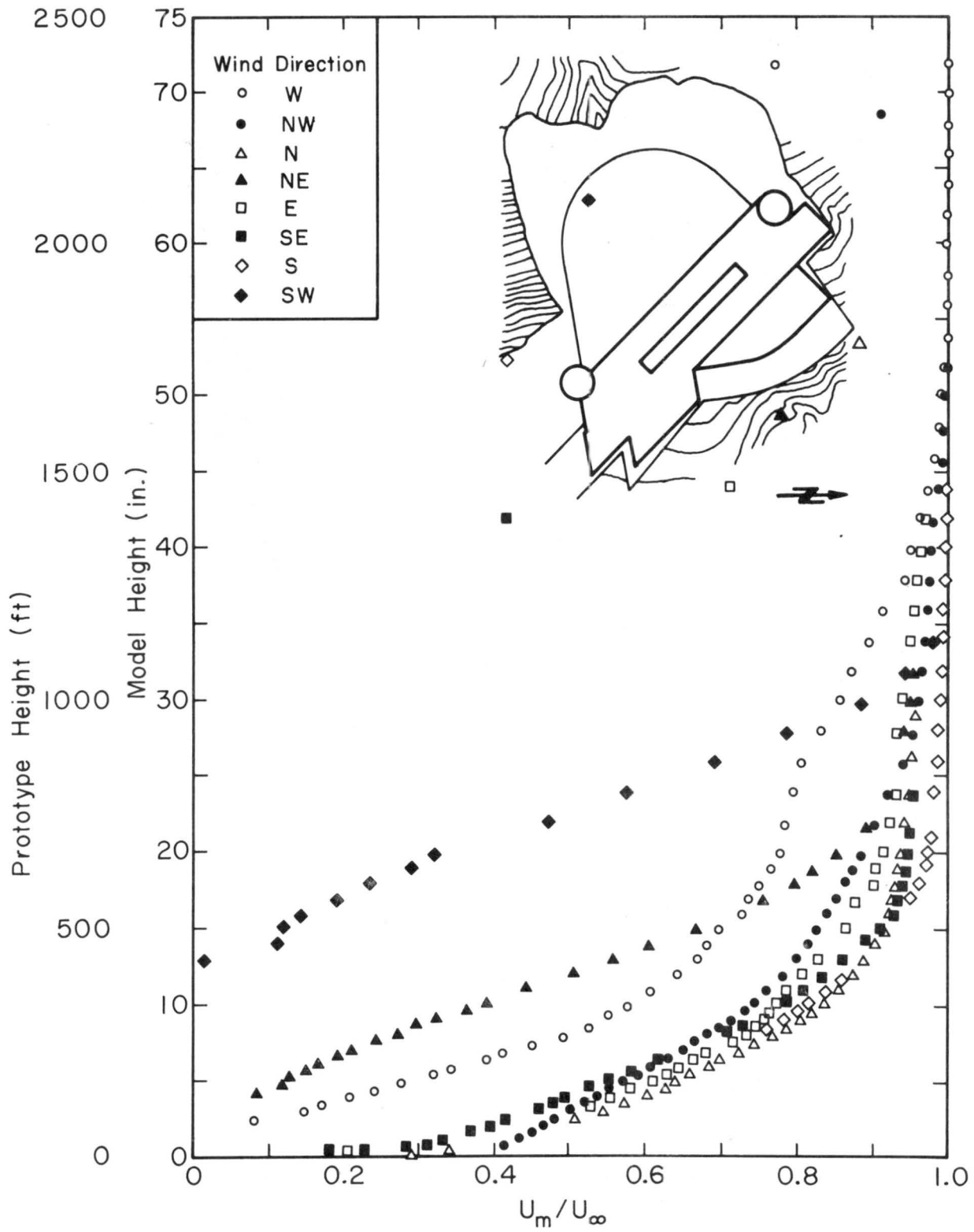


Fig. 22 Mean Velocity Profiles at 300 ft Upwind of Building:  
Free Stream Wind Speed = 45 ft/sec.

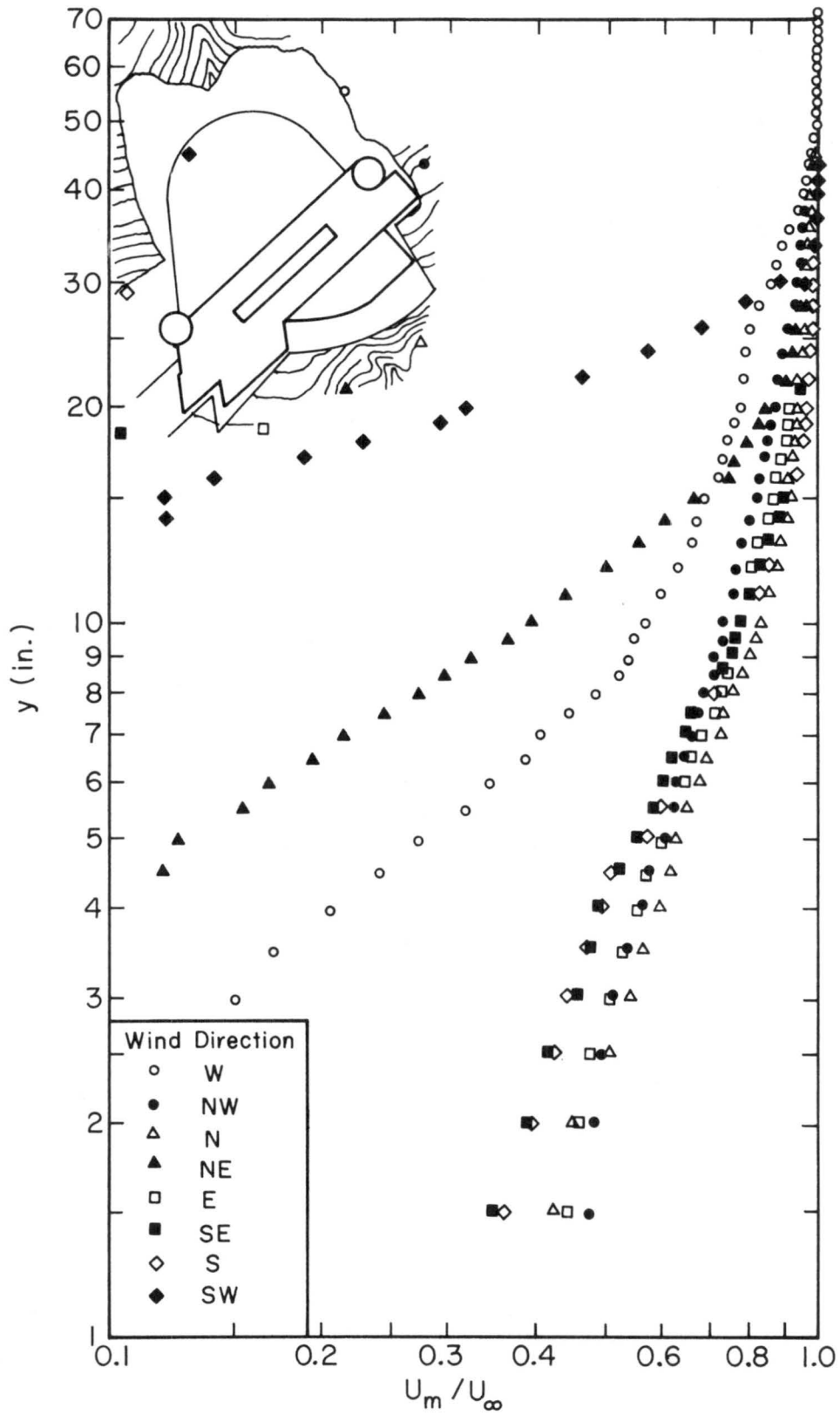


Fig. 23 Log-Log Plots of Mean Velocity Profiles at 300 ft Upwind of the Building.

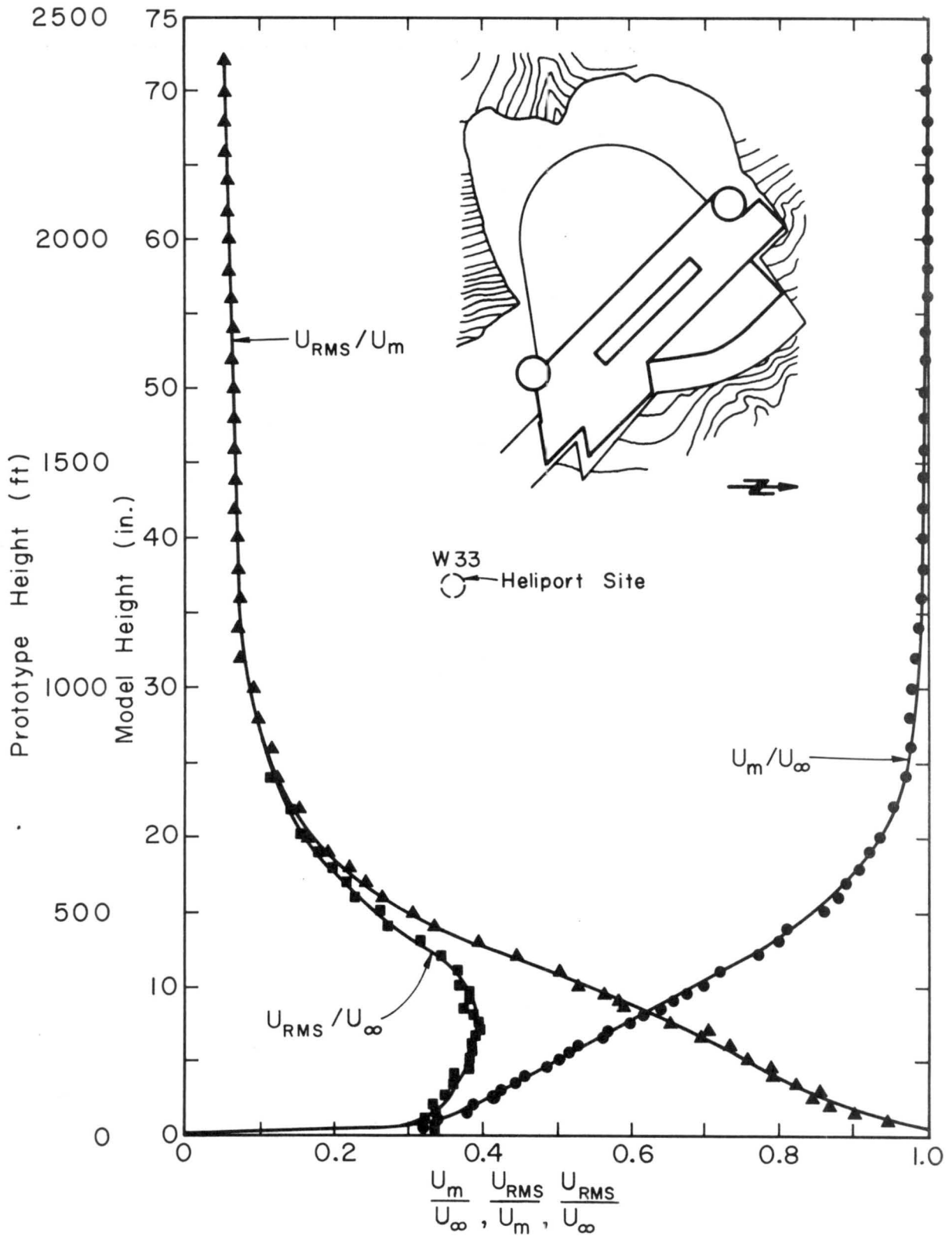


Fig. 24 Mean Velocity and Turbulence Intensity Profiles at the Heliport for the Case of Wind Approaching from W.

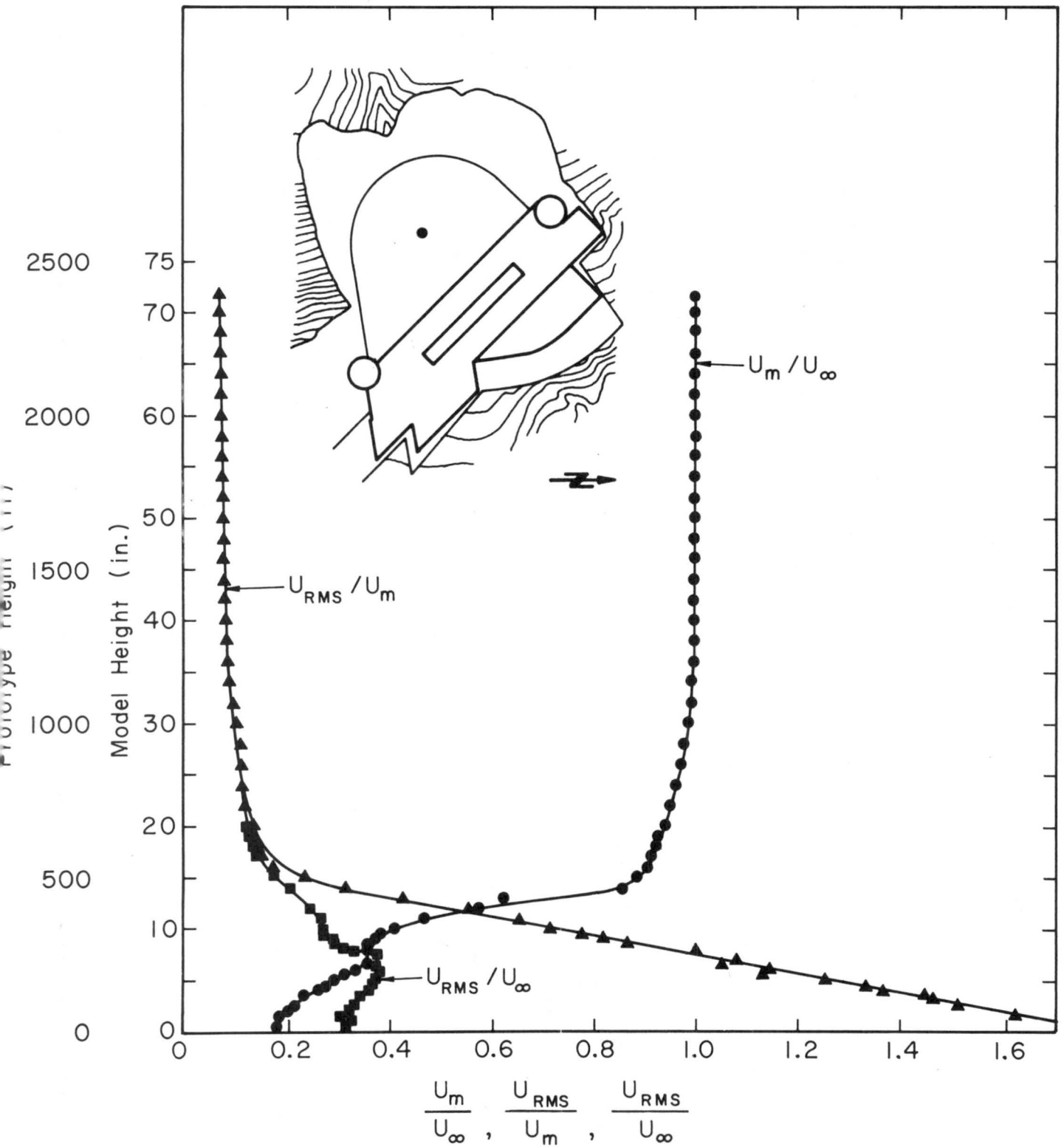
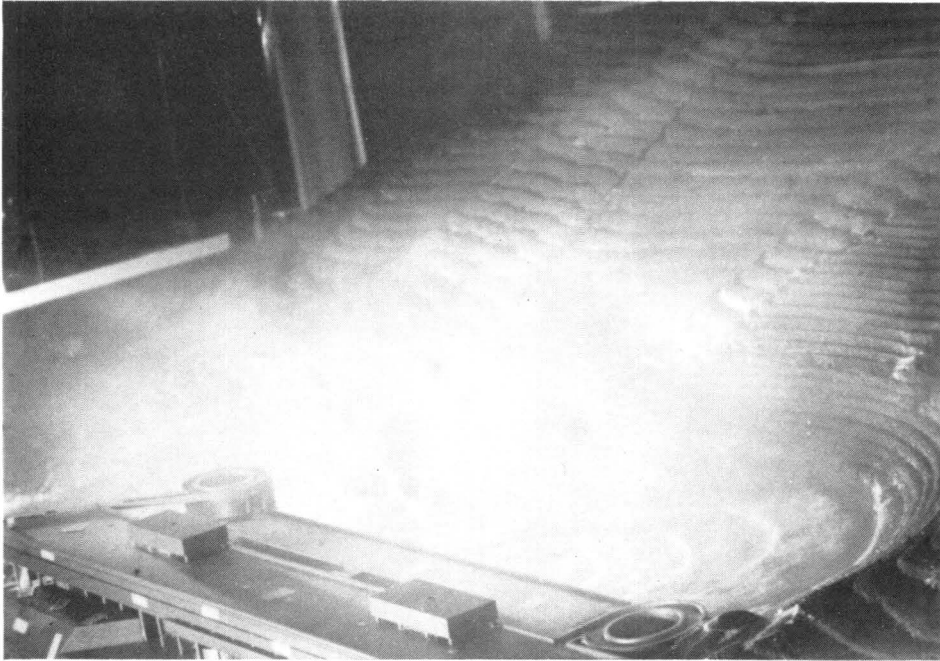
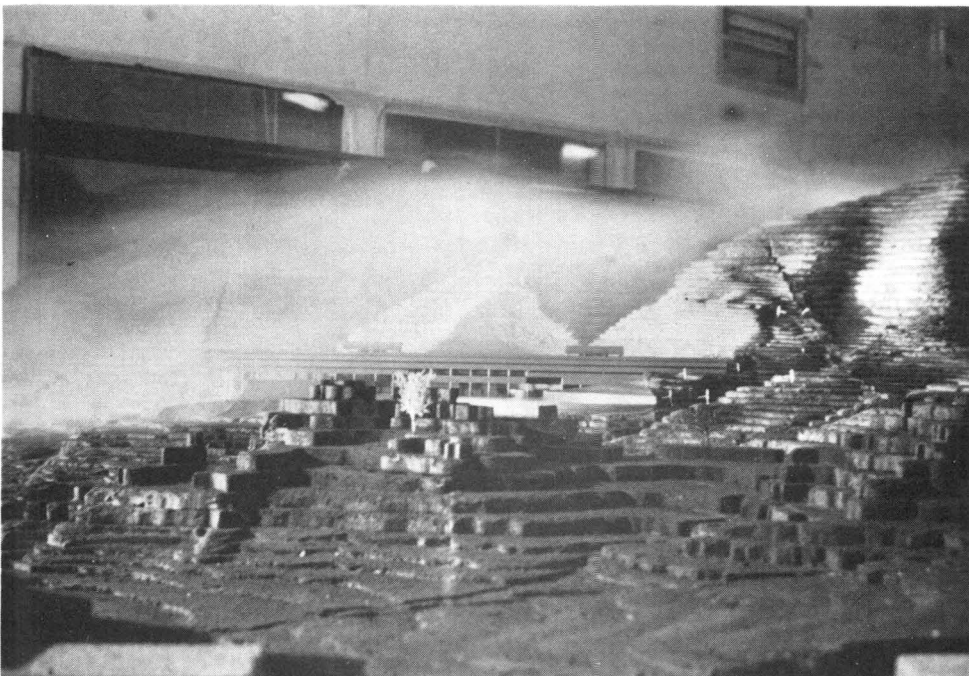


Fig. 25 Mean Velocity and Turbulence Intensity Profiles in the Parking Area for the Case of Wind Approaching from W.



(a) Wind Approaching from SW

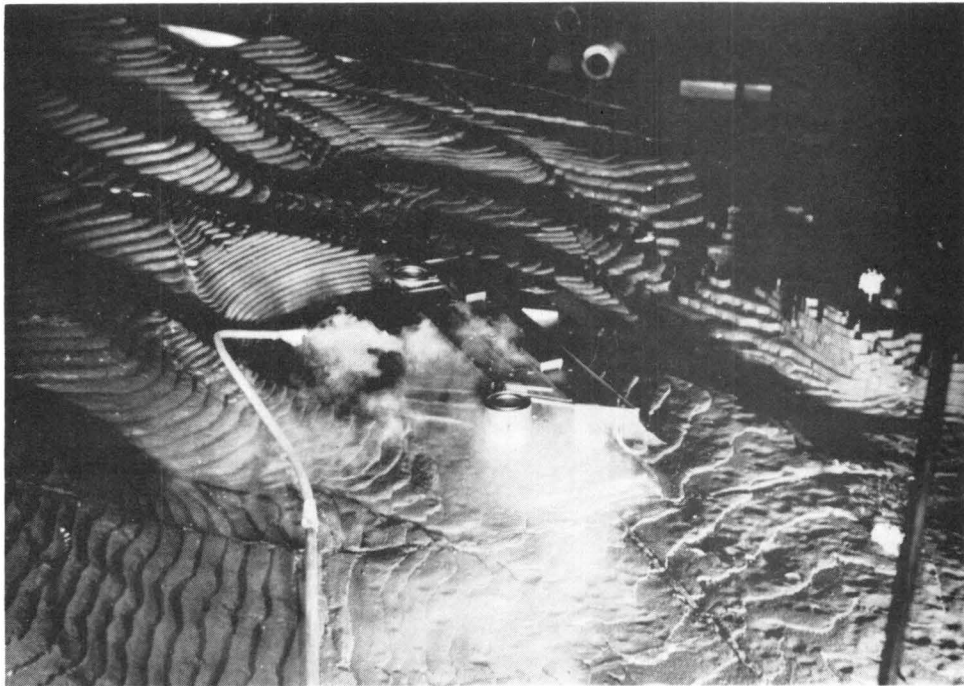


(b) Wind Approaching from NW

Figure 26 General Approach Flow Pattern



(a) Wind Approaching from West.



(b) Wind Approaching from North.

Figure 27 Wake Flow Due to the Building.

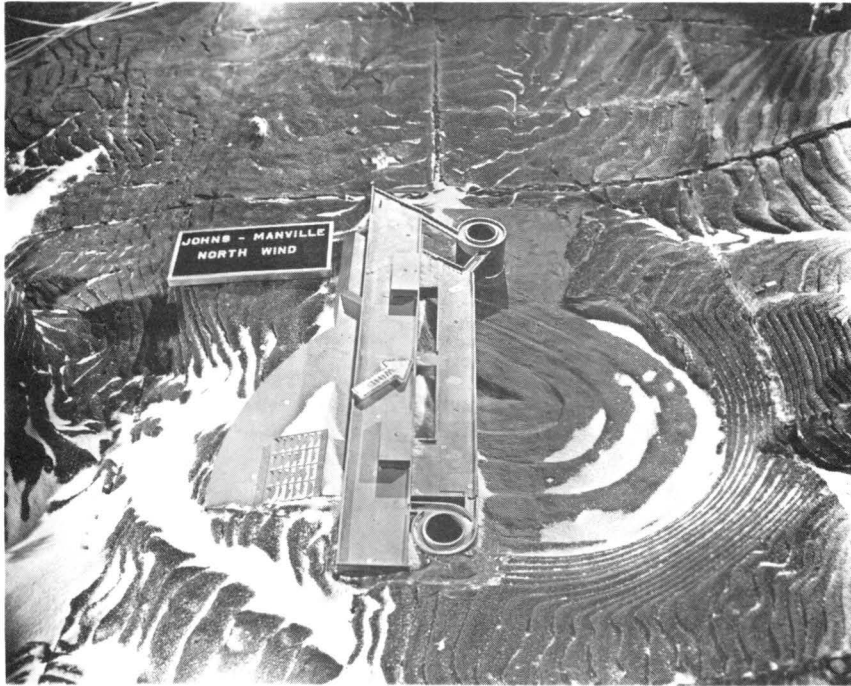


Figure 28 Snow Drift Locations Due to Winds Approaching from the North.

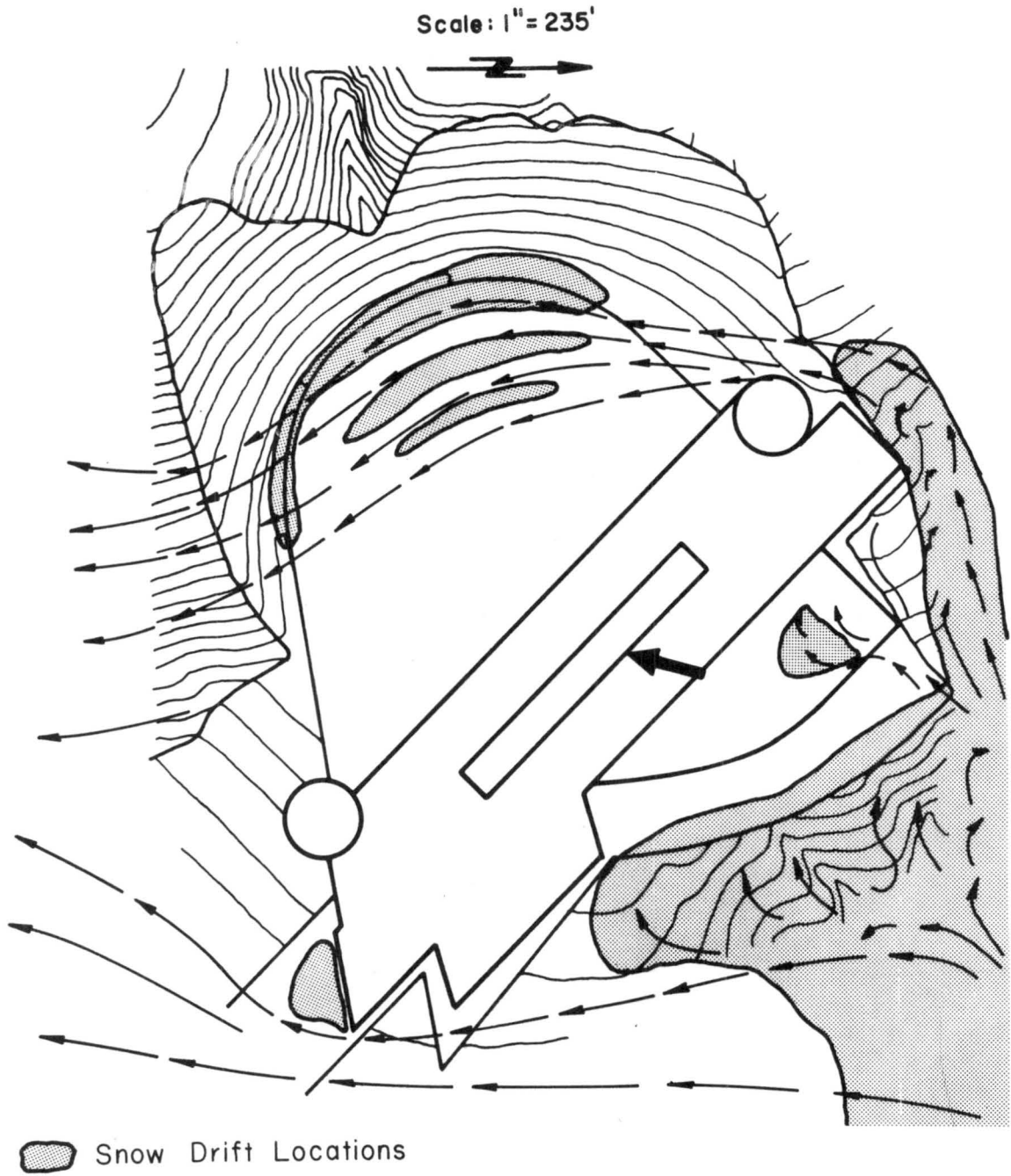


Fig. 29 Mean Drift Paths Due to N Wind.

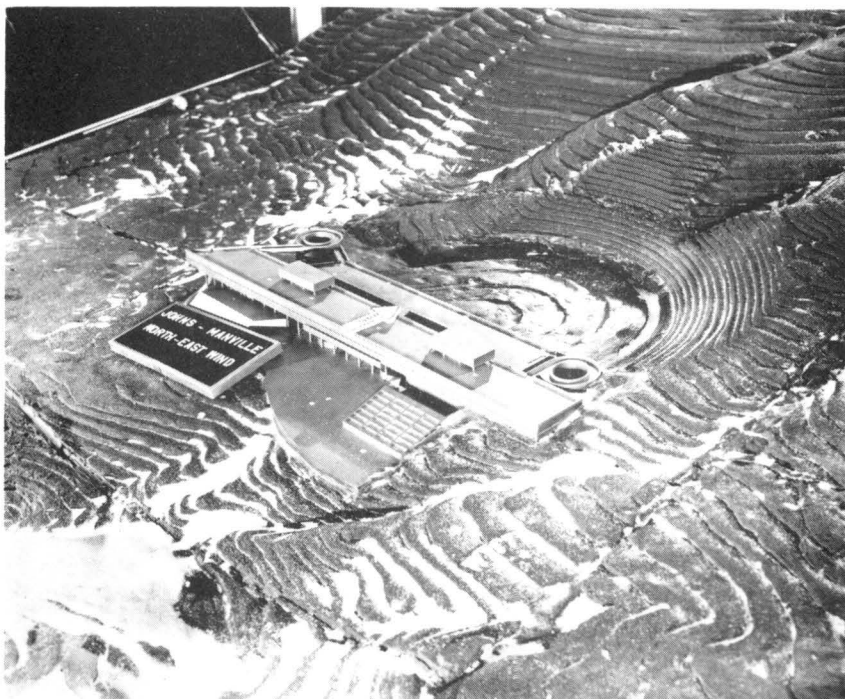
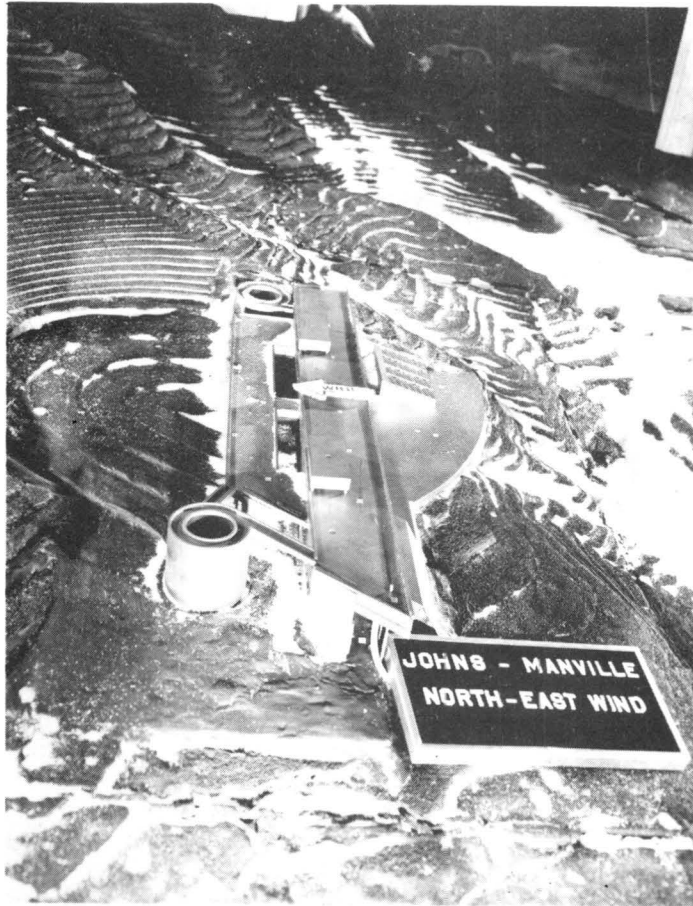


Figure 30 Snow Drift Locations Due to Winds Approaching from the Northeast.

Scale: 1" = 235'

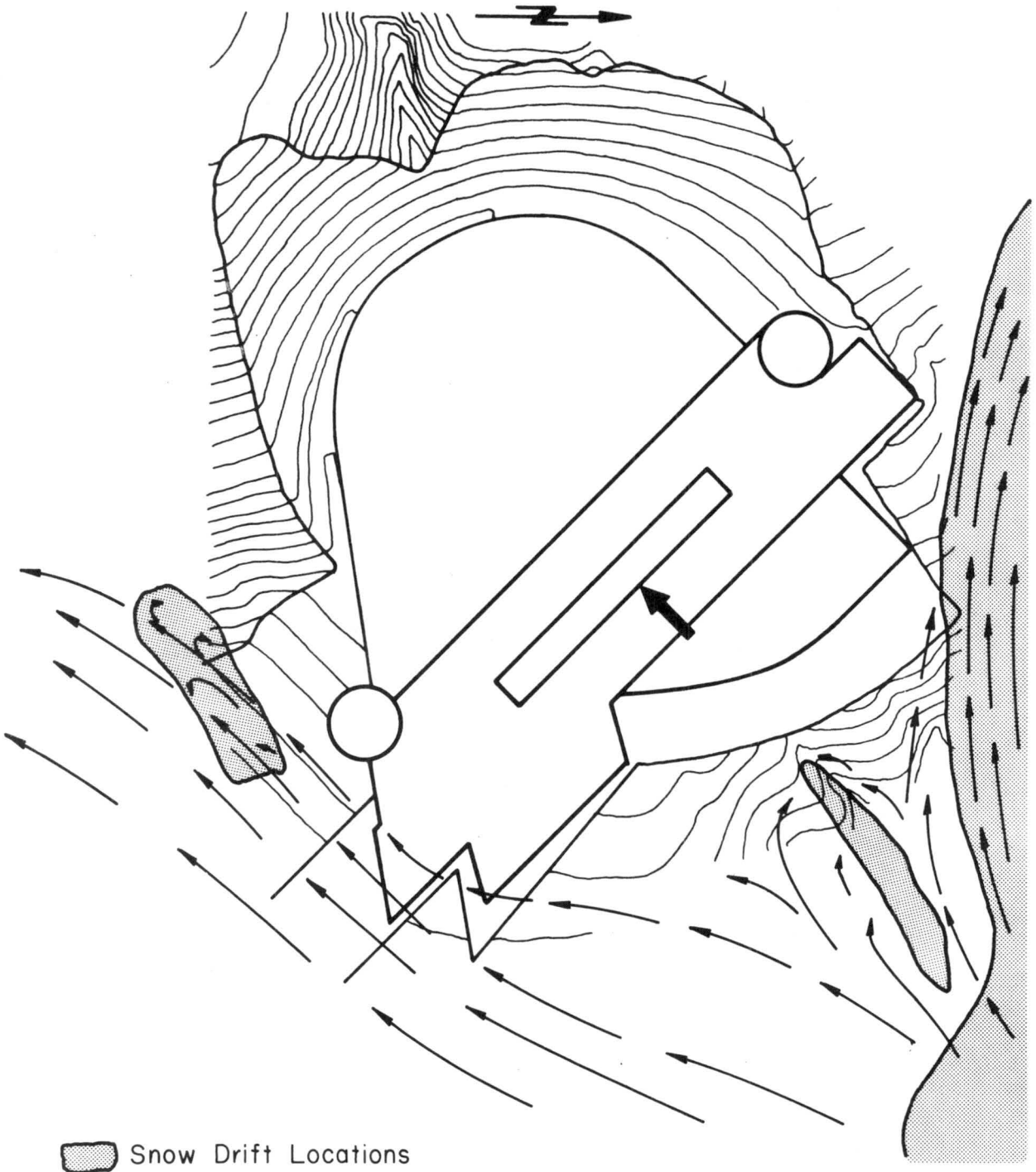


Fig. 31 Mean Drift Paths Due to NE Wind.



Figure 32 Snow Drift Locations Due to Winds Approaching from the East.

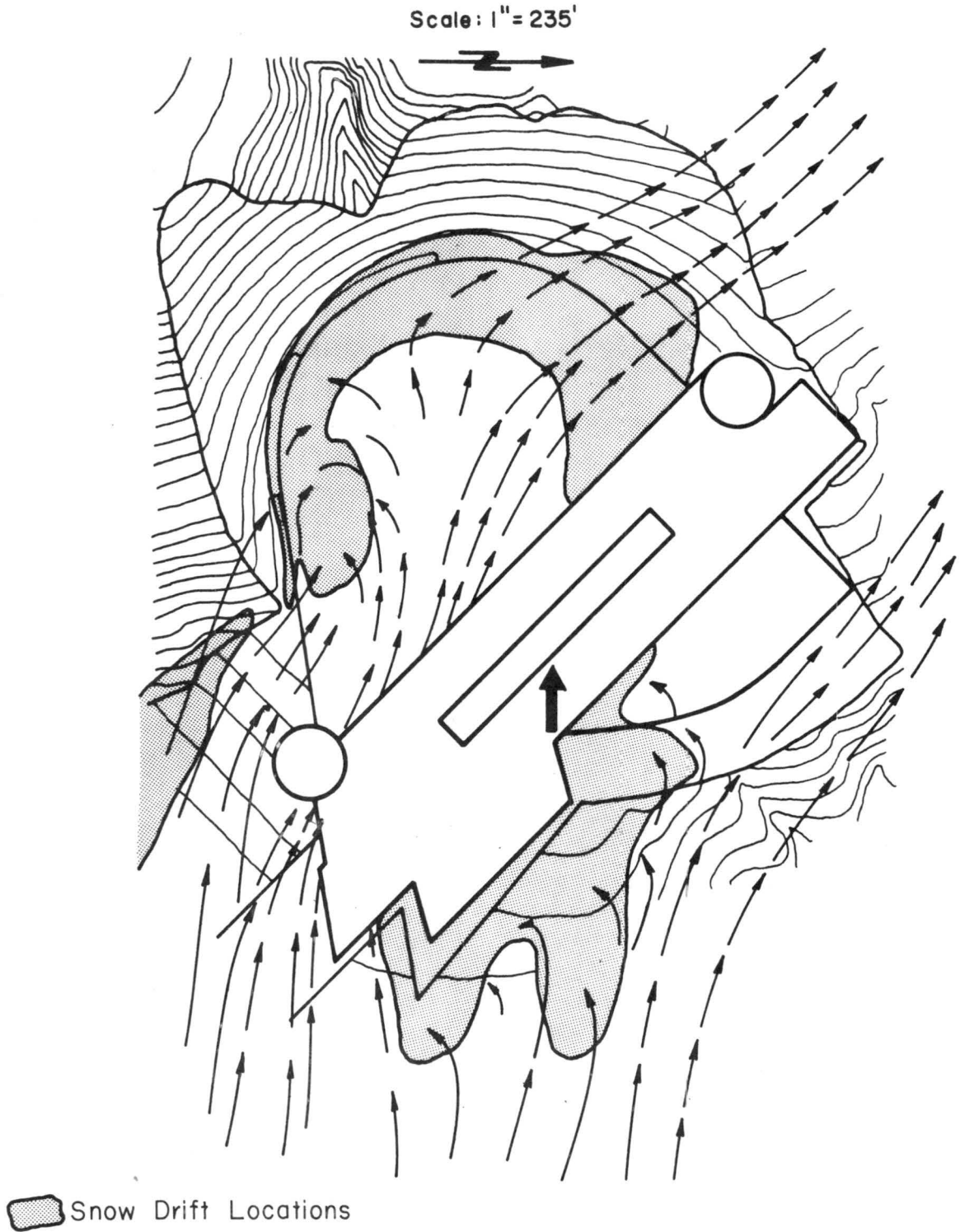


Fig. 33 Mean Drift Paths Due to the E Wind.

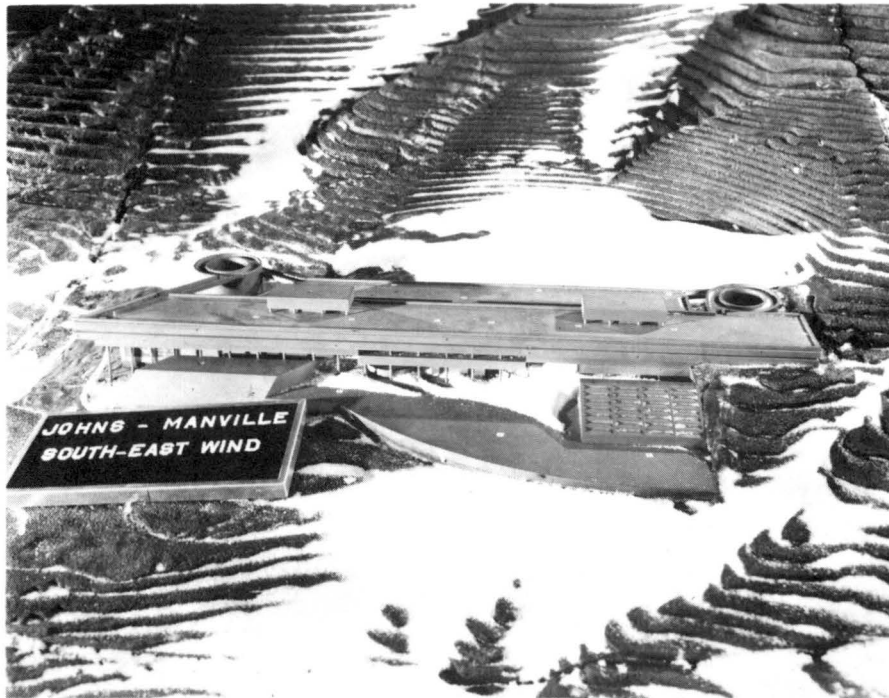


Figure 34 Snow Drift Locations Due to Winds Approaching from the Southeast.

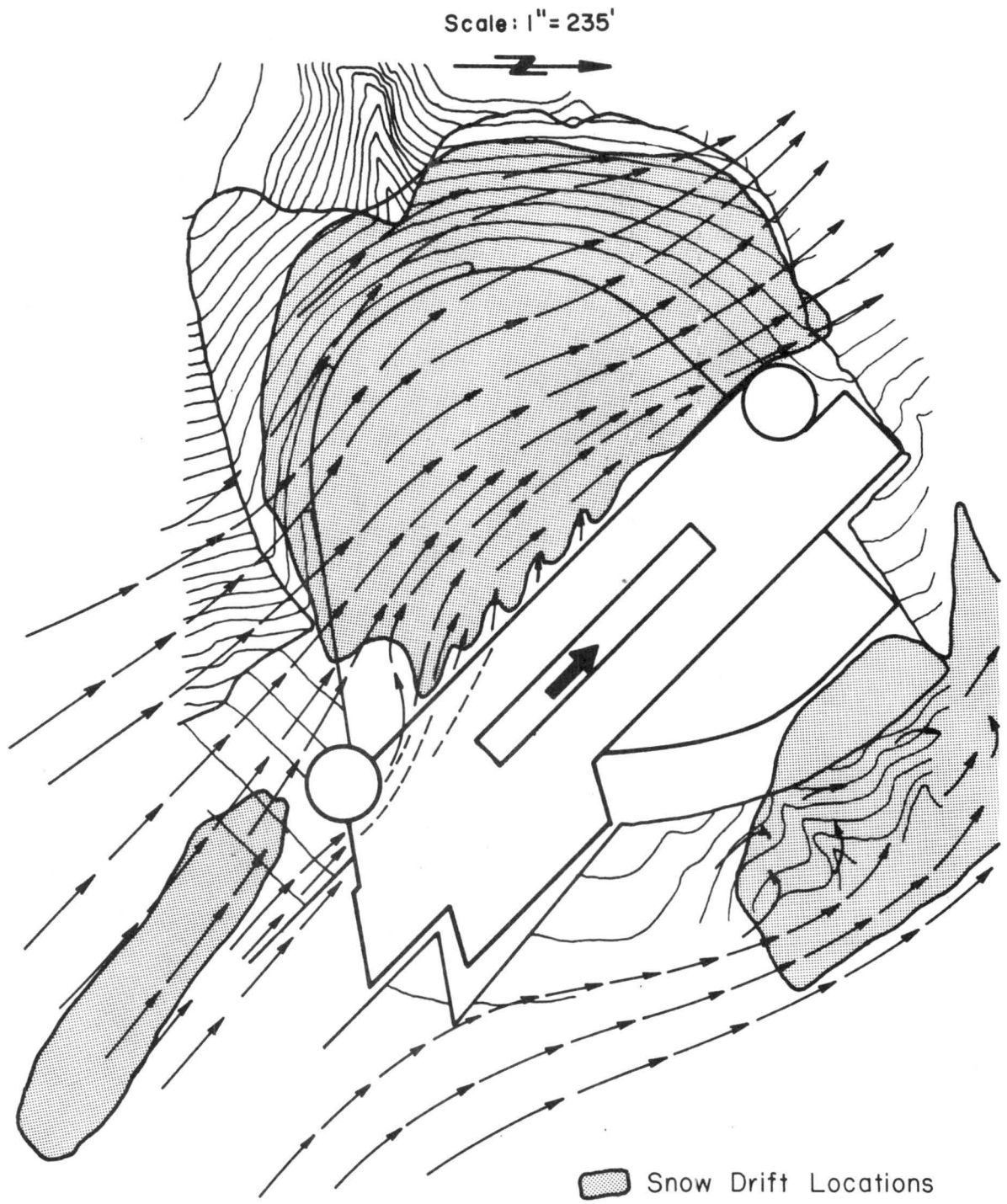


Fig. 35 Mean Drift Paths Due to the SE Wind

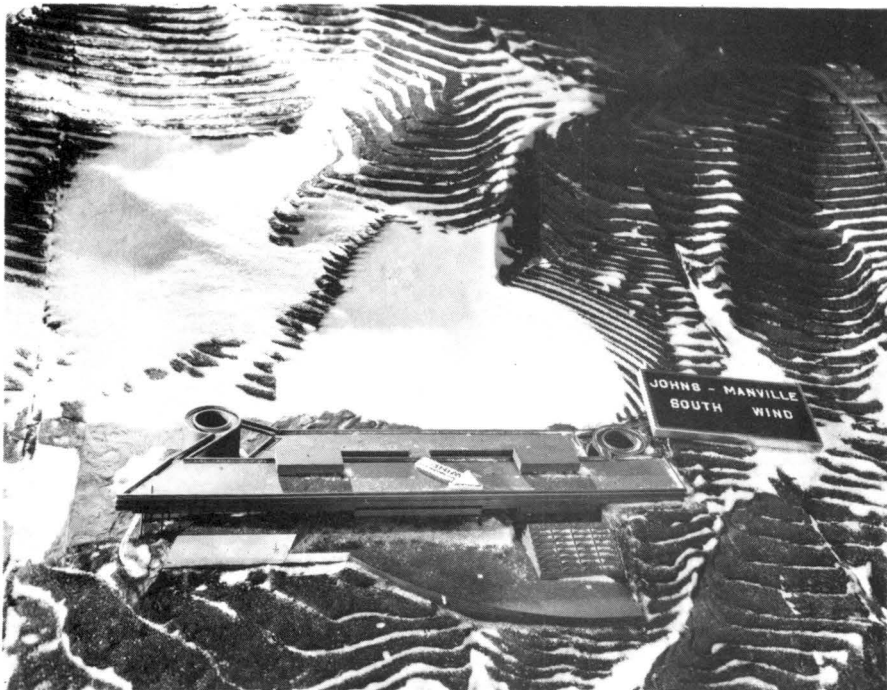
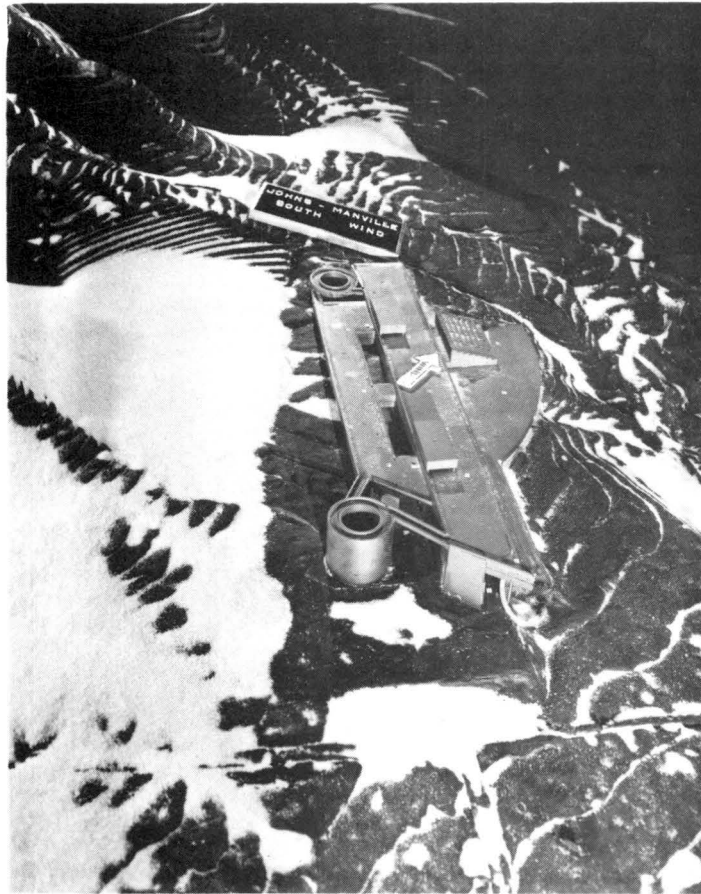


Figure 36 Snow Drift Locations Due to Winds Approaching from the South.

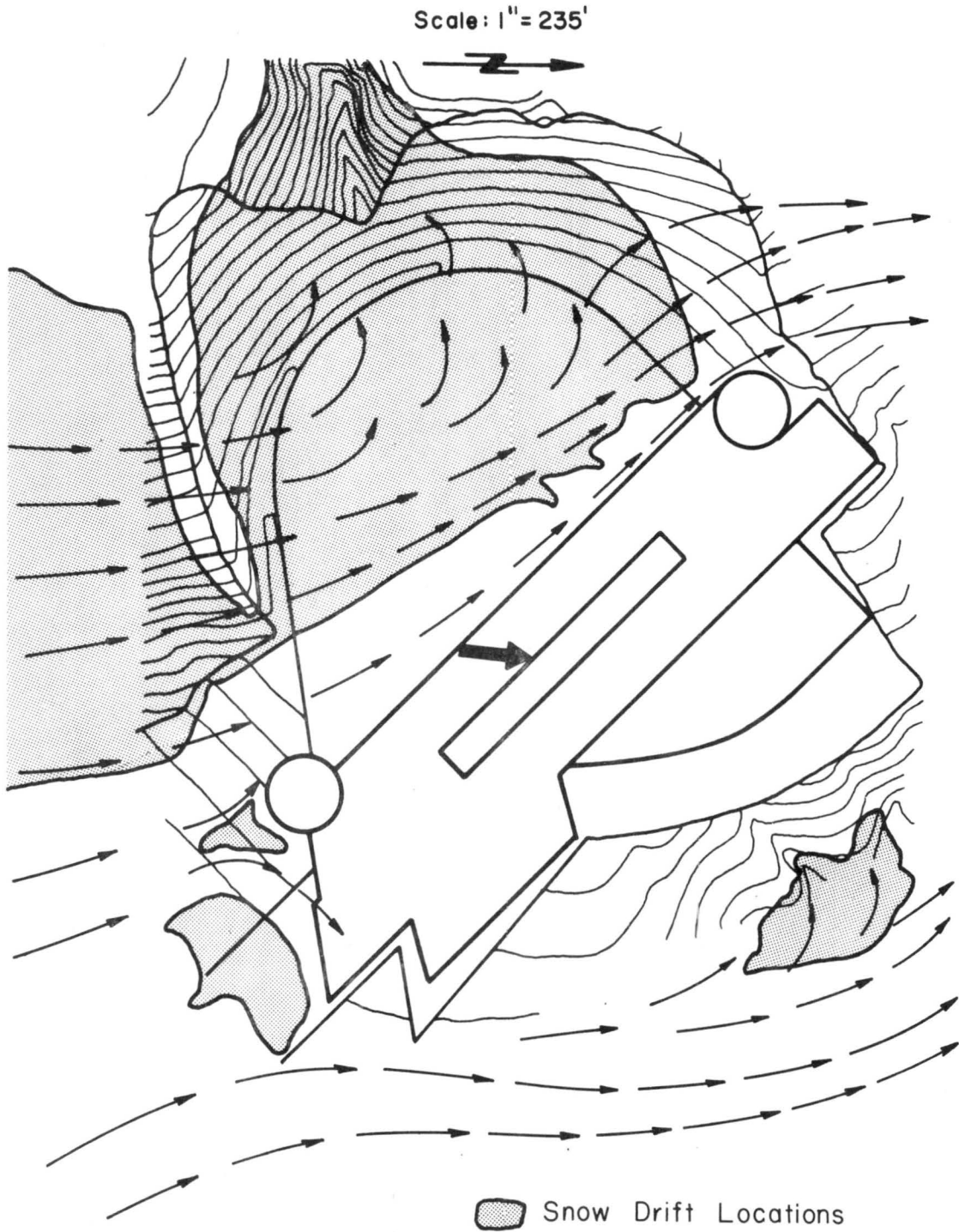


Fig. 37 Mean Drift Paths Due to the S Wind.

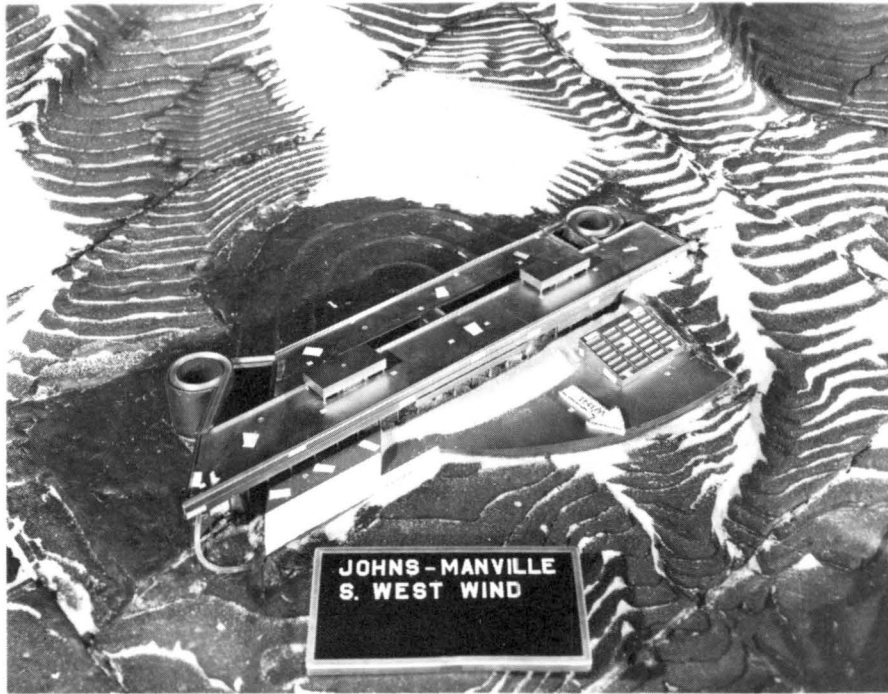


Figure 38 Snow Drift Locations Due to Winds Approaching from the Southwest.

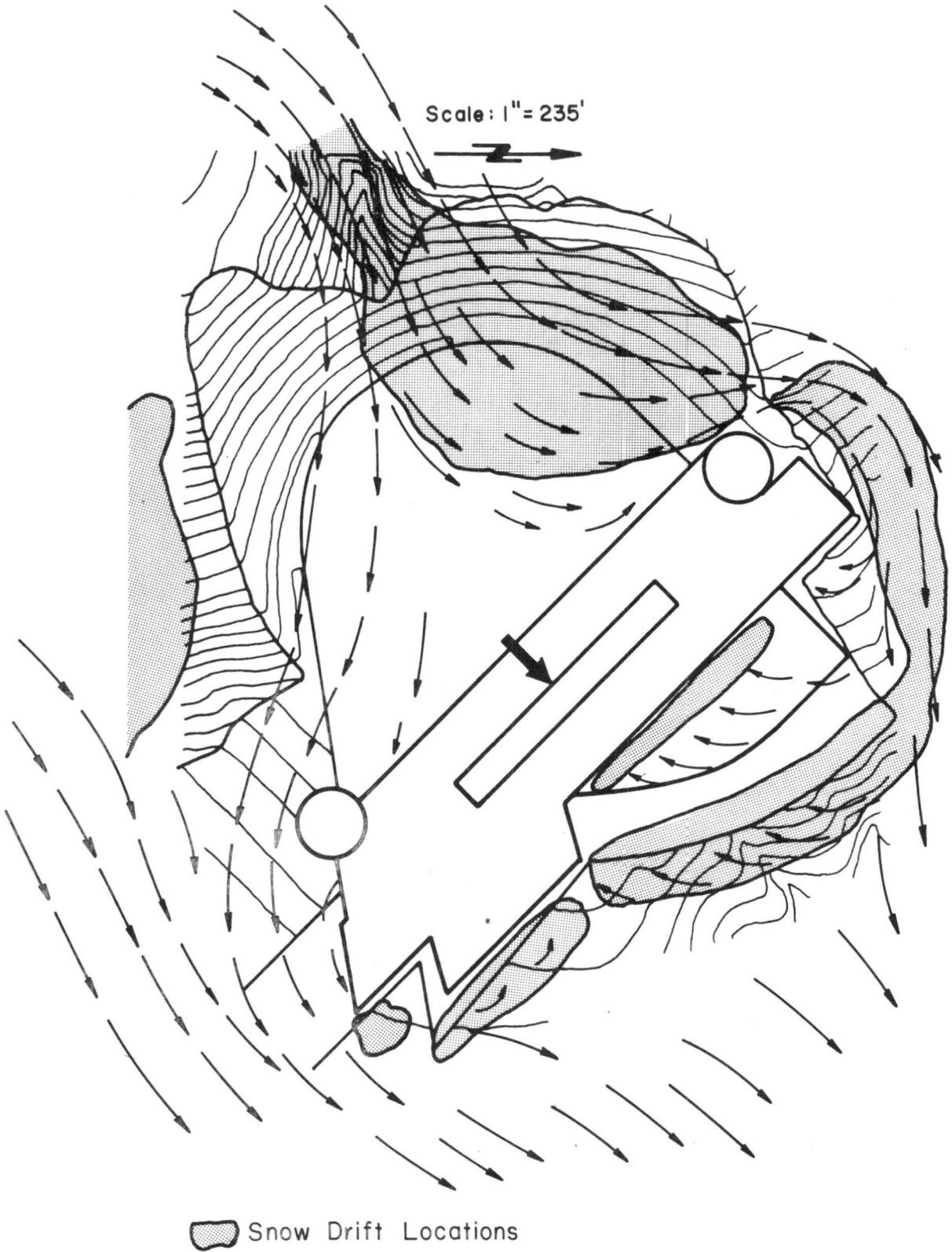


Fig. 39 Mean Drift Paths Due to the SW Wind.

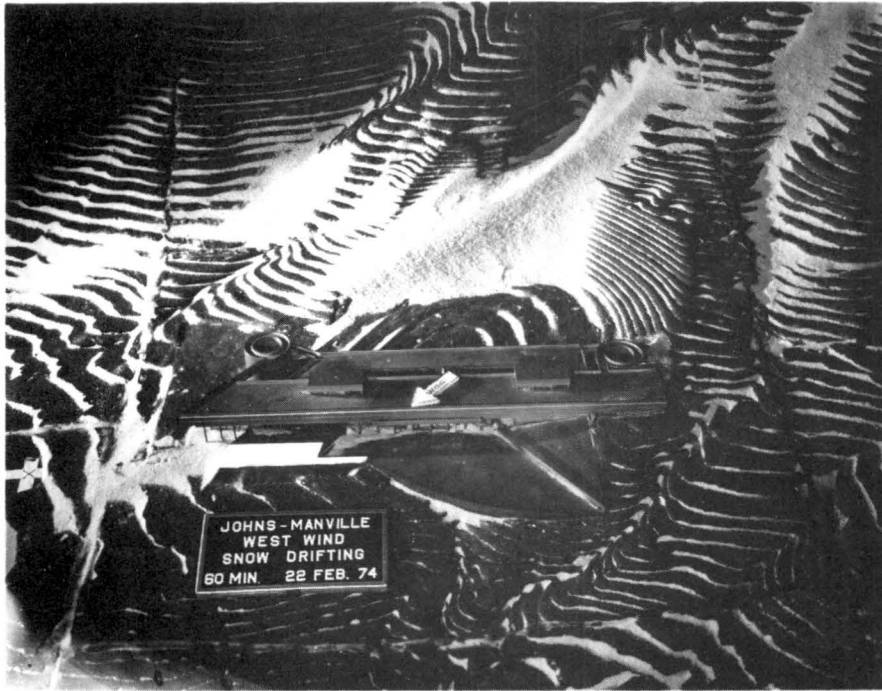


Figure 40 Snow Drift Locations Due to Wind Approaching from the West.

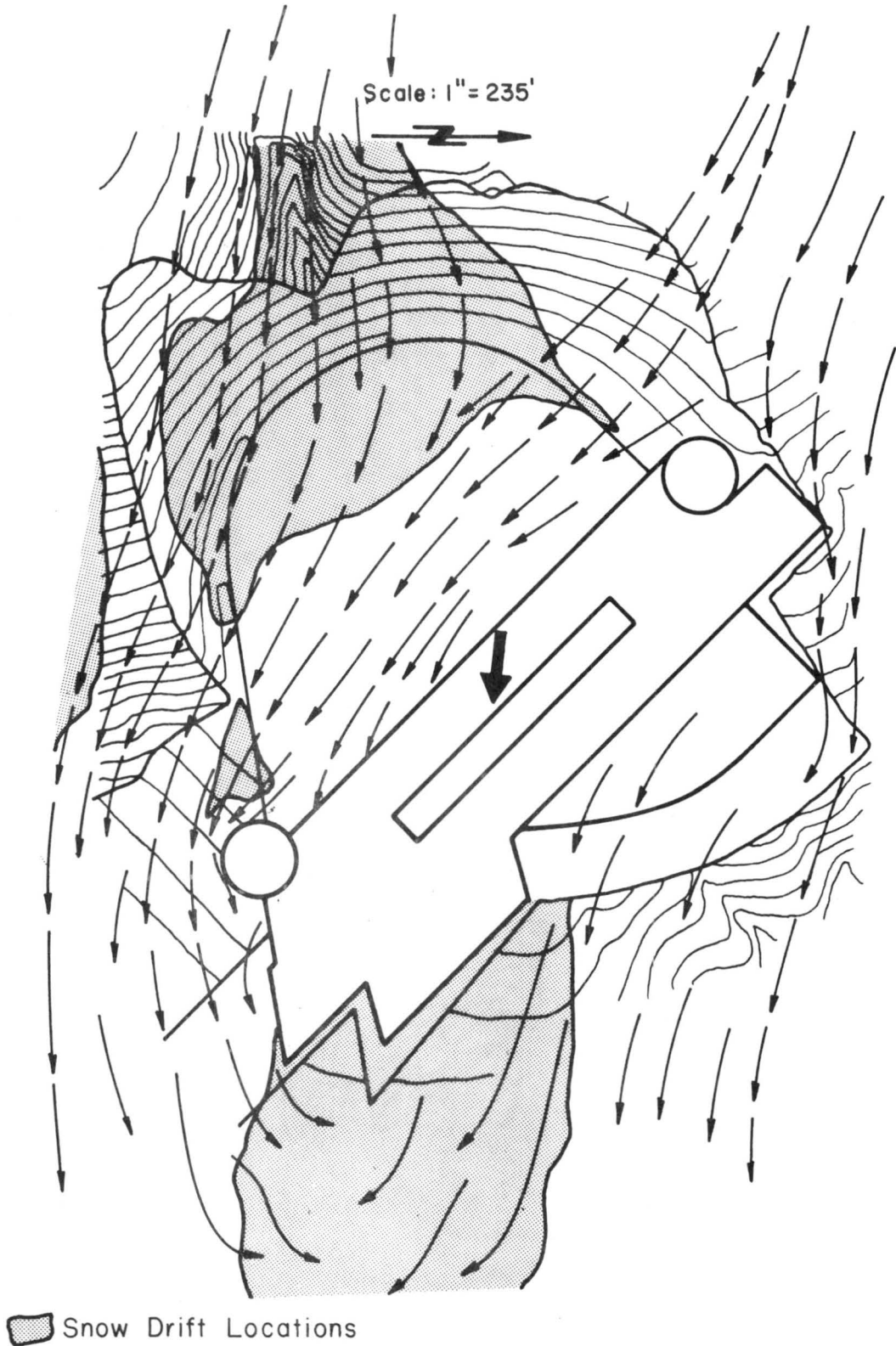


Fig. 41 Mean Drift Paths Due to the W Wind.

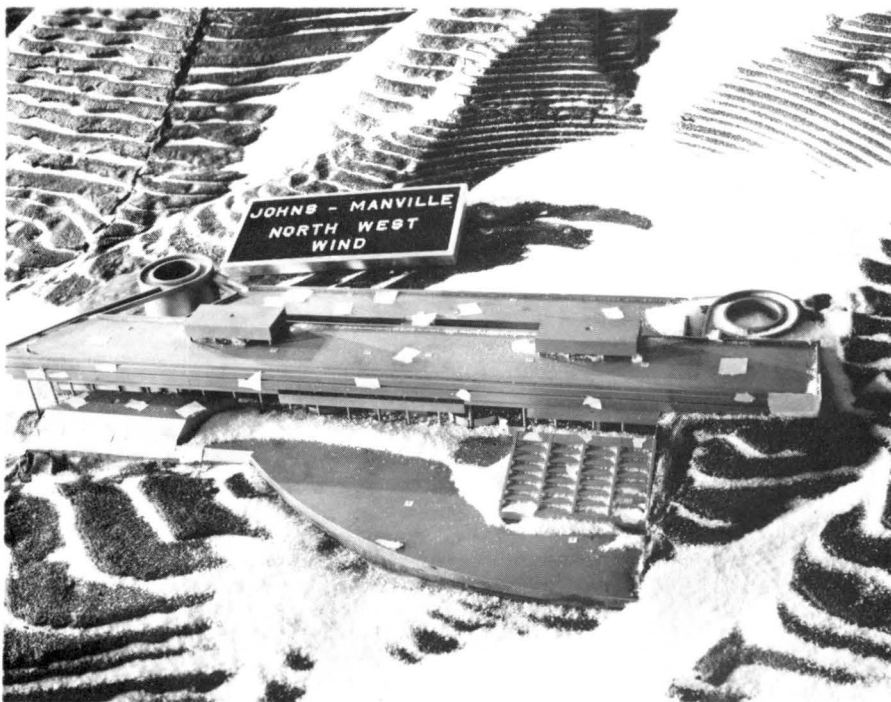


Figure 42 Snow Drift Locations Due to Wind Approaching from the Northwest.

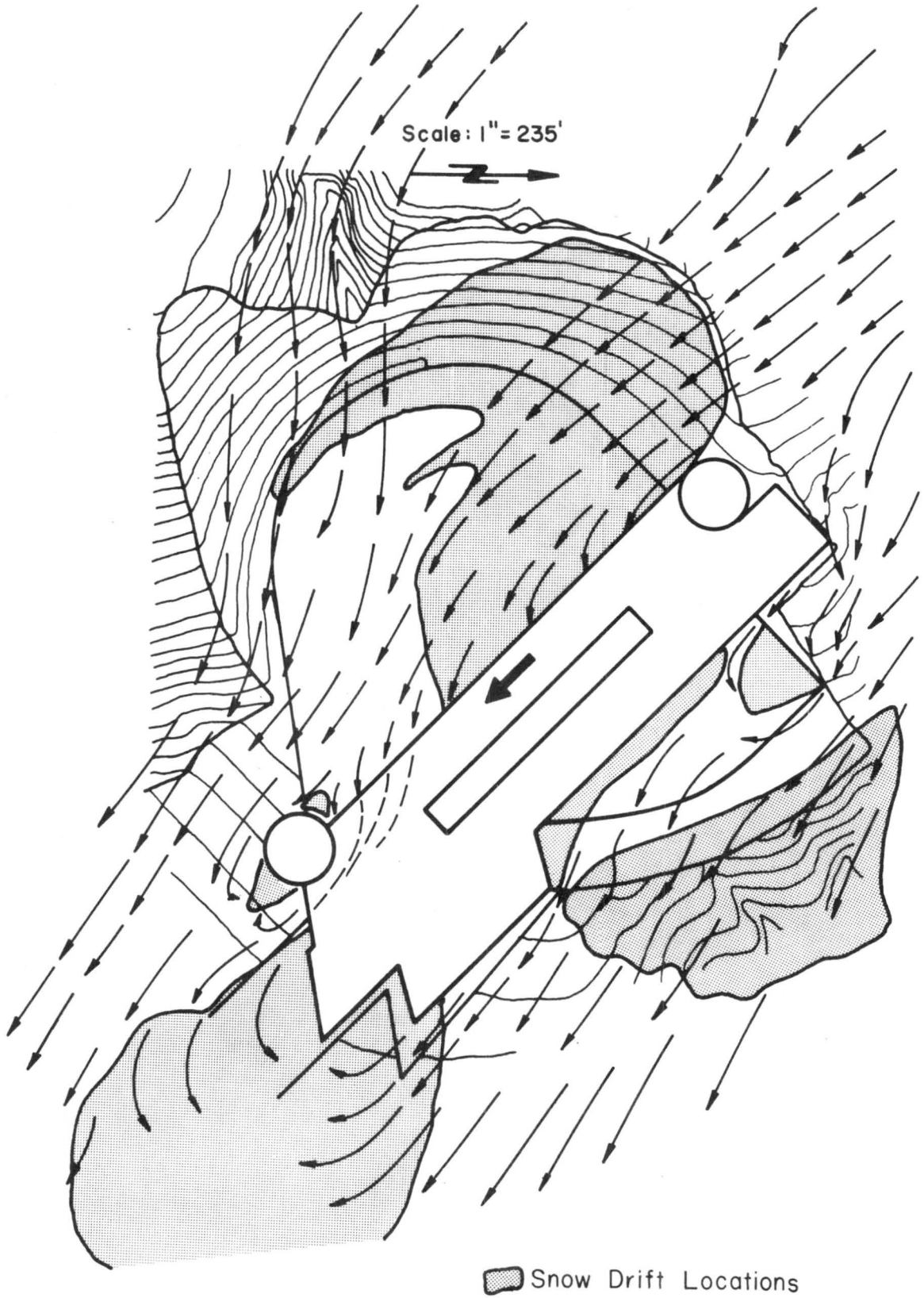


Fig. 43 Mean Drift Paths Due to NW Winds.

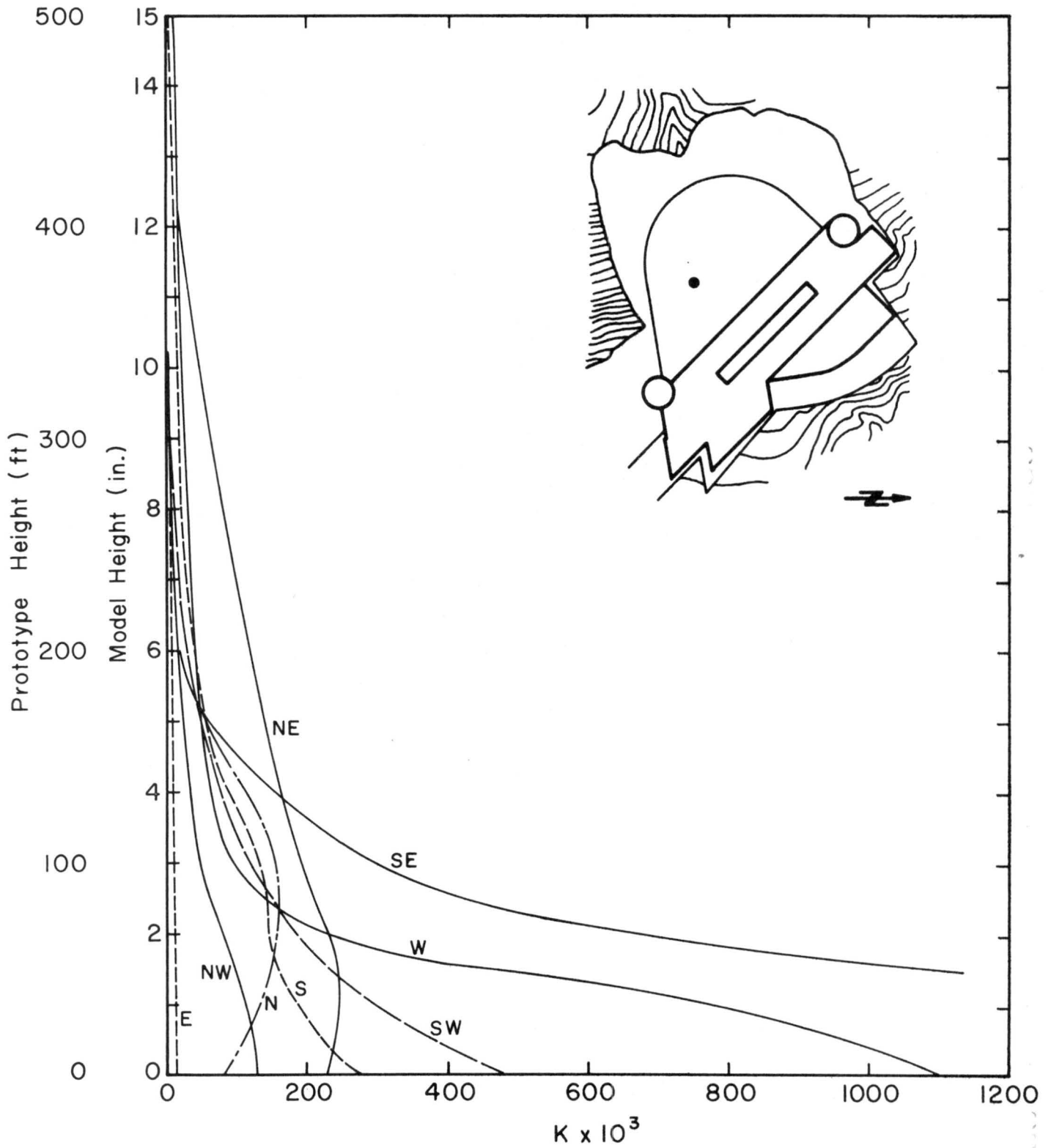


Fig. 44 Vertical Profiles of Concentration Coefficients in the Parking Area for the Cases of Wind Approaching from the N, NE, E, SE, S, SW, W and NW.

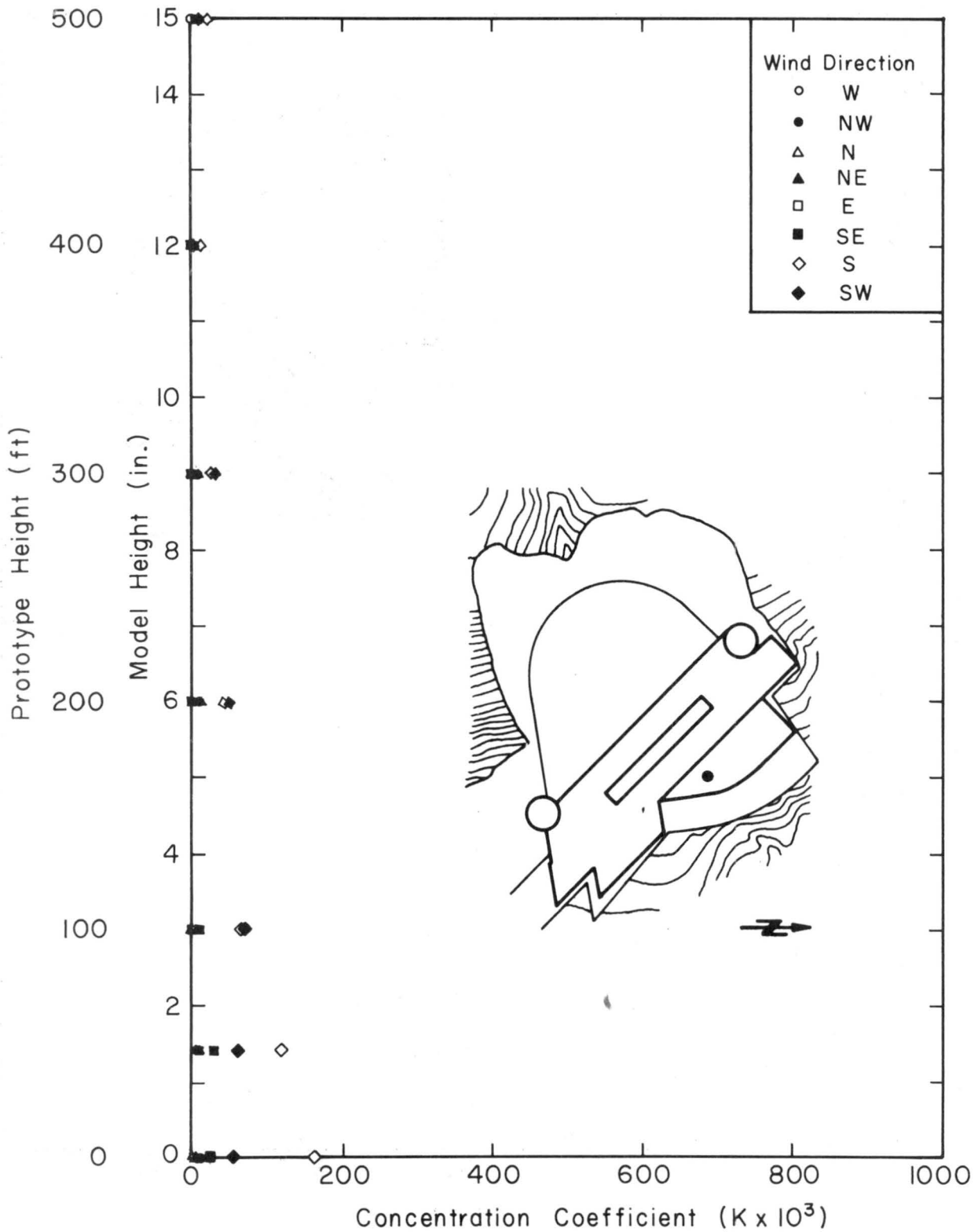


Fig. 45 Vertical Profiles of Concentration Coefficients on the Northeast Side of Building for the Cases of Wind Approaching from the N, NE, E, SE, S, W and NW.

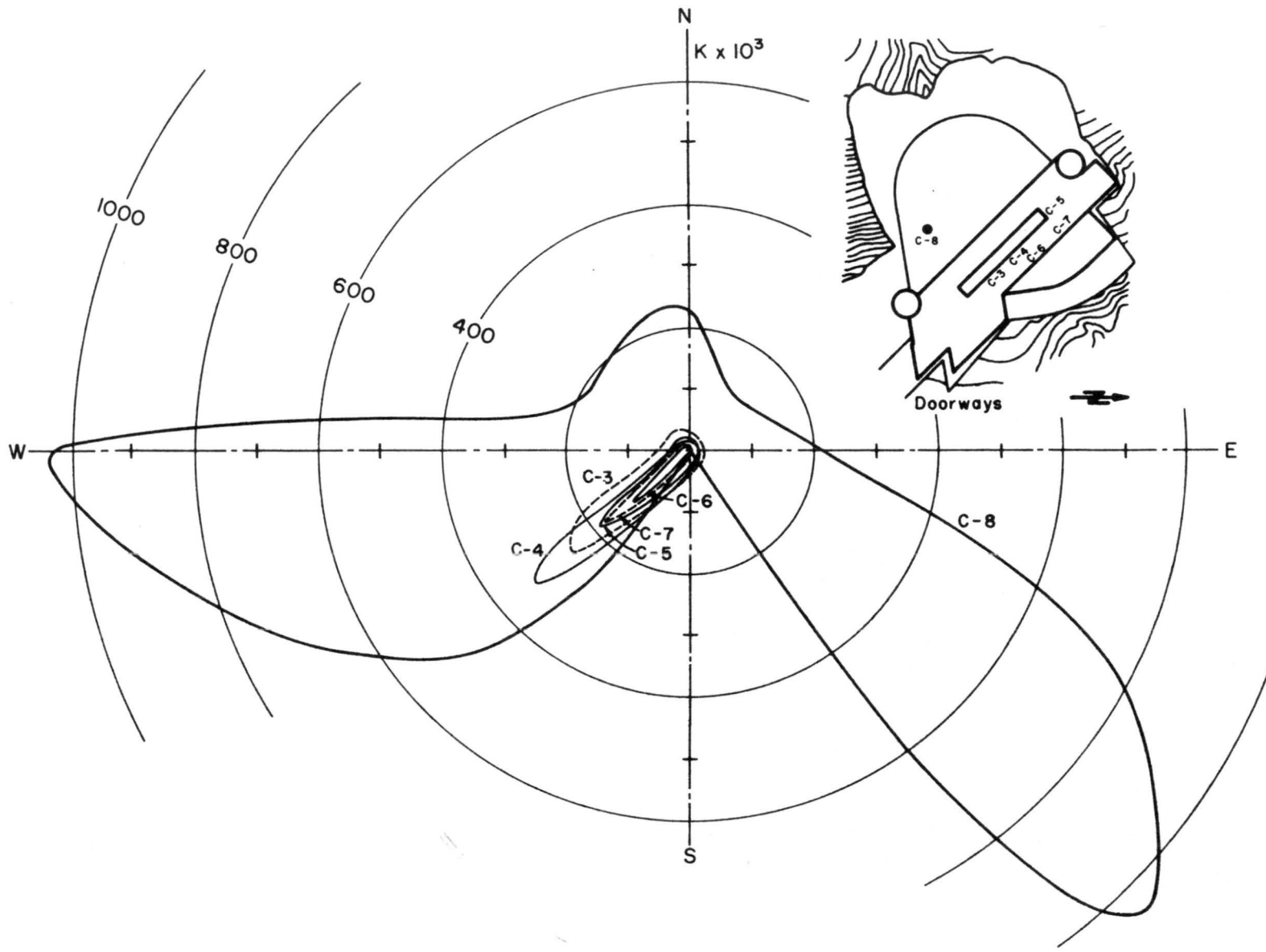


Fig. 46 Effect of Wind Directions on Concentration Coefficients at C3, C4, C5, C6, C7 and C8.

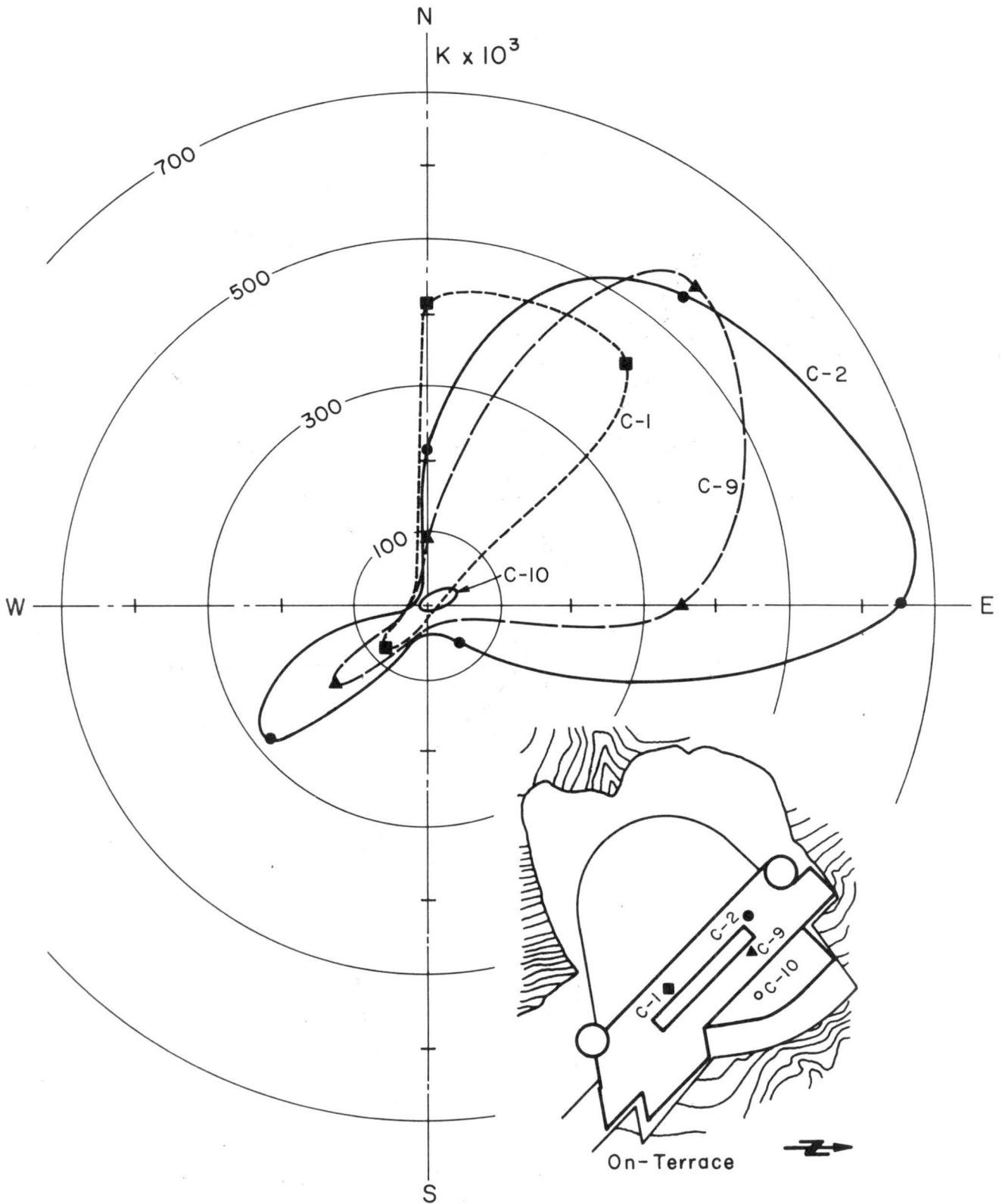


Fig. 47 Effect of Wind Direction on Concentration Coefficients at C1, C2, C9 and C10.

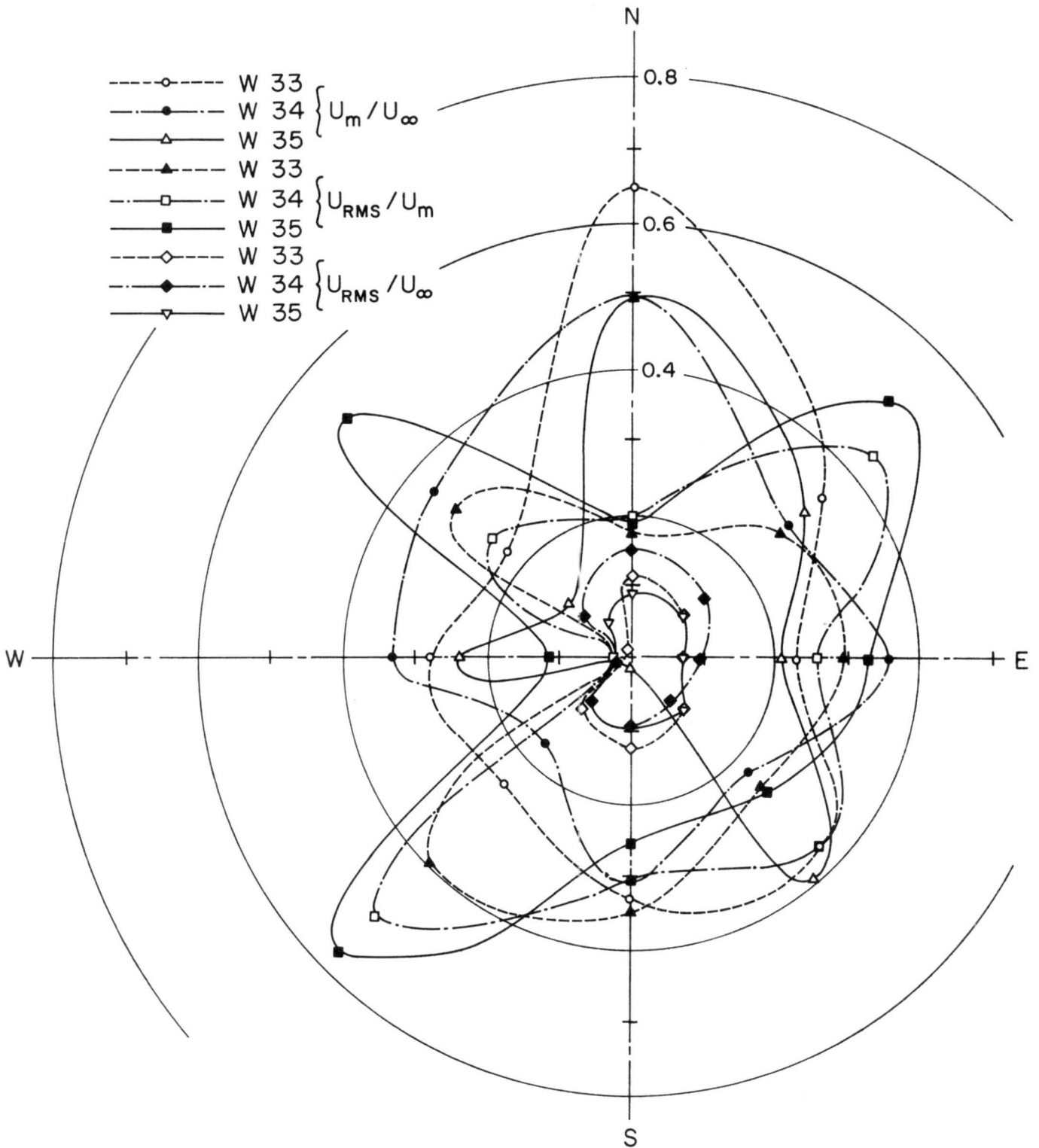


Fig. 48 Radial Plot of Local Mean Winds and Gusts in Heliport at W33, W34 and W35.